

INFORMATION TO USERS

This manuscript has been reproduced from the microfilm master. UMI films the text directly from the original or copy submitted. Thus, some thesis and dissertation copies are in typewriter face, while others may be from any type of computer printer.

The quality of this reproduction is dependent upon the quality of the copy submitted. Broken or indistinct print, colored or poor quality illustrations and photographs, print bleedthrough, substandard margins, and improper alignment can adversely affect reproduction.

In the unlikely event that the author did not send UMI a complete manuscript and there are missing pages, these will be noted. Also, if unauthorized copyright material had to be removed, a note will indicate the deletion.

Oversize materials (e.g., maps, drawings, charts) are reproduced by sectioning the original, beginning at the upper left-hand corner and continuing from left to right in equal sections with small overlaps. Each original is also photographed in one exposure and is included in reduced form at the back of the book.

Photographs included in the original manuscript have been reproduced xerographically in this copy. Higher quality 6" x 9" black and white photographic prints are available for any photographs or illustrations appearing in this copy for an additional charge. Contact UMI directly to order.

UMI

A Bell & Howell Information Company
300 North Zeeb Road, Ann Arbor MI 48106-1346 USA
313/761-4700 800/521-0600

NOTE TO USERS

The original manuscript received by UMI contains pages with slanted print. Pages were microfilmed as received.

This reproduction is the best copy available

UMI

THE USE OF STREAMBED TEXTURE TO INTERPRET
PHYSICAL AND BIOLOGICAL CONDITIONS AT
WATERSHED, REACH, AND SUBREACH SCALES

by

John M. Buffington

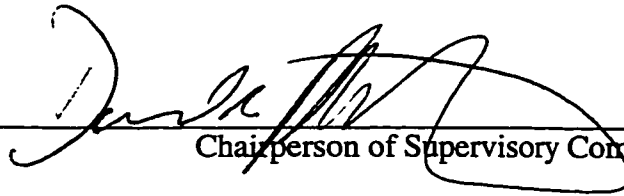
A dissertation submitted in partial fulfillment of the
requirements for the degree of

Doctor of Philosophy

University of Washington

1998

Approved by



Chairperson of Supervisory Committee

Program Authorized
to Offer Degree

Geological Sciences

Date

September 24, 1998

UMI Number: 9916629

UMI Microform 9916629
Copyright 1999, by UMI Company. All rights reserved.

**This microform edition is protected against unauthorized
copying under Title 17, United States Code.**

UMI
300 North Zeeb Road
Ann Arbor, MI 48103

Doctoral Dissertation

In presenting this dissertation in partial fulfillment of the requirements for the Doctoral degree at the University of Washington, I agree that the Library shall make its copies freely available for inspection. I further agree that extensive copying of this dissertation is allowable only for scholarly purposes, consistent with "fair use" as prescribed in the U.S. Copyright Law. Requests for copying or reproduction of this dissertation may be referred to University Microfilms, 1490 Eisenhower Place, P.O. Box 975, Ann Arbor, MI 48106, to whom the author has granted "the right to reproduce and sell (a) copies of the manuscript in microform and/or (b) printed copies of the manuscript made from microform."

Signature 

Date 9/24/98

University of Washington

Abstract

THE USE OF STREAMBED TEXTURE TO
INTERPRET PHYSICAL AND BIOLOGICAL
CONDITIONS AT WATERSHED, REACH, AND
SUBREACH SCALES

by John M. Buffington

Chairperson of the Supervisory Committee: Associate Professor David R. Montgomery
Department of Geological Sciences

Physical controls on bed-surface grain size and consequent implications for aquatic habitat are examined at a variety of spatial scales. Data compiled from laboratory studies show that reach-average median surface grain size (D_{50}) varies inversely with sediment supply, while field studies of forest gravel-bed rivers conducted here demonstrate that D_{50} varies directly with bed shear stress as modified by hydraulic resistance due to channel walls, bars, and wood. Textural response is evaluated relative to a theoretical prediction of competent D_{50} . I hypothesize that surface textures are altered through size-selective erosion or deposition caused by imbalances between sediment supply and transport capacity. Moreover, changes in surface texture that smooth or roughen the bed should alter both the boundary shear stress and the critical shear stress of grains moving over the bed, thereby creating a feedback process between bed-surface texture, sediment flux, and supply-transport state. At subreach scales, my field studies demonstrate that bed surfaces are composed of textural patches, the number and frequency of which varies directly with the magnitude and frequency of hydraulic roughness, due presumably to greater spatial divergence of transport capacity and sediment supply forced by the roughness elements. Bed-surface textures were classified using a new procedure that combines visual and quantitative measurements of patch grain-size distributions and offers reasonable statistical discrimination of differences in both mean grain size and variance between textural patches.

I further examined the correspondence between bed shear stress and surface grain size in two forest pool-riffle channels using a theoretical shear-stress partitioning model. Reach-average velocities calculated from the model are within 7-8% of those measured in

the field using a salt-tracer, providing support for the model. Observed values of D_{50} are in close agreement with those predicted from modeled bankfull bed stresses, indicating that surface grain size of the sites is in quasi-equilibrium with bankfull channel hydraulics.

Greater textural variation at subreach scales creates a broader diversity of aquatic habitats for animals that rely on specific substrate sizes. Furthermore, textural fining caused by bar and wood roughness has the potential to create usable salmonid spawning-gravels in channels that otherwise would be too coarse. Coupling field measurements and theoretical predictions via digital elevation models, I propose a watershed-scale framework for assessing the potential influence of hydraulic roughness on salmonid spawning-habitat availability. Application of the model indicates that textural fining caused by bar and wood resistance can control more than 90% of the potential spawning habitat in mountain drainage basins studied here, with bar roughness most important for lower-mainstem reaches (41-73% of the potential habitat), and wood roughness important for upper-mainstem channels (25-53% of the potential habitat).

Table of Contents

List of Figures.....	iii
List of Tables.....	x
Introduction.....	1
Chapter 1: Effects Of Sediment Supply And Hydraulic Roughness On Surface Textures Of Gravel-Bed Rivers.....	6
Overview	6
Introduction	6
Study Sites and Methods	9
Results and Discussion	12
Implications	22
Conclusions.....	24
Chapter 2: A Procedure For Classifying And Mapping Textural Facies In Gravel-Bed Rivers.....	49
Overview	49
Introduction	49
Classifying and Mapping Textural Patches.....	51
Field Test.....	54
Discussion and Conclusion	58
Chapter 3: Hydraulic Roughness And Shear-Stress Partitioning In Forest Pool-Riffle Channels.....	76
Overview	76
Introduction	76
Study Site and Field Methods.....	77
Hydraulic Roughness and Shear-stress Partitioning	80
Results and Discussion	90
Grain-size Response to Hydraulic Roughness.....	93
Conclusion	93
Chapter 4: Watershed-Scale Availability Of Salmonid Spawning Habitat As Influenced By Hydraulic Roughness.....	113
Overview	113

Introduction	114
Study Sites	116
Methods	117
Results.....	121
Discussion.....	121
Conclusions.....	123
List of References.....	136

List of Figures

Number	Page
Figure 1.1: Channel morphologies studied in northwestern Washington and southeastern Alaska: a) plane-bed; b) wood-poor pool-riffle; c) wood-rich pool-riffle.	32
Figure 1.2: Pool spacing as a function of wood loading and land use at the Alaskan study sites. Pool spacing is expressed in channel widths per pool, defined as $(L/W_{bf})/\#pools$, where L is reach length and W_{bf} is bankfull width. Wood loading is defined as $\#pieces/(W_{bf} \cdot L)$. Logged sites were clearcut to channel margins and/or cleared of in-channel wood.	33
Figure 1.3: Reach-average median surface grain size versus bed shear stress, stratified by equilibrium transport rate ($q_b=q_s$) in laboratory channels. The heavy line is a theoretical prediction of the competent median grain size as a function bed stress (eqn 1.3, $\tau_c=\tau'$, see text).....	34
Figure 1.4: Reach-average textural fining (predicted D_{50s} (eqn 1.3)-observed D_{50s}) as a function of sediment supply during equilibrium transport ($q_b=q_s$) in laboratory channels (data of Fig. 1.3).....	35
Figure 1.5: Typical topographic and textural maps of the three channel morphologies investigated: a) plane-bed (Hoko River 2), b) wood-poor pool-riffle (Hoko River 1), and c) wood-rich pool-riffle (Mill Creek). See Table 1.3 for texture definitions.....	36
Figure 1.6: Box plots of the number of a) textural types (i.e., facies types) and b) textural patches per reach for the Olympic study sites. The line within each box is the median value of the distribution, box ends are the inner and outer quartiles, whiskers are the inner and outer tenths, and circles are the extrema. n is the number of observations per distribution.	39
Figure 1.7: Textural patch frequency as a function of wood frequency at the Olympic study sites. The fitted curve is forced to one patch in plane-bed reaches with zero pieces of wood.....	40

- Figure 1.8: Reach-average bed-surface grain size (D_{50s}) versus total bankfull boundary shear stress (τ_{0bf}), stratified by channel type. The channel types studied represent a general cumulative addition of wall, bar, and wood roughness, resulting in a progressive decrease in bed shear stress (eqn 1.2) and corresponding textural fining. The solid and dashed lines are predictions of the theoretical competent median grain size for low roughness (eqn 1.3, $\tau_c = \tau' = \tau_0$) and bed load sediment supplies of 0, 0.1, and 1.0 kg/m²s, respectively (see text). Circled point is a plane-bed channel recently impacted by sediment input from a debris flow. 41
- Figure 1.9: Box plots of reach-average a) width-to-depth ratio, b) amplitude-wavelength ratio of streamwise wall topography (one side of channel), c) amplitude-wavelength ratio of bar topography and d) wood loading. See Fig. 1.6 caption for box plot definition. Values used for these plots are listed in Table 1.1. 42
- Figure 1.10: Amplitude-wavelength ratio of a) wall topography and b) bar topography as functions of wood loading. Mill Creek (far right point) is excluded from the curve fits. 43
- Figure 1.11: Box plots of reach-average, dimensionless bar wavelength and amplitude. See Fig. 1.6 caption for box plot definition. 44
- Figure 1.12: Median bed-surface grain size versus total bankfull shear stress, stratified by reach morphology [sensu Montgomery and Buffington, 1997]. The solid line is the predicted competent D_{50s} (see Fig. 1.8 caption). Data sources are: dune-ripple [Simons and Albertson, 1963; Chitale, 1970; Williams, 1978; Higginson and Johnston; 1988]; plane-bed and pool-riffle [current study]; step-pool and cascade [D. R. Montgomery, unpublished]. 45
- Figure 1.13: Apparent dimensionless critical shear stress as a function of relative roughness (D_{50s}/h). Here, we use a modified Shields equation [Bathurst et al., 1983] that accounts for downslope gravitational forces and intergranular friction angle ($\tau^*_{c50s} = \tau_{c50s} / [(\rho_s - \rho)gD_{50s}(\cos\theta \tan\Phi_{50} - \sin\theta)]$), where θ is the channel slope angle (0.6-11.3°) and Φ_{50} is the

median friction angle for D_{50s}). For the 6 mm and 2.5 mm experiments, Φ_{50} is calculated from Buffington et al.'s [1992] equation 7, while for the nearly uniform 22.5 mm and 12 mm experiments we assume $\Phi_{50} \approx 45^\circ$ [Miller and Byrne, 1966]. τ_{c50s} is based on extrapolation to zero particle motion and is corrected for wall effects using the Einstein [1934; 1942] approach [Mizuyama, 1977]. The 22.5 mm and 12 mm values are median grain sizes of laboratory mixtures, which are approximately equal to D_{50s} due to the use of well-sorted mixtures..... 46

Figure 1.14: Figure 1.8 redrawn, showing standard errors of reach-average values of D_{50s} . Where error bars are not shown the error is smaller than the symbol size. Standard errors of D_{50s} are also listed in Table 1.1..... 47

Figure 1.15: Comparison of median grain sizes preferred by spawning salmonids and those found in channels with wall, bar, and wood roughness. The spawning gravel median grain sizes are compiled from Kondolf and Wolman [1993] and are typically based on McNeil-type sampling [McNeil and Ahnell, 1960] that combines surface and subsurface material. Furthermore, these samples are typically underweight [sensu Church et al., 1987] and, in some cases, truncated at arbitrary upper grain sizes [Kondolf and Wolman, 1993]. Consequently, the reported ranges of median spawning gravels likely contain considerable error and may be biased toward small sizes due to coarse-tail truncation and combining surface and subsurface material (the latter is typically finer than surface sizes)..... 48

Figure 2.1: Textural and topographic maps of a) Skunk Creek and b) Mill Creek, forest pool-riffle channels of the Olympic Peninsula, western Washington, USA. Each facies type is named according to our textural classification (discussed later). D_{50s} is the median bed-surface grain size of a textural patch, and σ_{gs} is Folk's [1974] graphic standard deviation ($[\phi_{84} - \phi_{16}]/2$, where ϕ_{84} and ϕ_{16} are the \log_2 grain sizes [Krumbein, 1936] for which 16% and 84% of the surface grain sizes are finer..... 65

Figure 2.2: Cartoon illustrating basic strategies for sampling bed-surface sediments in a stream reach: a) facies-stratified random, b) facies-stratified systematic (grid/transect), c) unstratified random, and d) unstratified systematic. Textural patches are indicated by different fill patterns, and sample locations are shown by black dots. In (b), the interval of sample sites within patches is scaled to individual patch area, with each patch having the same number of samples..... 67

Figure 2.3: Two-level ternary classification for bed-surface facies. Level I decomposes the basic sextahedron of major size classes into seven ternary diagrams for classifying textures according to their relative abundance of three major size classes; standard grain size names and divisions are used (Table 2.1). Level II further delineates the grain size composition of the dominant size class (see figure text for symbol key and examples)..... 68

Figure 2.4: Technically dissimilar textures (sgC and gsC) grouped as functionally similar (circled points), but distinctly different from gcS and csG textures in the same reach. 70

Figure 2.5: Cartoon illustrating bed-surface textures with a) similar means, but different variances, and b) different means, but similar variances. 71

Figure 2.6: Level I grain size composition of textures sampled at our study sites. 72

Figure 2.7: Distributions of grain size mean, median, and standard deviation for the sampled textures shown in Figure 2.6..... 73

Figure 2.8: Modified classification ternaries, subdivided at a) the 60th percentile and b) the 60th and 80th percentiles. The modified ternaries increase the number of textural categories from 15 to 27 and 39, respectively. 74

Figure 2.9: Comparison of surface (D_{50s}) and subsurface (D_{50ss}) median grain sizes of textural patches in forest channels of the Olympic Peninsula, western Washington, USA. Surface grain-size distributions were determined from patch-spanning, random, pebble counts [Wolman, 1954] of 100+ grains. Subsurface grain-size distributions were determined from sieved bulk samples, following the Church et al. [1987] sampling criterion (i.e., the largest grain is $\leq 1\%$ of the total sample weight). The reported linear regression is forced through zero. 75

Figure 3.1: Location of study sites.....100

Figure 3.2: Salt-concentration curve from Trap Creek. See text for symbol definitions.	101
Figure 3.3: Cartoon of successive scales of roughness identified at the study sites.	102
Figure 3.4: Cartoon of boundary layers and successive addition of roughness length-scales in a two-component system of grain skin-friction and bar form-drag.	103
Figure 3.5: Cartoon of a segmented velocity profile in a two-component system of grain and bar-form roughness. The portion of the profile near the bed is influenced by grain skin-friction, while that away from the bed and above the height of the bars is influenced by the combined effects of skin friction and bar form-drag.	104
Figure 3.6: Study-site maps of channel topography and wood debris for a) Bambi Creek and b) Trap Creek.	105
Figure 3.7: Variation of cross-sectional values of bankfull channel width (W , circles) and depth (h , squares) at Bambi Creek (solid symbols) and Trap Creek (open symbols).	107
Figure 3.8: Detrended bed-surface profiles of a) Bambi Creek and b) Trap Creek	108
Figure 3.9: Profiles of downstream width undulations at a) Bambi Creek and b) Trap Creek.	109
Figure 3.10: Reach-average flow velocity as a function of relative flow depth (h / h_{bf}).	110
Figure 3.11: Pie charts illustrating the proportion of the total, reach-average, bankfull boundary shear stress represented by each shear-stress component in a) Bambi Creek and b) Trap Creek.	111
Figure 3.12: Comparison of roughness-corrected velocity profile to that assuming skin friction only in a) Bambi Creek and b) Trap Creek.	112
Figure 4.1: Effects of hydraulic roughness on reach-average median bed-surface grain size (D_{50}) (redrafted from Buffington and Montgomery [in review (b)]). For a given total boundary shear stress (τ_0), D_{50} systematically decreases away from the predicted value of competent median grain size (largest mobile D_{50}) with increasing hydraulic roughness and lowered bed stress (τ'). D_{50} ranges preferred by different salmonid species [Kondolf and Wolman, 1993] are shown at the right of the figure, with open circles	

	indicating the inner and outer quartiles of each distribution of median grain sizes.....	127
Figure 4.2:	Location of study sites.....	128
Figure 4.3:	Field-relationships between channel depth and drainage area for a) the Boulder River and Finney Creek drainage basins (data from Montgomery et al. [1998]), and b) the Willapa River watershed (data from Massong [1998]).	129
Figure 4.4:	Predicted channel-segment types for the Boulder River watershed. Characteristics of each channel type are presented in Table 4.1. Pink segments (headwater reaches) are generally not preferred by salmonids due to slopes > 4% and associated boulder-bed morphologies. Cyan segments (lower mainstem reaches) are plane-bed channels with usable spawning-gravel sizes. Green segments (lower mainstem reaches) are usable pool-riffle channels. Deep blue segments (upper mainstem reaches) are usable wood-forced pool-riffle segments. Numbers and lengths of each channel type are listed in the figure key.....	130
Figure 4.5:	Predicted channel-segment types for the Finney Creek basin. See Figure 4.4 for explanation of legend.....	131
Figure 4.6:	Predicted channel-segment types for the Willapa River watershed. In addition to the channel types discussed in the Figure 4.4 caption, red segments shown here (lower mainstem reaches) are lower-gradient pool-riffle and dune-ripple channels predicted to have grain sizes smaller than those typically preferred by spawning salmonids.....	132
Figure 4.7:	Typical frequency distributions of reach slope in natural pool-riffle and plane-bed channels [Montgomery and Buffington, 1997; 1998] compared with slope distributions of pool-riffle and plane-bed segment-types identified in this analysis. Numbers of reaches per channel type in each basin are reported in Figures 4.4-6.	133
Figure 4.8:	Typical textural maps for plane-bed, pool-riffle, and wood-forced pool-riffle channel types redrafted from Buffington and Montgomery [in review (a; b)]. σ_g is Folk's [1974] graphic standard deviation in units of phi [Krumbein, 1936].....	134

Figure 4.9: Box plots of a) the number of different types of textural patches per reach and b) the total frequency of textural patches per reach in plane-bed, pool-riffle, and wood-forced pool-riffle channels (redrafted from Buffington and Montgomery [in review (b)]). n is the number of channels surveyed per morphologic type.....135

List of Tables

Number	Page
Table 1.1: Reach-average channel characteristics	26
Table 1.2: Empirical fit of equation 1.1 to observed equilibrium transport rates	28
Table 1.3: Surface texture composition of the Olympic channels	29
Table 1.4: Comparison of roughness characteristics between channel types	31
Table 2.1: Standard grain-size divisions and names	62
Table 2.2: Statistical accuracy of textural classification.....	63
Table 2.3: Statistical significance of greater classification detail.....	64
Table 3.1: Reach-average physical characteristics of the channels and their hydraulic roughness elements	95
Table 3.2: Calculated shear stress components and roughness length-scales.....	97
Table 3.3: Comparison of measured and calculated reach-average flow velocities and total channel roughness.....	98
Table 3.4: Comparison of measured and calculated reach-average median bed-surface grain size	99
Table 4.1: Stream-segment types.....	125
Table 4.2: Stream-segment statistics.....	126

Acknowledgments

I gratefully appreciate the comments, stimulating discussions, and encouragement provided by my advisors: Dave Montgomery, Bill Dietrich, Catherine Petroff, and Derek Booth.

I am indebted to Brooke Stewart and Kyle Nichols for providing able field assistance in challenging work environments.

Financial support for various portions of this work was provided by the Washington State Timber, Fish & Wildlife agreement (TFW-SH10-FY93-004, FY95-156) and the Pacific Northwest Research Station of the U.S.D.A. Forest Service (cooperative agreement PNW 94-0617).

Dedication

To my wife Mélanie for constant support and encouragement.

And to my son, Jack, for reminding me of the important things in life.

Introduction

Alluvial channels are nonlinear dynamic systems that can exhibit a variety of responses to perturbations of hydraulic discharge or sediment supply. For example, many alluvial channels are free to adjust their width, depth, slope, bed-form morphology, channel pattern, and bed-surface texture in response to changes in discharge and sediment supply. Several morphologic adjustments may occur simultaneously for a given perturbation, with many responses feeding back on one another, adding to the non-linearity of alluvial processes.

Given sufficient time and constancy of water and sediment inputs these process-feedbacks may result in a quasi-equilibrium channel form that passes the imposed sediment and water loads with little morphologic change. The concept of channel equilibrium is a well-established paradigm in fluvial geomorphology and hydraulic engineering, and has been described in many different ways, depending on both the time-scale and morphologic features of interest. Based on field observations in Utah and California, as well as laboratory flume studies, Gilbert [1877; 1914; 1917] hypothesized that alluvial channels adjust to imbalances between sediment supply and transport capacity through sediment deposition or scour that ultimately causes reach-scale changes in channel gradient and establishment of quasi-equilibrium. In a study of sand-bed irrigation canals in the Punjab, Lindley [1919] described morphologically-stable channels as being 'in regime' with the imposed sediment and water discharges. Mackin [1948] used the expression 'at grade' to describe valley-scale equilibrium of channel gradient. In a study of Colorado irrigation ditches, Lane [1953] recognized that bed-surface grain size was in equilibrium with bankfull hydraulics, resulting in a substrate that became mobile only at discharges greater than or equal to the bankfull stage. Henderson [1963] later described Lane's canals and 'threshold channels' and applied the concept to gravel-bed rivers, in general, based on observations made by Wolman and Leopold [1957] and Wolman and Miller [1960]. Since then, many field studies [Kellerhals, 1967; Andrews, 1989], laboratory studies [Wolman and Brush 1961; Ikeda et al., 1988], and theoretical models [Li et al., 1976; Parker, 1978a, b; Chang, 1980; Pizzuto, 1990] have investigated the processes that enable channel equilibrium and have sought to predict equilibrium-channel morphology.

The likelihood of channel morphology equilibrating with the imposed hydrology and sediment load depends on the shape and duration of the local hydrograph, as well as the time-scale of adjustment for the morphologic feature of interest. In arid regions, channels experience infrequent, intense floods of short duration (on the scale of several hours) that may not offer sufficient time for morphologic adjustment to the imposed discharges and sediment loads. In mountain drainage basins of the Pacific Northwest, hydraulic discharge is typically perennial, with flood events occurring one or more times a year and having durations on the order of one or more days, allowing significantly more time for morphologic adjustments. In intermontaine regions of the United States, flood flows typically result from spring snow-melt and are characterized by long, gradually-varying discharge curves that occur on the order of tens of days to months and allow even more time for morphologic adjustments. Although channels adjust and respond to smaller discharge events as well, it is typically the flood events that dominate channel morphology [Wolman and Miller, 1960; Carling, 1988].

Independent of the question of the spatial and temporal scales over which channels may attain particular types of equilibrium, many alluvial rivers are quite responsive to perturbations of discharge or sediment supply, even if such disturbances occur on short time-scales. In particular, bed-surface texture of poorly sorted rivers may be one of the most responsive and easily altered channel characteristics. Here, I explore physical controls on bed-surface grain size of gravel-bed rivers in hydraulically-complex forest environments of southeastern Alaska and northwestern Washington. Through a series of investigations I examine and interpret textural morphology of gravel-bed rivers at a variety of spatial scales. I also explore linkages between the physical processes that control bed-surface grain size and the availability of habitat for aquatic animals that rely on specific substrate sizes. An underlying goal of the dissertation is to be able to interpret physical and biological conditions from inspection of streambed texture. The dissertation is organized into four 'chapters' that are separate papers dealing with different aspects of physical and biological processes related to surface texture of gravel-bed rivers.

The first paper investigates the effects of sediment supply and hydraulic roughness on bed-surface textures at reach and subreach scales. Data compiled from laboratory studies are used to examine the effects of sediment supply, while a field study of forest gravel-bed channels with different characteristic morphologies and roughness configurations is conducted to investigate the effects of hydraulic resistance. Results

demonstrate that reach-average median surface grain size varies systematically with both sediment supply and hydraulic roughness due to channel walls, bars, and wood. Grain size response is evaluated here relative to a theoretical prediction of channel competence, providing an end-member reference state for conditions of low sediment supply and low hydraulic roughness. Results also show that textural response to sediment supply in laboratory studies is several times less than that due to resistance caused by channel walls, bars, and wood. Textural changes are likely caused by size-selective erosion or deposition resulting from local differences between sediment supply and transport capacity. Furthermore, changes in surface texture that roughen or smooth the bed likely effect the local velocity structure and boundary shear stress, as well as the critical shear stress for grains traveling over the bed. Consequently, a feedback process may develop between bed-surface texture and sediment flux, providing a mechanism for partial or complete channel adjustment to imbalances between sediment supply and transport capacity [Dietrich et al., 1989; Lisle et al., 1993]. The field data also demonstrate that at subreach-scales the number and frequency of textural patches (i.e., grain size facies) varies directly with the magnitude and frequency of hydraulic roughness, due presumably to greater spatial divergence of transport capacity and sediment supply forced by the roughness elements.

The second paper proposes and investigates a standard method for classifying and mapping textural facies in gravel-bed rivers. Textural patches are commonly observed in natural and laboratory gravel-bed channels and are of significance for both physical and biological processes at subreach scales. Facies maps also provide a natural template for stratifying other physical and biological measurements and produce a retrievable and versatile data base that can be used as a component of channel monitoring efforts. Nevertheless, there is no standard, quantitative procedure for classifying bed-surface textures. Consequently, a classification method is developed here that combines visual identification of textural patches with quantitative grain size measurement. Drawing from accepted sedimentological techniques, I classify bed-surface textures using grain-size ternary diagrams. A field test of the classification indicates that it affords reasonable statistical discrimination of bed-surface textures, in terms of both patch mean grain size and variance.

The third paper examines sources and magnitudes of hydraulic roughness in two forest, gravel-bed channels of southeastern Alaska. Shear stress associated with each source of roughness is calculated from a stress-partitioning model based on boundary-layer

theory and physical dimensions of each scale of roughness. Six sources of roughness are identified at the study sites: skin friction of bed-surface grains; form drag due to bars; form drag caused by downstream undulations of channel width; form drag caused by wood debris (typically logs); momentum losses due to the combined effects of cross-section shape, width-to-depth ratio, and differences in skin friction between the channel walls and bed; and momentum losses due to planform curvature (i.e., channel sinuosity). The stress-partitioning model is tested by comparing predicted reach-average velocities to those measured in the field from salt-tracers. Results demonstrate that predicted velocities are reasonably similar to measured values, providing support for the stress-partitioning model. Moreover, the reach-average median bed-surface grain size at each site is in close agreement with that predicted from the bankfull bed stress corrected for hydraulic roughness, and is several times smaller than that predicted from the unpartitioned, total boundary shear stress. These findings indicate that bed-surface grain size is in quasi-equilibrium with bankfull channel hydraulics at the study sites, and provide further support for the hypothesis that bed-surface grain size varies directly with boundary shear stress as modified by channel roughness elements. Despite similarities of channel slope, grain size, width-to-depth ratio, channel sinuosity, and amplitude-wavelength ratio of bars, the two channels have very different wood loadings that result in an order of magnitude difference in reach-average hydraulic roughness.

The fourth paper explores the potential effect of hydraulic roughness on the availability of salmonid spawning gravel at reach and watershed scales in three mountain drainage basins in Washington state. Field relationships between channel depth and drainage area are coupled with channel slopes determined from digital elevation models to predict reach-average bankfull boundary shear stresses and corresponding competent grain sizes. These predictions are combined with 1) reported ranges of gravel sizes preferred by salmonids and 2) the empirical results of the first paper to predict the potential influence of bar and wood roughness on bed-surface grain size and consequent spawning-habitat availability. Results demonstrate that bar and wood roughness can significantly enhance spawning-habitat availability in channels that are otherwise too coarse for spawning. Moreover, without textural fining caused by hydraulic roughness, such as that due to bars and wood, the predicted availability of spawning habitat is virtually nonexistent in the steep drainage basins examined here. The distribution and location of channel types predicted to provide usable spawning habitat in each basin is remarkably similar despite differences in

watershed size, physiography, underlying lithology, and geologic history. This type of analysis provides a general framework for assessing potential spawning habitat as controlled by hydraulic roughness, and can be used to reconstruct potential historical spawning grounds or focus watershed-scale habitat-restoration efforts.

The above investigations combine process-based observations and theory, allowing defensible interpretations of physical processes and biological implications in complex forest environments.

Chapter 1: Effects Of Sediment Supply And Hydraulic Roughness On Surface Textures Of Gravel-Bed Rivers¹

Overview

Analysis of data from flume experiments and field investigations indicates that reach-average median bed-surface grain size (D_{50s}) of poorly sorted gravel-bed channels varies systematically with both sediment supply and hydraulic roughness caused by channel walls, bars, and wood. For a given reach-average bed stress, D_{50s} varies inversely with the rate of sediment supply, while for a range of sediment loadings D_{50s} varies directly with bed stress as modified by hydraulic resistance. Textural change is evaluated relative to a theoretical prediction of channel competence that provides an end-member condition of low hydraulic resistance and low equilibrium transport. Textural response to wall, bar, and wood roughness in natural channels is typically several times greater than that observed for sediment supply alone in laboratory channels. We hypothesize that textural change results from size-selective erosion or deposition caused by imbalances between sediment supply and transport capacity. Moreover, changes in surface texture that smooth or roughen the bed should alter both the boundary shear stress and the critical shear stress of grains moving over the bed, thereby creating a feedback process between bed-surface texture, sediment flux, and the supply–transport state of the channel.

Introduction

Rivers with self-formed beds transport and sort the alluvium supplied to them according to basic principles of mass continuity (i.e., sediment output minus input equals change in sediment storage). Bedrock and aggrading alluvial channels are examples of extreme, opposing inequalities between bed load transport capacity (q_c , output potential) and sediment supply (q_s , input). Bedrock channels have transport capacities far in excess of sediment supply ($q_c \gg q_s$), resulting in exportation of all sediment, and scour to the underlying valley floor [Gilbert 1877; 1914; Montgomery et al., 1996]. In contrast,

¹ Co-authored paper by John M. Buffington and David R. Montgomery, in review with *Water Resources Research*.

aggrading alluvial channels represent a sediment supply significantly in excess of transport capacity ($q_s \gg q_c$). Sources of sediment supply include both upstream input and alluvium stored in the channel bed and banks. Transport capacity is defined here as the potential bed load transport rate (i.e., the transport rate of a channel unlimited by sediment supply). We define bed load transport rate (q_b) as a power function of the difference between the bed shear stress (τ') and the critical stress for grain motion (τ_c)

$$q_b = k (\tau' - \tau_c)^n \quad (1.1)$$

where k and n are empirical values [du Boys, 1879; O'Brien and Rindlaub, 1934; Meyer-Peter and Müller, 1948]. The bed shear (τ') is defined as the total boundary shear stress (τ_0) corrected for momentum losses caused by hydraulic roughness elements other than grain skin friction [e.g., Einstein and Banks, 1950; Einstein and Barbarossa, 1952; Nelson and Smith, 1989]

$$\begin{aligned} \tau' &= \tau_0 - \tau'' - \tau''' - \dots - \tau^n \\ \text{bed} &= \text{total} - \text{walls} - \text{bed forms} - \dots - \text{other} \end{aligned} \quad (1.2)$$

The critical, grain-mobilizing, shear stress for a grain size of interest (τ_{ci}) is a function of submerged grain weight, particle protrusion into the flow, and intergranular friction angle [Wiberg and Smith, 1987; Kirchner et al., 1990; Buffington et al., 1992]; the latter two depend on sediment sorting (σ) and the size of the particle of interest (D_i) relative to its neighbors (D_i/D_{50s} , where D_{50s} is the median bed-surface grain size) [Wiberg and Smith, 1987; Kirchner et al., 1990; Buffington et al., 1992].

Dietrich et al. [1989] recently suggested that selective transport and altered bed-surface texture provide a mechanism for alluvial channels to adjust to less extreme imbalances of sediment supply and transport capacity than those of bedrock and aggrading alluvial channels. In particular, the broad grain-size distributions of gravel-bed rivers (typically sand to cobble) allow for considerable selective transport and dynamic textural response to local perturbations of sediment supply or transport capacity. For example, a local transport capacity greater than supply ($q_c > q_s$) may result in winnowing of fine grains (as is common below both natural [Rice, 1994] and anthropogenic dams [Leopold et al., 1964]), which will, in turn, create a rougher surface with greater intergranular friction

angles, increasing critical shear stresses for grains moving over the bed (τ_{ci}) [Wiberg and Smith, 1987; Kirchner et al., 1990; Buffington et al., 1992], thereby retarding bed load transport rates (eqn. 1.1) and partially counteracting the difference between transport capacity and sediment supply. Altered bed-surface roughness also effects local velocity structure and shear stress [Naot, 1984], creating an additional feedback between bed-surface texture, shear stress, and transport capacity. Given sufficient time, constancy of sediment and water inputs, and availability of mobile sediment, the above process feedbacks may ultimately result in equilibration of the transport rate with the imposed sediment supply rate [Dietrich et al., 1989; Lisle et al., 1993]. Selective transport that results in bed-surface coarsening and armor development also makes the bed surface less mobile and alters the timing and total contribution of subsurface sediment to the supply of bed load material [Milhous, 1973; Parker and Klingeman, 1982; Carling and Hurley, 1987].

While it has been well-documented that alluvial channels can respond to perturbations of sediment supply or transport capacity through macro-scale changes in channel width, depth, slope, scour depth, and bed form morphology [Gilbert, 1914; Leopold and Maddock, 1953; Schumm, 1971; Montgomery and Buffington, 1998], textural response to such perturbations has received less attention. Furthermore, textural change may have important implications for both sediment yield (eqn. 1.1) and the availability of aquatic habitat for animals that prefer specific grain sizes, such as salmonids [Kondolf and Wolman, 1993] and macroinvertebrates [Cummins and Lauff, 1969; Reice, 1980].

In this paper, we conduct a systematic analysis of the effects of sediment supply and hydraulic roughness [i.e., altered τ' (eqn. 1.2)] on surface textures of gravel-bed channels having wide grain-size distributions. We hypothesize that for a given bed shear stress, surface grain size will be inversely related to sediment supply. Sediment supplies that overwhelm the local transport capacity should cause deposition of fine-grained particles (those typically in transport) and reduction of bed-surface grain size. It is expected that greater sediment loads will cause increased deposition and greater textural fining. Conversely, reduced sediment supply should result in surface winnowing and textural coarsening. Similarly, for a given sediment supply we hypothesize that bed-surface grain size will vary directly with bed shear stress as modified by hydraulic roughness elements. Hydraulic resistance that lowers the effective bed stress should decrease the bed load

transport capacity, again, resulting in deposition of fine-grained material and reduced bed-surface grain size. The magnitude of textural fining should reflect both the decrease in competence and the degree of fine-sediment deposition forced by hydraulic roughness and lower bed stresses. Textural response to both sediment supply and hydraulic roughness is evaluated here relative to a theoretical prediction of channel competence, providing an end-member reference state for both low equilibrium transport and low hydraulic roughness.

Study Sites and Methods

Sediment supply

There are three components of the sediment supply that may influence bed-surface textures: 1) the rate of sediment supply (kg/m·s); 2) the caliber (i.e., size) of the sediment comprising the supply; and 3) the size distribution (i.e., sorting) of the supply. In this study, we focus on textural response to the rate of sediment supply.

To examine textural response to sediment-supply rate we compiled data from previously published laboratory studies that met the following criteria: 1) experiments were conducted in sediment-feed flumes (i.e., non recirculating) with surface textures, bed slope, and water surface slope allowed to equilibrate with an imposed discharge and sediment feed rate; 2) each source conducted experiments at several feed rates, using a constant size distribution; 3) experiments were allowed to run to a state of equilibrium transport (defined as equality of both the rate and size distribution of sediment input and output); and 4) grain-size distributions of the equilibrium bed surface were reported. We found only four studies that met these criteria [Parker et al., 1982; Kuhnle and Southard, 1988; Dietrich et al., 1989; Lisle et al., 1993].

Hydraulic roughness

To examine textural response to hydraulic roughness [and therefore altered τ' (eqn. 1.2)] a field study of three types of gravel-bed channels was conducted in forest mountain drainage basins of northwestern Washington and southeastern Alaska. The three channel morphologies are: plane-bed [sensu Montgomery and Buffington, 1997]; wood-poor pool-riffle; and wood-rich pool-riffle (Fig. 1.1). These three channel types represent a general cumulative addition of wall, bar, and wood-debris roughness and a progressive decrease in τ' for a given τ_0 (eqn. 1.2).

Olympic sites—We surveyed fourteen channels on the Olympic Peninsula of

northwestern Washington. The Olympic Peninsula is characterized by mountainous terrain and a coastal rain forest of Sitka spruce (*Picea sitchensis*), western hemlock (*Tsuga heterophylla*), red cedar (*Thuja plicata*), and Douglas fir (*Pseudotsuga taxifolia*). Bedrock geology of the Peninsula is predominantly composed of Eocene to Miocene marine basalts and sediments [Tabor and Cady, 1978a; b]. The Olympic study sites occupy watersheds influenced by Pleistocene glaciation and are typically incised into fluvioglacial deposits. Channel widths and slopes of our study sites ranged from 5-13 m and 0.0040-0.0265, respectively (Table 1.1).

Logging activity on the Olympic Peninsula is generally intensive, with some forests on their third harvest rotation. Most study sites had riparian buffers composed of mixed shrub and conifer, although some study sites had been clear cut to channel margins, resulting in riparian forests of mixed shrub and red alder (*Alnus rubra*). Coniferous buffers were typically second growth, indicating a long history of logging disturbance. Hillslope failures are common in the Peninsula and are attributed to reduced root strength after timber harvesting. Relict debris flow deposits form channel-margin terraces in three of the study reaches and indicate both long runout paths and the potential for periodic large sediment inputs.

Olympic methods—At each study site, three cross sections and a center-line bed profile were surveyed in reaches that were 8 to 18 channel widths long. Detailed topographic, textural, and wood maps also were constructed using a digital theodolite. Bed surfaces were commonly composed of spatially distinct textural patches (i.e., grain size facies) of differing particle size and sorting. A standard procedure was developed to classify textural patches [Buffington and Montgomery, in review (a)]. Surface grain-size distributions of each patch type were determined from random pebble counts [Wolman, 1954] of 100+ grains. These samples were, in turn, spatially averaged by patch area to determine reach-average grain-size distributions. Particle sizes suspendable at bankfull stage were removed from the grain-size distributions to separate bed load from suspended load distributions. The maximum suspendable size was calculated from Dietrich's [1982] settling velocity curves, assuming a Corey shape factor of 0.7, a Power's roundness of 3.5, and a settling velocity equal to the bankfull shear velocity.

Alaskan sites—We supplemented our Olympic survey with data from twenty-seven, southeast Alaskan, coastal channels studied by Wood-Smith and Buffington [1996] (Table 1.1). The Alaskan study areas are characterized by steep glaciated terrain, maritime

climate, and rain forests predominantly composed of Sitka spruce and western hemlock. Hillslopes are commonly grooved by avalanche chutes and slope failures. The geology of southeastern Alaska is characterized by all major rock types of ages ranging from Proterozoic(?) to Quaternary [Gehrels and Berg, 1992], largely accreted during the Cretaceous to Eocene [Goldfarb et al., 1988; Gehrels et al., 1990]. Southeastern Alaska was profoundly influenced by Pleistocene glaciation [Reed, 1958] and many of the study sites drain glacially-carved valleys and cirques. The Alaskan study sites include both pristine old growth environments and areas heavily disturbed by timber harvesting. Pristine channels were characterized by high wood loading, while disturbed channels were generally clear cut to the stream banks and had most or all of their in-channel wood removed [Wood-Smith and Buffington, 1996]. Channel widths and slopes of our study sites ranged from 5-29 m and 0.0017-0.0267, respectively (Table 1.1).

Alaskan methods—At each study site, five cross sections and a center-line bed profile were surveyed with an engineer's level over reaches that were 8 to 23 channel widths long. A bank-to-bank random pebble count [Wolman, 1954] of 100+ grains was conducted at each cross section. Reach-average grain-size distributions were determined from simple averages of these samples, with the suspendable load removed as described above.

The Alaskan channels exhibit a continuum of wood loading that strongly influences pool spacing at the sites (Fig. 1.2). We used the median value of this continuum (0.010 pieces/m²) to separate wood-poor and wood-rich pool-riffle channels. This division corresponds well with land use history at these sites (Fig. 1.2). Because all in-channel wood was inventoried in the Olympic streams, while only pool-forming wood was recorded in the Alaskan channels, it was necessary to derive a conversion factor for the two types of wood measurement before the data sets could be combined. Using previously published data from similar channel types and physiographic regions [Montgomery et al., 1995], we developed a reasonable correlation between pool-forming wood pieces/m² and non-functioning wood pieces/m² ($y=0.23 x^{0.53}$, $r^2=0.46$), from which the total wood loading is calculated as the sum of these two quantities. We find that the median value of 0.010 pool-forming pieces/m² is equivalent to a total wood loading of about 0.030 pieces/m²; this value was used to separate the Olympic pool-riffle channels into wood-rich and wood-poor categories, providing a common definition of channel type for the Olympic and Alaskan sites. Total wood loading at the study sites varied from 0-0.15 pieces/m²

(Table 1.1).

It is worth noting that plots of pool spacing versus wood loading (Fig. 1.2) can be potentially spurious because bankfull width (W_{bf}) and reach length (L) appear in both the abscissa and ordinate ($1/(W_{bf} \cdot L)$ vs. L/W_{bf}). In particular, the data exhibit an inverse power function not unlike that expected for a spurious self-correlation of $1/L$ versus L . However, our study reaches have a narrow, constant range of lengths that are roughly 10-20 channel widths across all wood loadings. Therefore, the potential for spurious correlation vanishes, as the common factors in the abscissa and ordinate reduce to $1/(10-20 W_{bf}^2)$ versus 10-20. A similar plot by Montgomery et al. [1995; their Fig. 4] is non-spurious for the same reasons.

Results and Discussion

Sediment supply

With the compiled laboratory data, we examined changes in the equilibrium bed-surface texture caused by altered rates of sediment supply. In each study, sediment-supply caliber and grain-size distribution are held constant, while the channel morphology, hydraulics, and bed load transport rate are allowed to equilibrate with an imposed sediment feed rate.

The compiled data demonstrate that for fairly constant bed shear stresses in each study, reach-average median bed-surface grain size systematically coarsens in response to decreasing rate of sediment supply (Fig. 1.3). Furthermore, bed load transport rates are brought into equilibrium with lowered sediment supply rates through winnowing and surface coarsening, increasing τ_c for grains moving over the bed and reducing q_b (eqn. 1.1), while τ' remains fairly constant in each study. These observations confirm the hypothesis that channels with wide grain-size distributions can adjust texturally to sediment supply perturbations. Here, we use D_{50s} as representative of the bed surface as a whole. τ' is the channel depth-slope product corrected for wall effects [Houjou et al., 1990] and bed form drag where present [Nelson and Smith, 1989]; the depth-slope product is defined as ρghS , where ρ is fluid density (1000 kg/m^3), g is gravitational acceleration, h is flow depth, and S is water surface slope. Channel morphologies in these studies include: plane-bed; low-amplitude dunes (bed load sheets [Whiting et al., 1988]); and pool-riffle. Although macro-scale changes in channel slope, width, depth, and bed morphology also provide mechanisms for equilibrating differences between rates of sediment supply and

transport, our analysis shows that bed-surface textural response is an active component of channel response to altered sediment supply (Fig. 1.3).

The heavy black line shown in Figure 1.3 is a theoretical prediction of the upper limit of textural coarsening predicted from the Shields [1936] equation

$$D_{50s} = \frac{\tau_{c50s}}{\tau_{c50s}^* (\rho_s - \rho) g} \quad (1.3)$$

where τ_{c50s} is the critical shear stress for incipient motion of D_{50s} (set equal to the imposed τ' value), τ_{c50s}^* is the corresponding dimensionless critical stress (set equal to 0.030, a conservative value for visually-based methods that minimizes error caused by neglect of roughness elements [Buffington and Montgomery, 1997]), and ρ_s is the sediment density (set equal to 2650 kg/m³). This equation predicts the theoretical competent median grain size (i.e., maximum mobile D_{50s}) for the imposed τ' . Because τ_{c50s} is set equal to τ' , the prediction also corresponds with an end-member condition of zero equilibrium transport (eqn. 1.1). As expected, the compiled data approach this maximum limit of textural coarsening at low sediment supplies and low equilibrium transport rates (Fig. 1.3). It is emphasized, however, that equation 1.3 predicts a hypothetical grain size, the occurrence of which depends on particle-size availability as dictated by the grain-size distribution of the sediment supply.

We also find that the difference between the predicted and observed D_{50s} is correlated with the equilibrium transport rate, causing the compiled data to collapse into a single function (Fig. 1.4) despite differing 1) bed shear stress, 2) reach-average median surface grain size, 3) caliber of supplied sediment, and 4) sorting of supplied sediment in the four studies. A power function of this sort confirms the form of the bed load transport equation assumed in this analysis (eqn. 1.1), the rationale for which is as follows. Inspection of equation 1.3 shows that grain size is linearly proportional to its critical shear stress. By relating the observed D_{50s} to its critical shear stress ($D_{50s_{obs}} \propto \tau_{c50s}$), and relating the predicted, competent D_{50s} to the imposed bed stress ($D_{50s_{pred}} \propto \tau'$), equation 1.1 can be rewritten as

$$q_b = k_1 (\tau' - \tau_c)^{n_1} = k_2 (D_{50s_{pred}} - D_{50s_{obs}})^{n_2} \quad (1.4a)$$

$$\Rightarrow (D_{50s_{pred}} - D_{50s_{obs}}) = k_3 q_b^{n_3} \quad (1.4b)$$

which agrees with the relationship observed in Figure 1.4.

Equilibrium transport rates of the compiled data are also well described by equation 1.1 (Table 1.2). In fitting equation 1.1 to the data we calculated τ' as described above (depth-slope product corrected for wall effects and bed form drag). In each study, the grain-size distribution of the bed load is finer than that of the bed surface, except at the highest transport rates, where the two distributions become similar. Consequently, when fitting equation 1.1 to the data it is necessary to calculate a τ_c value that specifically represents movement of the bed load material. Two mechanisms for entraining bed load material can be envisioned: 1) mobilizing fine-grained, in situ particles resting on the bed surface; and 2) mobilizing coarse-grained armor particles, causing the release of finer-grained material trapped under and around the larger clasts. Therefore, we consider two different τ_c values, representing the above two cases: the critical shear stress of the median grain size of the load over that of the surface material (τ_{c50l} as a function of D_{50l}/D_{50s} , case 1); and the critical shear stress of the median bed-surface grain size (τ_{c50s} , case 2). For both cases, we calculated τ_c from the Shields equation ($\tau_{ci} = \tau_{ci}^* (\rho_s - \rho) g D_{50i}$) using several different hypothetical Shields numbers expressed as power functions of D_i/D_{50s} ($\tau_{ci}^* = \alpha (D_i/D_{50s})^\beta$) (Table 1.2); we also examined different exponents of this power function, representing moderately versus strongly selective transport (i.e., $\beta = -0.8$ to -0.4) (Table 1.2). In all cases, the compiled data conform to equation 1 and have reasonably high correlation coefficients (Table 1.2), however the fitted coefficient (k) and exponent (n) of equation 1.1 are strongly dependent on the choice of τ_{ci}^* and τ_c .

While it is commonly believed that n has a value of about 1.5, we could find only three studies that report experimentally determined n values [O'Brien and Rindlaub, 1934 (data of Gilbert, 1914); Meyer-Peter and Müller, 1948; Chien, 1956 (data of USWES, 1935)]. These studies report that $n=1.3-1.8$. However, our analysis indicates that n can be quite variable, and likely depends on investigator choice of 1) characteristic grain size (i.e., particular D_i and particular grain-size distribution (e.g., surface, subsurface, or laboratory mixture [Buffington and Montgomery, 1997])), 2) method of determining τ_{ci} , and 3) method of correcting τ' for channel roughness.

It is emphasized that the above analysis represents an end-member condition of equilibrium transport, realization of which in natural channels depends on the local

hydrologic regime (i.e., the frequency, duration, and nature of runoff events), as well as the spatial and temporal scales of interest.

Hydraulic roughness: subreach-scale response

Detailed field measurements at the Olympic sites allow examination of subreach-scale textural response to hydraulic roughness. Representative maps of each channel type (plane-bed, wood-poor pool-riffle, and wood-rich pool-riffle) illustrate characteristic variations in topography, wood loading, and surface texture (Fig. 1.5). The number of textural types observed in a reach varied from one to seven, with textures composed of grain sizes ranging from silt to small boulder (Table 1.3). t-tests indicate that almost all textural types within a reach are significantly different from one another, while most patches of the same textural type within a reach are statistically similar (0.10 significance, two-tailed t-test assuming unequal and unknown variance).

Facies mapping demonstrates that channel type and roughness configuration strongly influence the number, frequency, and spatial arrangement of surface textures. Plane-bed channels exhibit one to four grain-size facies, but are frequently mono-textural (Table 1.3, Fig. 1.6a). Each of the wood-poor pool-riffle channels are composed of four textural types, while wood-rich pool-riffle channels exhibit three to seven facies types per reach (Table 1.3, Fig. 1.6a). Similarly, the total number of textural patches within a reach ranges from 1-8 in plane-bed channels, but increases to 13-24 in wood-poor pool-riffle channels and 17-55 in wood-rich pool-riffle streams (Table 1.3, Fig. 1.6b). Furthermore, the spatial arrangement of textures is progressively more complicated in the three channel types studied (Fig. 1.5).

Textural patches likely represent spatial divergence of sediment supply and transport capacity, causing local, size-selective variations in sediment flux that lead to patch development. Our field observations suggest that increased frequency and magnitude of flow obstructions (i.e., bars and wood) enhance the spatial divergence of sediment flux and patch development. For example, the number of textural patches in a reach is related to the frequency of wood obstructions (Fig. 1.7). Although the stochastic nature of wood recruitment creates complex, irregular textural patterns within our study sites, more predictable patterns of textural patches have been documented in channels with less chaotic arrangements of flow obstructions. For example, regular patterns of textural patches are found in self-formed meandering channels due to systematic downstream and cross-

channel variations in shear stress and sediment flux caused by channel curvature, topographically-induced convective accelerations, and lateral bed slope [Dietrich et al., 1979; Dietrich and Smith, 1984; Parker and Andrews, 1985].

Hydraulic roughness: reach-scale response

The three channel types studied (plane-bed, wood-poor pool-riffle, and wood-rich pool-riffle) represent a cumulative addition of wall, bar, and wood roughness and, presumably, a progressive decrease in τ' for a given τ_0 (eqn. 1.2). Our field data demonstrate that for a given reach-average, total, bankfull shear stress (τ_{0bf}), channels with greater roughness [and therefore lower τ'_{bf} (eqn. 1.2)] have systematically smaller reach-average surface grain sizes (Fig. 1.8). This result is consistent with several other studies that demonstrate that wood removal from forest channels causes bed-surface coarsening, presumably due to increased bed stress resulting from the loss of wood roughness elements [Lisle, 1995].

Here, τ_{0bf} is defined as $\rho gh_{bf}S_c$, where h_{bf} is the bankfull depth averaged over the bed, and S_c is the center-line bed slope (Table 1.1). While we did not find any practical difference in results using the bankfull depth averaged over the bed versus averaged over the entire cross section, we chose the former because 1) it is of most physical relevance to the channel bed and observed grain sizes; and 2) many of the study sites had broad, low-angle banks that caused substantial reduction in the average flow depth when the bank regions were included. The banks of the study sites are generally immobile, fine-grained, cohesive soils rooted by significant riparian vegetation ranging in scale from grasses and herbs to large conifers. For comparison with other studies, bankfull depths averaged over the entire cross section also are reported in Table 1.1.

Roughness configuration—The scatter of D_{50s} values in Figure 1.8 for a given τ_{0bf} and channel type reflects site-specific differences in roughness configuration. For example, wood creates hydraulic roughness primarily through form drag, the magnitude of which depends on the frequency, size, orientation, and flow height of the in-channel logs and rootwads. Similarly, the form drag caused by bars depends on their amplitude and wavelength [Nelson and Smith, 1989]. Several sources contribute to what we collectively call wall roughness: 1) proximity of walls (so-called width-to-depth effects) and associated momentum diffusion [Leighly, 1932; Parker, 1978b]; 2) roughness length scale (i.e., skin friction) of the material forming the walls [Einstein, 1934; 1942; Houjou et al., 1990]; 3)

downstream variations in channel width that effectively force lateral form drag analogous to bed form drag; and 4) riparian vegetation protruding from the banks [Andrews, 1984].

Roughness magnitude—Although we did not quantify hydraulic roughness through either direct measurement of τ' or calculation of resistance coefficients (e.g., Darcy-Weisbach f , Manning n , etc.), the physical channel characteristics that cause wall, bar, and wood roughness show a statistically significant increase in magnitude across the three channel types studied (Fig. 1.9). For example, while there is no significant difference in width-to-depth ratios $[(W/h)_{bf}]$ amongst the channel types (Fig. 1.9a, Table 1.4), there is a significant increase in streamwise wall topography and consequent form drag; streamwise variation of channel width results in wave-form wall topography at the study sites, the amplitude-wavelength ratio of which $[(\alpha/\lambda)_w]$ increases significantly across the three channel types (Fig. 1.9b, Table 1.4), indicating a progressive increase in hydraulic roughness due to greater wall form drag.

Differences in wall skin friction and protrusion of riparian vegetation into the channel were not quantified. However, the greatest amount of vegetative protrusion into the channel typically occurred at the wood-poor pool-riffle sites where growth of riparian shrubs and deciduous trees was stimulated by recent clear cutting.

Like streamwise wall topography, the amplitude-wavelength ratio of bars $[(\alpha/\lambda)_b]$ shows a statistically significant increase across the three channel types (Fig. 1.9c, Table 1.4), indicating a progressive increase in roughness due to bed form drag. Two scales of bars are included in Figure 1.9c: macro scale bars ($\alpha_b > 0.5 h_{bf}$) and meso scale bars ($0.25 h_{bf} < \alpha_b < 0.5 h_{bf}$). Bar forms were identified visually from detrended bed profiles.

There is also a significant increase in wood loading across the three channel types (Fig. 1.9d, Table 1.4), indicating a progressive increase in hydraulic roughness due to wood form drag. Wood loading plays an important morphologic and hydrologic role at the study sites, not only influencing pool spacing (Fig. 1.2) and textural patch frequency (Fig. 1.7), but also controlling the amplitude-wavelength ratio of both wall and bed topography (Fig. 1.10). Forest channels commonly exhibit considerable width variation within a single reach [Trimble, 1997] due to morphologic forcing caused by in-channel wood. Wood obstructions can force flow against banks, causing scour and the development of locally wide sections of channel, or they can armor banks and maintain locally narrow channel widths; both effects commonly occur within a single reach. While wood loading also influences bed topography (Fig. 1.10b), we find that wood affects the spacing of bars

more so than their amplitude (Fig. 1.11). Our findings indicate that beyond creating its own form drag and hydraulic roughness, wood forces greater wall and bed topography and consequently greater form drag at our study sites (Fig. 1.10). Wall form drag caused by downstream variations in channel width is a particularly important source of roughness in forest channels. We find that the amplitude-wavelength ratio of wall topography for each side of the channel is typically twice that of bar topography (cf. Fig. 1.9b-c).

Grain-size response—The progressive increase in wall, bar, and wood roughness causes a systematic reduction in reach-average D_{50s} at our study sites (Fig. 1.8). Channels with the same value of total bankfull shear stress (τ_{0bf}) have smaller grain sizes as roughness increases and diminishes the effective bed stress. These observations are consistent with the hypothesis that surface texture should vary directly with τ' for a given sediment supply. Roughness due to walls, bars, and wood lowers τ' (eqn. 1.2), decreasing channel competence and likely causing size-selective deposition of sediment that is in transport (typically finer-grained than the bed surface), both of which reduce the bed-surface grain size. This process also smoothes the bed and lowers τ_c for grains moving over that surface, thereby allowing partial or complete transport of the imposed load despite lower bed stresses. While the grain-size response observed in the field data is consistent with the above hypothesis, it cannot be fully tested, as no measures of sediment supply or bed load transport rate were made.

The heavy black line shown in Figure 1.8 is a theoretical prediction of the upper limit of textural coarsening predicted from the Shields [1936] equation as per equation 1.3, but with τ_{c50s} set equal to τ_{0bf} . We use τ_{0bf} here because it is the practical limit of shear stress in natural channels with well-developed floodplains and self-formed beds (i.e., all sizes mobile at typical high flows). Setting $\tau_{c50s}=\tau_{0bf}$ in equation 1.3 predicts the theoretical competent D_{50s} (i.e., maximum mobile D_{50s}) of a hydraulically-simple, low-roughness, plane-bed channel [i.e., one where τ' is approximately equal to τ_0 due to the absence of other roughness elements (eqn. 1.2)]. Furthermore, because we set $\tau_{c50s}=\tau_{0bf}=\tau'_{bf}$, this prediction corresponds with a zero transport rate (eqn. 1.1). The two dashed lines below the heavy one are predictions of theoretical competence for the same hydraulically-simple channel, but with equilibrium transport rates of 0.1 and 1.0 kg/m·s, respectively, based on the empirical data of Figure 1.4. As expected, the field data show that surface grain sizes systematically approach these theoretical competence curves at low hydraulic roughness (plane-bed morphology), as τ'_{bf} approaches τ_{0bf} . The degree to

which the data approach these curves also depends on the supply–transport state of the channel; the curves are for the special case of channel equilibrium.

We emphasize, again, that the predicted values of competent D_{50s} are hypothetical, the occurrence of which depends on sediment-size availability as dictated by the grain-size distribution of the sediment supply. Furthermore, only gravel-bed channels with plane-bed morphologies [sensu Montgomery and Buffington, 1997] have the potential to realize the theoretical competent D_{50s} . Both lower-gradient sand-bed rivers and steeper-gradient boulder-bed rivers have characteristic channel morphologies and accompanying roughness elements that cause $\tau' \ll \tau_0$, and therefore $D_{50s_{obs}} \ll D_{50s_{pred}}$ (Fig. 1.12). Sand-bed rivers typically have a dune-ripple morphology [Montgomery and Buffington, 1997] characterized by multiple scales of bed forms (ripples, dunes, bars) that provide significant form drag, while steeper-gradient boulder-bed channels typically have step-pool and cascade morphologies [Montgomery and Buffington, 1997] characterized by tumbling flow, low width-to-depth ratios, and boulder form drag, all of which create considerable channel roughness [Marcus et al., 1992]. Dune-ripple channels also exhibit sediment transport at stages significantly less than bankfull, indicating that the observed D_{50s} should be much less than a theoretical competent D_{50s} predicted from bankfull shear stress (Fig. 1.12).

Even when limited to gravel-bed morphologies (plane-bed and pool-riffle channels), equation 1.3 overpredicts the competent D_{50s} in channels with steep slopes due to unaccounted-for effects of relative roughness (D_{50s}/h). For given values of ρ , ρ_s , and τ^*_{c50s} , equation 1.3 specifies a unique D_{50s}/h value for each value of S

$$D_{50s} = \frac{\tau_{c50s}}{\tau^*_{c50s} (\rho_s - \rho) g} = \frac{\rho g h S}{\tau^*_{c50s} (\rho_s - \rho) g} \quad (1.5a)$$

$$\Rightarrow \frac{D_{50s}}{h} = \frac{\rho S}{\tau^*_{c50s} (\rho_s - \rho)} \quad (1.5b)$$

Consequently, high values of D_{50s}/h are predicted for channels with steep slopes. As grain size becomes a significant proportion of the flow depth, it causes form drag that diminishes τ' and the competent D_{50s} , an effect that is not accounted for in equations 1.3 and 1.5a. Laboratory data from experiments by Mizuyama [1977] illustrate the effect of relative

roughness on critical shear stress. Figure 1.13 shows the apparent change in τ^*_{c50s} as a function of D_{50s}/h . The τ^*_{c50s} values are apparent because the τ' values used to calculate τ^*_{c50s} were not corrected for relative roughness and grain form drag. Based on equation 1.5b and Mizuyama's [1977] data we estimated the influence of relative roughness and grain form drag on the predicted competence of our study sites. Our field sites have slopes of 0.4-2.7%, which correspond with predicted relative roughnesses of $D_{50s}/h=0.08-0.55$ (calculated from equation 1.5b, with $\rho=1000 \text{ kg/m}^3$, $\rho_s=2650 \text{ kg/m}^3$, and $\tau^*_{c50s}=0.03$). Figure 1.13 indicates that a change in relative roughness from 0-0.08 causes a 4% change in apparent τ^*_{c50s} , while a change in D_{50s}/h from 0-0.55 causes a 32% change in apparent τ^*_{c50s} . Because the competent D_{50s} is linearly proportional to τ^*_{c50s} (eqn. 1.5a), a 4-32% change in apparent τ^*_{c50s} indicates that the competent D_{50s} is overpredicted by an equivalent percentage. However, more than 80% of our study sites have slopes $<1.5\%$, indicating less than 17% overprediction of competence for the majority of our data.

Plots of dimensionless critical shear stress versus relative roughness have the potential to be completely spurious because channel depth and grain size are common factors to both the ordinate and abscissa [Abrahams et al., 1988]. In such plots, there is the potential for a ratio-type, spurious self-correlation [Kenney, 1982] caused by plotting grain size and depth versus their inverses. Consequently, the expected spurious correlation is a doubly negative relationship. In contrast, the Figure 1.13 data demonstrate a positive correlation, suggesting that the observed relationship is "real", rather than spurious. A positive relationship between dimensionless critical shear stress and relative roughness is commonly observed in incipient motion studies [Buffington and Montgomery, 1997].

Roughness versus sediment supply—The observed grain size response to wall, bar, and wood roughness is considerably greater than that predicted for sediment supply alone (dashed curves, Fig. 1.8). The data demonstrate that textural fining in response to hydraulic roughness can be several times greater than that predicted for bed load supply rates of $1 \text{ kg/m}\cdot\text{s}$ (a reasonable upper limit of typical, non-catastrophic, sediment loads). However, one of the plane-bed study sites, recently impacted by a debris flow (circled point, Fig. 1.8), shows considerable deviation from the other plane-bed channels, presumably in response to catastrophic sediment loading of the debris flow. Infrequent, catastrophic sediment inputs from hollow failures and resultant debris flows are characteristic of the steep, mountainous terrain of northwestern Washington and southeastern Alaska. Evidence for such impacts observed at our field sites include 1)

landslide tracks entering a channel, in some cases accompanied by a debris jam, and 2) fresh debris flow levees, inundating and scouring riparian vegetation. Although six of our study sites showed evidence of debris-flow input (Table 1.1), only one of the most recently affected channels showed a strong textural response to debris-flow loading (circled point, Fig. 1.8).

Because we did not quantify either the rate or caliber of sediment supply at the field sites, one may wonder if the textural fining observed in Figure 1.8 is due to systematic changes in either of these factors, rather than a systematic increase in hydraulic roughness and lowered τ' . It is unlikely that the observed textural fining represents either an underlying increase in sediment supply rate or a decrease in supply caliber for the following reasons: 1) the highest sediment loading is expected for sites in logged basins, where high sediment production rates occur due to road runoff [Reid and Dunne, 1984] and mass wasting caused by both poor road design [Montgomery, 1994] and reduced root strength following timber harvest [Sidle et al., 1985]. However, the logged sites (predominantly wood-poor pool-riffle) do not show the highest degree of textural fining. The channels with the greatest amount of textural fining (wood-rich pool-riffle) are predominantly roadless old growth sites with a lower frequency of mass wasting events. Therefore, the observed textural fining is not due to an increasing sediment supply rate; 2) lithology (a strong control on grain strength and caliber) is highly variable across the sites and is uncorrelated with the three channel types; and 3) drainage area (a crude surrogate for sediment supply rate and caliber) is uncorrelated with channel type.

The strong grain size response to hydraulic roughness (Fig. 1.8), and the lack of evidence for an underlying covariance with sediment supply that would explain the observed textural fining, suggests that site-specific differences in sediment supply rate and caliber are overwhelmed by wall, bar, and wood roughness at our study sites, except where recent catastrophic sediment inputs have occurred (circled point, Fig. 1.8). The dominant control of wall, bar, and wood roughness on D_{50s} at our sites is further supported by comparison of observed textural fining with that predicted for normal, non-catastrophic, sediment loads (dashed curves, Fig. 1.8).

Standard error of D_{50s} —Because the reported D_{50s} values are reach averages of bed surfaces with progressively greater numbers of textural types, it is important to examine the standard error associated with the calculated reach-average D_{50s} and its potential influence on our interpretation of the data. The standard error of the reach-average D_{50s} is defined as

$$SE_{50s} = \frac{s_{50s}}{\sqrt{n}} \quad (1.6)$$

where s_{50s} is the standard deviation of texture median grain sizes weighted by their area, and n is the number of textural types per reach. We find that the standard errors are substantial at some sites, but the pattern of decreasing grain size with increasing roughness due to walls, bars, and wood is maintained and is not obscured by the standard errors (Fig 1.14). For the most part, the standard errors are small because even in very patchy reaches there is typically a dominant textural type that occupies $\geq 50\%$ of the bed-surface area (Table 1.3), which skews the distribution of textural types and resultant reach-average D_{50s} toward the grain-size characteristics of the dominant textural type.

Use of the depth-slope product—Shear stress calculated from a depth-slope product assumes steady, uniform flow, which can be approximated in natural channels for slowly varying discharges and long reach lengths. Paola and Mohrig [1996] argue that to assume quasi-steady flow, significant discharge fluctuations should occur on time scales $\gg u/gS$ (where u is the downstream flow velocity), while quasi-uniform flow requires study reach lengths $\gg h/S$. Although our study sites are characterized by high velocities (~ 1 m/s at bankfull stage) and flashy hydrographs, the steep channel slopes ($\sim 10^{-3}$ - 10^{-2}) make u/gS quite small (< 2 min) and considerably less than the time scale for significant discharge variations during flood events (rising limb of hydrograph is typically ≥ 5 hr [Estep and Beschta, 1985; Smith et al., 1993]). Consequently, a quasi-steady flow approximation is valid for our study sites. However, the ratio of study reach length to h/S ranges from 0.4-10 (with an average of 3), and does not satisfy the criteria for quasi-uniform flow. Therefore, a depth-slope product may only partially approximate the actual reach-average shear stress at each study site.

Implications

Sediment supply—Because predicted and observed D_{50s} values are proportional to τ' and τ_c , respectively, the difference between $D_{50s_{pred}}$ and $D_{50s_{obs}}$ provides an indirect measure of excess shear stress ($\tau' - \tau_c$) which is well correlated with bed load transport rate in our analysis (Fig. 1.4). This suggests that for quasi-equilibrium conditions ($q_b \approx q_s$), local sediment supply rate can be inferred from the difference between observed and

predicted D_{50s} . Regardless of whether the caliber of the observed bed-surface grain size reflects textural response to sediment loading (Fig. 1.3) or is due to the particular size distribution of the supply, the difference between predicted and observed grain size is a measure of excess shear stress, and therefore a measure of both q_b and q_s for near-equilibrium channels.

Other indices of sediment loading have been proposed [e.g., Dietrich et al., 1989; Lisle and Hilton, 1992], but only offer qualitative assessments of sediment supply (i.e., high, medium, and low). Based on our findings, we propose that specific sediment loadings could be inverted from the difference between predicted and observed D_{50s} values in channels that are in quasi-equilibrium (Fig. 1.4). However, for natural gravel-bed channels with well-developed floodplains and self-formed beds (i.e., all sizes mobile at typical high flows), the theoretical competent D_{50s} in Figure 1.4 should be predicted from the bankfull bed stress (τ'_{bf}). Grain size response to wall, bar, and wood roughness observed in this study (Fig. 1.8) underscores the need to use roughness-corrected bed stresses for such calculations. An expedient approach for applying Figure 4 is to confine its use to hydraulically-simple, plane-bed reaches where correction for wall effects [sensu Houjou et al., 1990] may be the only roughness correction needed. Hydraulically-simple reaches are further recommended because the grain-size response to sediment supply observed in our analysis is fairly small (~15 mm over three orders of magnitude of sediment loading) and may be overwhelmed by parameter uncertainty in currently available formulas for stress correction of hydraulically-complex reaches. Application of Figure 1.4 also should be limited to channels with low slopes (<2%). Channels with steep slopes require both a relative roughness correction for prediction of competent D_{50s} (see Fig. 1.13 discussion) and use of a modified Shields equation that accounts for slope-driven gravity forces [Mizuyama, 1977; Bathurst et al., 1983; see also Fig. 1.13].

While Figure 1.4 may prove useful for assessing local bed load sediment supply, it is cautioned that our results are based on a limited set of flume data with small grain sizes ($D_{50s} \leq 13$ mm) and channels not entirely self-formed; except for the study of Lisle et al. [1993], the laboratory channels used in our compilation were constrained to specific widths. Furthermore, the caliber of sediment supply was held constant in each experiment, and although the data collapse into a single function despite differing caliber and size-distributions of sediment supply, the limited amount of available data does not allow a full exploration of the effects of these parameters. For example, everything else being equal,

bed-surface response to a supply of fine-grained sediment may be very different than to a supply of coarser-grained material. Due to these concerns further investigation of our findings is warranted before they are endorsed as a land management tool. Moreover, the condition of near-equilibrium transport may not be a realistic assumption for actively disturbed landscapes, such as watersheds that have been intensely clearcut and are experiencing high sediment loads due to accelerated landslide frequency, road runoff, and destabilized river banks. Nevertheless, where it is known that channels are aggrading, our proposed method provides a minimum estimate of local sediment supply rate; the difference between predicted and observed D_{50s} can provide an estimate of the bankfull q_b , which must be less than q_s for an aggrading system.

Hydraulic roughness—Textural fining caused by hydraulic roughness may have important implications for the availability of salmonid spawning habitat. Salmonids select specific grain sizes in which to spawn [Kondolf and Wolman, 1993]. Comparison of preferred spawning gravel sizes and our field data suggest that textural fining caused by channel walls, bars, and wood can create usable spawning gravels in channels otherwise too coarse to be hospitable for spawning (Fig. 1.15). Furthermore, bar and wood roughness create a greater variety of textural patches (cf. Fig. 1.5a-c), offering a range of aquatic habitats that may promote biologic diversity or be of use to specific animals at different life stages.

Conclusions

We find that gravel-bed channels with broad grain-size distributions exhibit systematic textural response to altered magnitudes of bed load sediment supply and hydraulic roughness (and therefore altered bed shear stress). Textural changes are likely caused by size-selective erosion or deposition resulting from local differences between sediment supply and transport capacity. Furthermore, changes in surface texture that roughen or smooth the bed likely effect the local velocity structure and boundary shear stress, as well as the critical shear stress for grains traveling over the bed. Consequently, a feedback process may develop between bed-surface texture and sediment flux, providing a mechanism for partial or complete channel adjustment to imbalances between sediment supply and transport capacity [Dietrich et al., 1989; Lisle et al., 1993]. However, altered bed-surface texture is only one of many potential morphologic responses in unconstrained alluvial channels. For example, perturbations of sediment supply or transport capacity also

may cause macro-scale changes of channel width, depth, slope, scour depth, and bed form morphology [Gilbert, 1914; Leopold and Maddock, 1953; Schumm, 1971; Montgomery and Buffington, 1998]. Nevertheless, our observations indicate that textural change can be an active, and potentially rapid, part of morphologic response to channel perturbations.

For the special case of a quasi-equilibrium state, surface grain size should be adjusted to the imposed bed shear stress and sediment supply. Consequently, inspection of bed-surface texture can provide important information regarding channel processes and magnitudes of both sediment supply and hydraulic roughness in equilibrium channels. For example, we find that the difference between the observed median grain size and that predicted from a theoretical competence expression can be correlated with specific magnitudes of equilibrium sediment supply, regardless of specific bed-surface grain size, bed stress, and caliber of sediment supply (Fig. 1.4).

We also find that at subreach-scales our study channels are composed of discrete textural patches that vary architecturally with channel morphology and roughness configuration (i.e., plane-bed to wood-forced pool-riffle). Previous studies demonstrate that textural patches also develop and evolve architecturally in response to altered sediment load in plane-bed and pool-riffle channels [Dietrich et al., 1989; Lisle et al., 1993]. Despite the common occurrence of textural patches in both natural [Dietrich and Smith, 1984; Ferguson et al., 1989; Kinerson, 1990; Wolcott and Church, 1990; Lisle and Madej, 1992; Paola and Seal, 1995; Powell and Ashworth, 1995] and laboratory channels [Iseya and Ikeda, 1987; Dietrich et al., 1989; Lisle et al., 1993], little is known about the processes and mechanics of patch development, patch interactions, and their role in bed load transport and channel stability.

Table 1.1: Reach-average channel characteristics

Channel	Sc	W _{bf} (m)	h _{bf} (m)*	L (m)	D _{50s} (mm)†	σ _{gs} (φ)†	SE _{50s} (mm)†	LWD/m ²	(α/λ) _b	(α/λ) _w
Olympic Channels										
<i>Plane-bed/incipient pool-riffle</i>										
Dry 2§	0.0126	6.84	0.59 (0.69)	60	67.1 (69.2)	1.24 (1.17)	0.0 (0.0)	0.0000	0.000	0.018
Alder†	0.0265	8.68	0.57 (0.64)	154	52.8 (58.0)	1.60 (1.28)	5.9 (5.5)	0.0015	0.010	0.023
Hoko 2	0.0160	5.12	0.34 (0.37)	60	54.8 (55.2)	1.34 (1.31)	0.0 (0.0)	0.0033	0.008	0.024
Hoh 1	0.0059	11.53	0.55 (0.62)	142	19.3 (41.9)	2.17 (1.19)	8.3 (0.8)	0.0006	0.008	0.008
Hoh 2	0.0114	10.08	0.51 (0.55)	95	56.8 (62.1)	1.59 (1.48)	7.6 (2.5)	0.0052	0.010	
<i>Wood-poor pool-riffle</i>										
Skunk 2	0.0126	6.79	0.83 (0.89)	85	39.3 (41.2)	1.11 (0.98)	9.1 (8.4)	0.0243	0.012	0.056
Hoko 1	0.0085	12.81	0.78 (0.89)	134	35.0 (35.7)	1.14 (1.09)	6.1 (6.1)	0.0157	0.033	0.060
Pins 1	0.0090	6.75	0.86 (0.92)	64	31.4 (34.0)	1.55 (1.29)	3.3 (3.4)	0.0278	0.012	0.042
<i>Wood-rich pool-riffle</i>										
Pins 2	0.0133	6.90	0.61 (0.66)	70	36.0 (39.5)	0.96 (0.92)	7.8 (7.2)	0.0580	0.026	0.112
Flu Hardy	0.0105	6.64	0.53 (0.55)	69.5	24.4 (29.1)	0.89 (0.85)	5.2 (2.6)	0.0455	0.044	0.118
Mill	0.0143	8.41	0.83 (1.04)	73	19.4 (24.0)	0.98 (0.87)	4.8 (4.1)	0.1450	0.048	0.120
Dry 1§	0.0222	7.96	0.60 (0.73)	70	53.4 (55.4)	0.96 (0.91)	10.8 (10.8)	0.0431	0.029	0.079
Skunk 1	0.0040	13.39	0.78 (0.85)	140	19.8 (23.8)	0.95 (0.86)	4.9 (2.2)	0.0352	0.030	0.072
Cedar	0.0046	10.95	0.72 (0.85)	100	27.2 (29.7)	0.72 (0.72)	5.9 (9.5)	0.0438	0.037	0.085
Alaskan Channels										
<i>Plane-bed/incipient pool-riffle</i>										
Maybeso 3	0.0024	27.07	1.03 (1.11)	324	36.4 (39.6)	>1.50 (1.17)	2.1 (2.8)	0.0132	0.007	0.021
Maybeso 4	0.0036	24.48	1.06 (1.12)	436	46.4 (47.7)	0.88 (0.82)	4.1 (3.9)	0.0058	0.004	0.020
Indian	0.0122	24.60	1.17 (1.32)	480	79.4 (85.1)	1.67 (1.54)	10.0 (9.3)	0.0025	0.014	0.054
Weaselet	0.0025	15.10	0.92 (1.01)	187	25.6 (48.2)	>2.34 (1.45)	8.8 (6.0)	0.0230	0.014	
<i>Wood-poor pool-riffle</i>										
12 Mile 1	0.0021	23.34	0.95 (1.05)	360	24.3 (26.6)	1.44 (0.89)	2.6 (2.1)	0.0106	0.010	0.045
12 Mile 2	0.0028	22.47	1.03 (1.10)	170	21.9 (24.9)	1.90 (0.90)	3.2 (3.0)	0.0108	0.016	0.040
Maybeso 1	0.0095	22.31	1.13 (1.24)	400	49.6 (53.2)	1.76 (1.51)	5.1 (5.6)	0.0000	0.015	
Maybeso 2	0.0065	29.12	0.97 (1.10)	500	36.2 (38.6)	1.30 (1.16)	4.3 (4.2)	0.0112	0.013	
Cable	0.0017	16.89	0.88 (0.96)	300	20.6 ^{ll}	>1.97 ^{ll}	6.4 ^{ll}	0.0234	0.023	0.083
FUBAR 1	0.0106	17.84	0.62 (0.66)	360	42.9 (47.5)	>1.50 (1.15)	9.2 (7.7)	0.0290	0.012	0.071
FUBAR 2	0.0127	16.32	0.79 (0.85)	300	57.6 (60.8)	1.58 (1.41)	4.5 (4.4)	0.0070	0.014	0.024
Muri	0.0150	14.29	0.59 (0.64)	300	44.3 (53.5)	>2.13 (1.29)	5.2 (4.3)	0.0123	0.015	0.060
Bambi	0.0102	4.6	0.32	80	16.3 (17.7)	>1.08 (0.85)	2.0 (1.7)	0.0136	0.025	0.075

Table 1.1 (continued)

Channel	S_c	W_{bf} (m)	h_{bf} (m)*	L (m)	D_{50s} (mm)†	σ_{gs} (ϕ)†	SE_{50s} (mm)†	LWD/m ²	$(\alpha/\lambda)_b$	$(\alpha/\lambda)_w$
<i>Wood-rich pool-riffle</i>										
Hook§	0.0110	21.37	0.82 (0.88)	250	27.4 (31.9)	>1.78 (1.07)	2.1 (1.6)	0.0405	0.040	0.100
Trap 1	0.0055	12.92	0.84 (0.95)	165	17.0 (17.8)	1.04 (0.97)	3.0 (2.8)	0.0644	0.040	
Trap 2	0.0074	15.59	0.66 (0.77)	220	15.4 (16.0)	1.30 (1.11)	1.7 (1.4)	0.0635	0.037	
Trap 3	0.0072	11.84	0.60 (0.66)	220	13.9 (16.5)	>1.72 (1.21)	1.7 (0.7)	0.0639	0.045	
Trap 4	0.0071	9.67	0.68 (0.76)	220	13.5 (16.2)	>1.83 (1.34)	1.1 (0.8)	0.0698	0.032	
Trap 5	0.0102	14.11	0.68 (0.75)	175	17.6 (21.2)	>1.54 (0.98)	1.4 (1.1)	0.0591	0.048	
Trap 6	0.0120	15.76	0.71 (0.78)	200	13.4 (18.7)	>1.88 (1.10)	1.5 (2.3)	0.0566	0.038	
E Fk Trap 1	0.0133	15.72	0.78 (0.87)	200	19.9 (23.5)	>1.84 (1.00)	1.4 (1.3)		0.038	
E Fk Trap 2	0.0127	10.65	0.58 (0.66)	172	24.5 (31.0)	1.79 (1.20)	3.9 (1.9)	0.0531	0.051	
Fowler 1	0.0063	18.03	0.65 (0.74)	225	14.1 (18.5)	>2.03 (1.55)	3.6 (3.6)	0.0313	0.023	0.058
Fowler 2	0.0054	11.46	0.68 (0.83)	210	19.0 (24.5)	>2.06 (1.57)	7.6 (9.5)	0.0358	0.034	0.048
Fish 1	0.0267	19.18	1.12 (1.33)	167	30.6 (40.9)	1.32 (0.90)	4.0 (3.3)	0.0601	0.052	0.126
Fish 2	0.0224	12.88	0.56 (0.60)	280	45.8 (48.3)	1.33 (1.23)	2.5 (2.4)	0.0311	0.034	0.077
Greens†	0.0220	12.90	0.66 (0.85)	260	34.9 (47.0)	>2.16 (1.58)	6.8 (5.7)	0.0303	0.039	0.055

S_c (center-line bed slope), W_{bf} (bankfull channel width), h_{bf} (bankfull channel depth), D_{50s} (median bed surface grain size), σ_{gs} (graphic

standard deviation [Folk, 1974]), LWD/m² (total wood loading, pieces/m²), $(\alpha/\lambda)_b$ (bar amplitude/wavelength), and $(\alpha/\lambda)_w$ (wall topography, amplitude/wavelength, one side of channel) are reach-average values. L is reach length. SE_{50s} is the standard error of the reach-average D_{50s} .

* First values are cross-sectionally averaged over the channel bed and banks, while those in parentheses are averaged over the channel bed only.

† Values in parentheses are for grain size distributions with suspendable sizes removed (see text).

‡ Evidence of recent catastrophic sediment inputs from debris flows.

§ Less recent debris flow input.

|| Bedload and suspended load material could not be differentiated as the maximum suspendable grain size was < 2 mm, the minimum resolution used for our surface pebble counts.

Table 1.2: Empirical fit of equation 1.1 to observed equilibrium transport rates

	$q_b = k (\tau' - \tau_c)^n = q_s$			$\tau_{c_i}^* = \alpha (D_i/D_{50s})^\beta$	
	k	n	r ²	α	β
τ_{c50l}	0.005	2.1	0.85	0.030	-0.8
	0.003	1.9	0.69	0.030	-0.4
	0.030	1.5	0.86	0.045	-0.8
	0.008	1.6	0.67	0.045	-0.4
τ_{c50s}	0.010	1.9	0.80	0.030	na*
	0.057 [†]	1.2	0.68	0.045	na*

τ_c is calculated as $\tau_{c_i}^*(\rho_s - \rho)gD_{50i}$ for hypothetical Shields numbers expressed as power-functions of D_i/D_{50s} , with assumed α and β values (last two columns) (see text).

* β values are not applicable for τ_{c50s} calculations because $D_i/D_{50s}=1$.

[†] empirical fit limited to seven of the thirteen experiments because six of the calculated τ_{c50s} values are greater than τ' .

Table 1.3: Surface texture composition of the Olympic channels

Channel	Texture*	% of Bed	Frequency (#/reach)	D _{50s} (mm) [†]	σ_{gs} (ϕ) ^{†,‡}
<i>Plane-bed/incipient pool-riffle</i>					
Dry 2	gC	100	1	67.1 (69.2)	1.24 (1.17)
Alder	G	0.4	1	~11	
	scG	9.0	4	21.8 (29.7)	1.76 (1.39)
Hoko 2	cG	90.6	1	56.1 (61.0)	1.58 (1.27)
Hoh 1	cG	100	1	54.8 (55.2)	1.34 (1.31)
	S	2	2	~2.0 (na)	
	cgS	63	3	9.0 (42.7)	2.76 (1.26)
Hoh 2	cG	35	3	38.9 (40.3)	1.10 (1.05)
	S	4	2	~2.0 (na)	
	cgS	4	1	9.0 (42.7)	2.76 (1.26)
	cG	0.5	1	38.9 (40.3)	1.10 (1.05)
	gC	91.5	1	61.4 (63.1)	1.54 (1.49)
<i>Wood-poor pool-riffle</i>					
Skunk 2	S	9.33	9	<2.0 (8.5)	>0.65 (0.40)
	G	11.19	9	9.9 (12.8)	1.41 (1.05)
	csG	8.22	4	25.0 (27.8)	1.37 (0.98)
Hoko 1	cG	71.24	2	50.4 (51.5)	1.10 (1.05)
	sg	5.10	7	~6.0	
	G	13.87	9	13.1 (13.8)	0.98 (0.87)
	cG _{mcvc}	61.58	4	38.4 (39.2)	1.24 (1.20)
	cG _{cvc}	19.45	3	47.4 (47.7)	0.92 (0.92)
Pins 1	S	1.16	3	~2.0 (na)	
	G _{efm}	4.15	6	9.2 (11.0)	1.32 (1.02)
	G _{fcm}	2.58	3	12.7 (14.1)	1.15 (1.04)
	cG	92.11	1	33.3 (35.6)	1.57 (1.31)
<i>Wood-rich pool-riffle</i>					
Pins 2	S	7.71	4	~2.0 (na)	
	sg	3.22	3	7.1 (8.7)	0.92 (0.47)
	cG _{mvcc}	48.47	3	29.6 (30.4)	0.93 (0.88)
	cG _{mcvc}	40.61	7	52.4 (52.8)	1.01 (1.00)
Flu Hardy	Z	3.98	2	~0.06 (na)	
	S	11.79	9	~2.0 (na)	
	G _{efm}	3.70	6	11.7 (12.0)	0.92 (0.90)
	G _{mcvc}	80.53	1	29.5 (29.9)	0.89 (0.85)

Table 1.3 (continued)

Channel	Texture*	% of Bed	Frequency (#/reach)	D _{50s} (mm)†	σ_{gs} (ϕ)†‡
Mill	Z	1.63	2	~0.06 (na)	
	S	15.89	21	~2.0 (na)	
	G _{vffm}	11.77	25	8.4 (10.4)	0.93 (0.67)
	G _{mvcc}	62.57	2	23.7 (24.5)	1.04 (0.94)
	G _{cvc}	8.15	5	39.6 (39.6)	0.58 (0.58)
Dry 1	S	0.94	3	~2.0 (na)	
	scG	4.79	2	9.3 (33.9)	2.34 (1.90)
	G	7.52	5	13.8 (15.7)	1.09 (0.87)
	cG	39.28	3	39.1 (39.6)	1.12 (1.09)
	gC	47.48	8	77.0 (77.0)	0.66 (0.66)
Skunk 1	S	16.15	32	~2.0 (na)	
	G _{vcmc}	62.31	6	21.2 (22.0)	0.96 (0.84)
	G _{mvcc}	21.54	4	29.2 (29.2)	0.91 (0.91)
	Z	5.61	2	~0.06 (na)	
	S	2.64	3	~2.0 (na)	
Cedar	sG	1.08	6	6.6 (7.2)	0.98 (0.84)
	G _{vcmc}	12.80	11	17.6 (17.6)	0.65 (0.65)
	G _{mvcc}	64.19	1	26.6 (26.8)	0.70 (0.70)
	cG	6.15	1	35.3 (35.3)	0.82 (0.82)
	gC	7.53	3	74.4 (74.4)	0.89 (0.89)

* Textures are named using the Buffington and Montgomery [in review (a)] classification scheme. Capital letters represent the dominant grain size (Z=silt, S=sand, G=gravel, C=cobble), preceding lower case letters represent less abundant grain sizes, read as adjectives modifying the upper case noun (s=sandy, g=gravelly, c=cobble), and succeeding lower case subscripts further describe the grain size composition of the dominant size class (vf=very fine, f=fine, m=medium, c=coarse, vc=very coarse). Order of lower case letters indicates relative abundance (least to greatest). For example, sG_{vm}=sandy, fine to medium gravel. Lower case subscripts are used to distinguish otherwise identical textural names (e.g., distinguishing coarse versus fine gravel textures). Sediment terms correspond with standard grain size classes [Table 1, Buffington and Montgomery, in review (a)].

† Values in parentheses are for grain size distributions with suspendable sizes removed (see text). 'na' indicates the entire suspension of a patch at bankfull flow.

‡ σ_{gs} is the graphic standard deviation, defined as $(\phi_{84}-\phi_{16})/2$ [Folk, 1974], where ϕ_{84} and ϕ_{16} are the log₂ grain sizes [Krumbein, 1936] for which 16% and 84% of the surface grain sizes are finer.

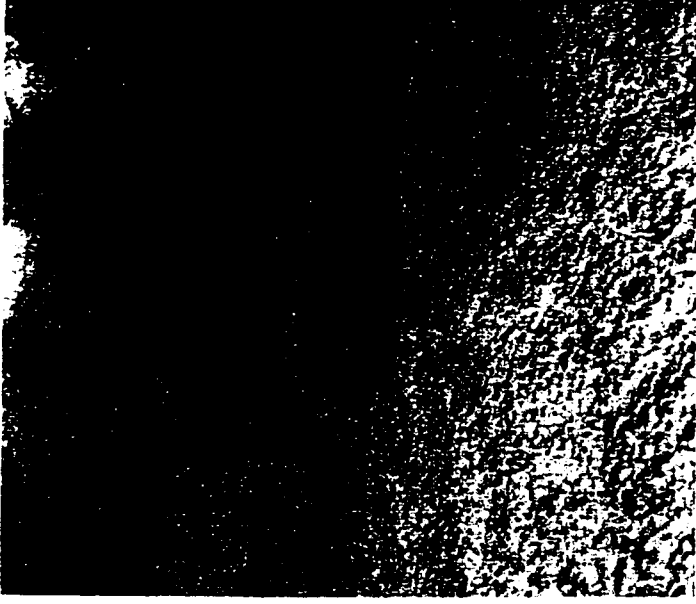
Table 1.4: Comparison of roughness characteristics between channel types

	P-value		
	$(W/h)_{bf}$	$(\alpha/\lambda)_w$	$(\alpha/\lambda)_b$
plane-bed vs. wood-poor pool-riffle	0.375	0.001	0.002
wood-poor pool-riffle vs. wood-rich pool-riffle	0.272	0.002	0.000
plane-bed vs. wood-rich pool-riffle	0.376	0.000	0.000
			wood pieces/m ²
			0.009
			0.000
			0.000

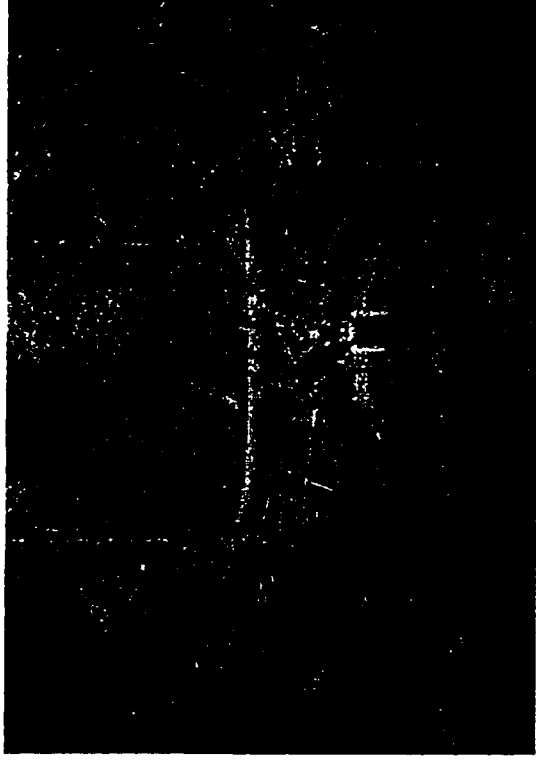
Reported P-values are for unpaired, one-tailed t-tests of the Figure 1.9 distributions, assuming unequal and unknown variance. Differences between distribution means are considered statistically significant when $P \leq 0.05$.



a)



b)



c)

Figure 1.1: Channel morphologies studied in northwestern Washington and southeastern Alaska: a) plane-bed; b) wood-poor pool-riffle; c) wood-rich pool-riffle.

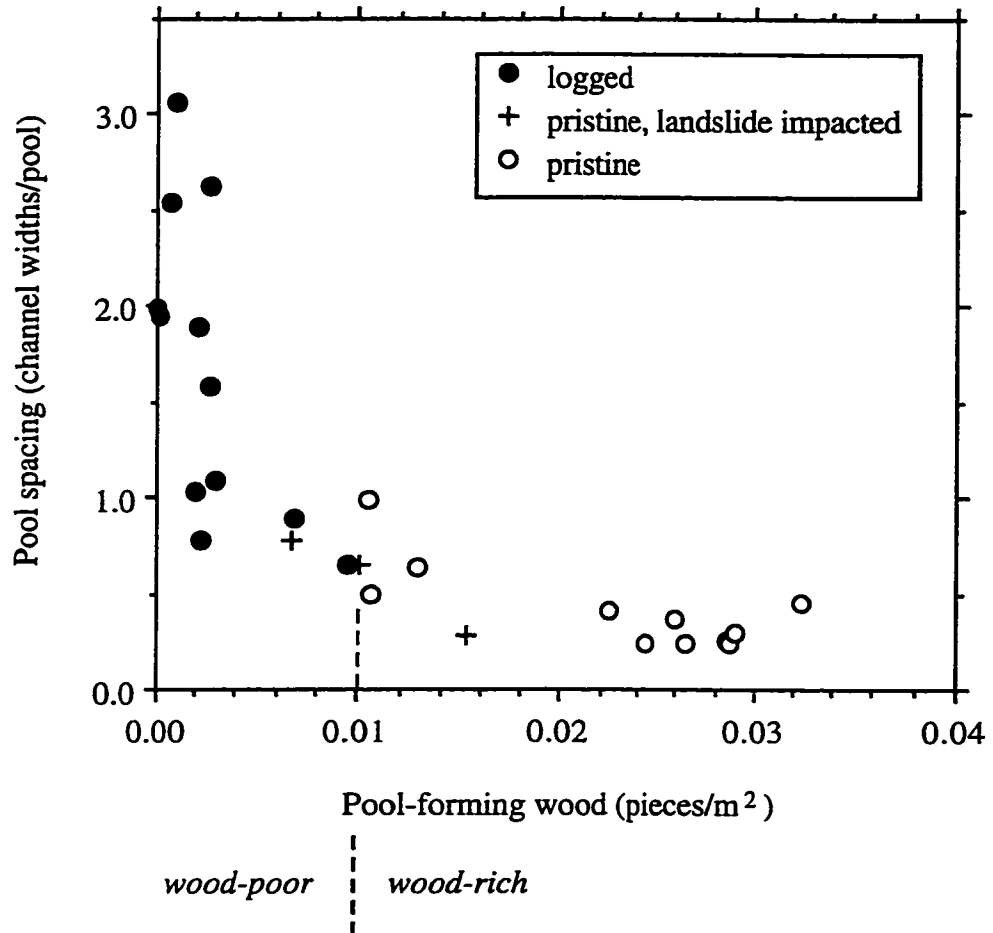


Figure 1.2: Pool spacing as a function of wood loading and land use at the Alaskan study sites. Pool spacing is expressed in channel widths per pool, defined as $(L/W_{bf})/\#\text{pools}$, where L is reach length and W_{bf} is bankfull width. Wood loading is defined as $\#\text{pieces}/(W_{bf} \cdot L)$. Logged sites were clearcut to channel margins and/or cleared of in-channel wood.

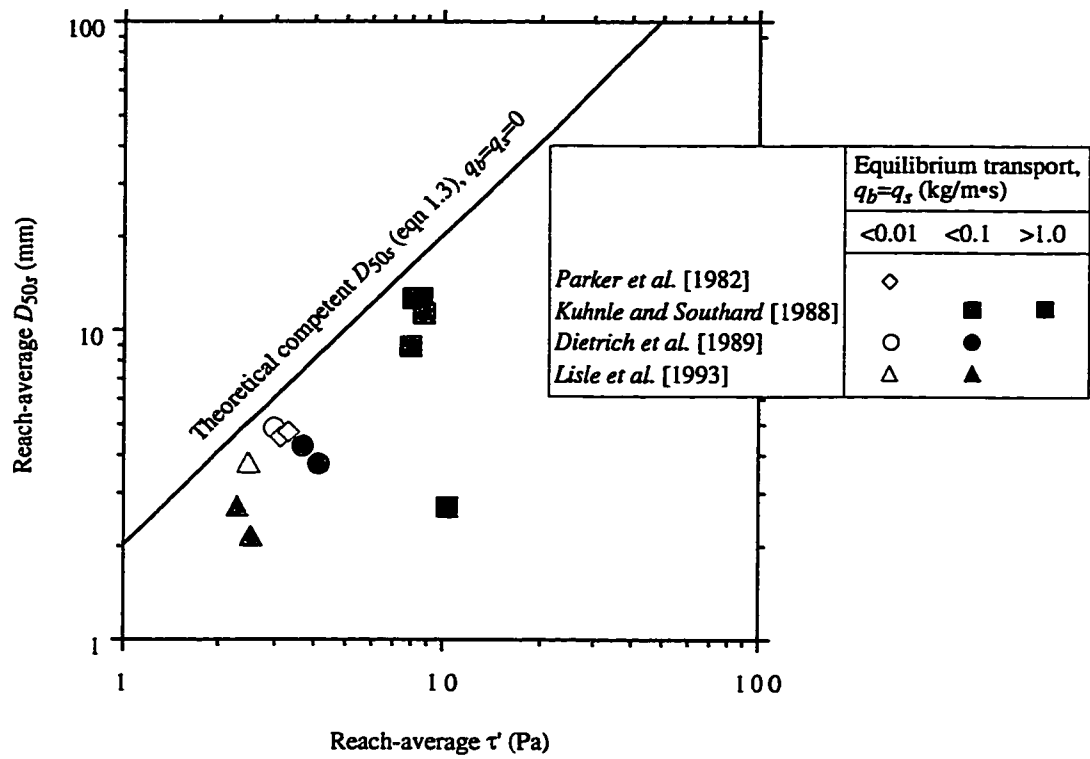


Figure 1.3: Reach-average median surface grain size versus bed shear stress, stratified by equilibrium transport rate ($q_b=q_s$) in laboratory channels. The heavy line is a theoretical prediction of the competent median grain size as a function bed stress (eqn 1.3, $\tau_c=\tau'$, see text).

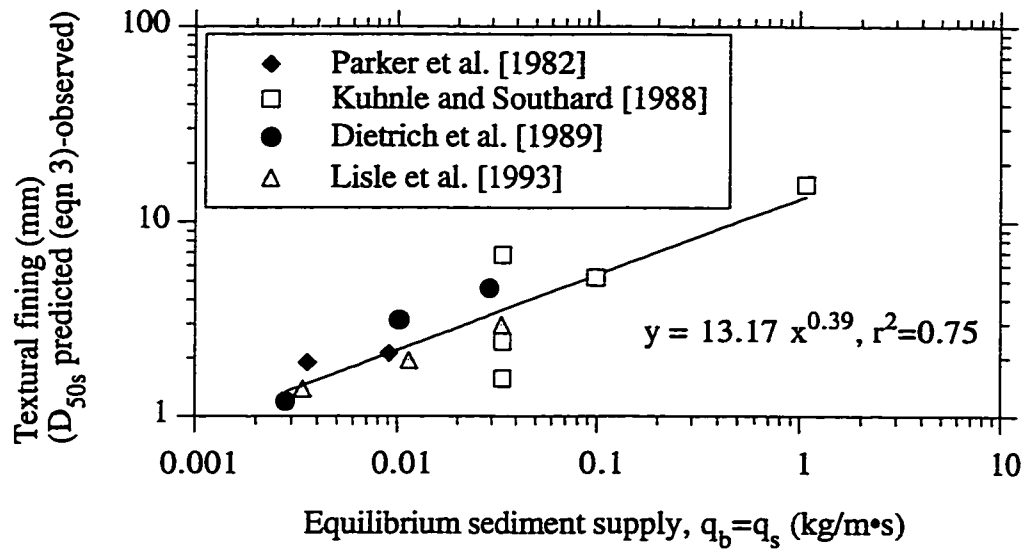


Figure 1.4: Reach-average textural fining (predicted D_{50s} (eqn 1.3)-observed D_{50s}) as a function of sediment supply during equilibrium transport ($q_b=q_s$) in laboratory channels (data of Fig. 1.3).

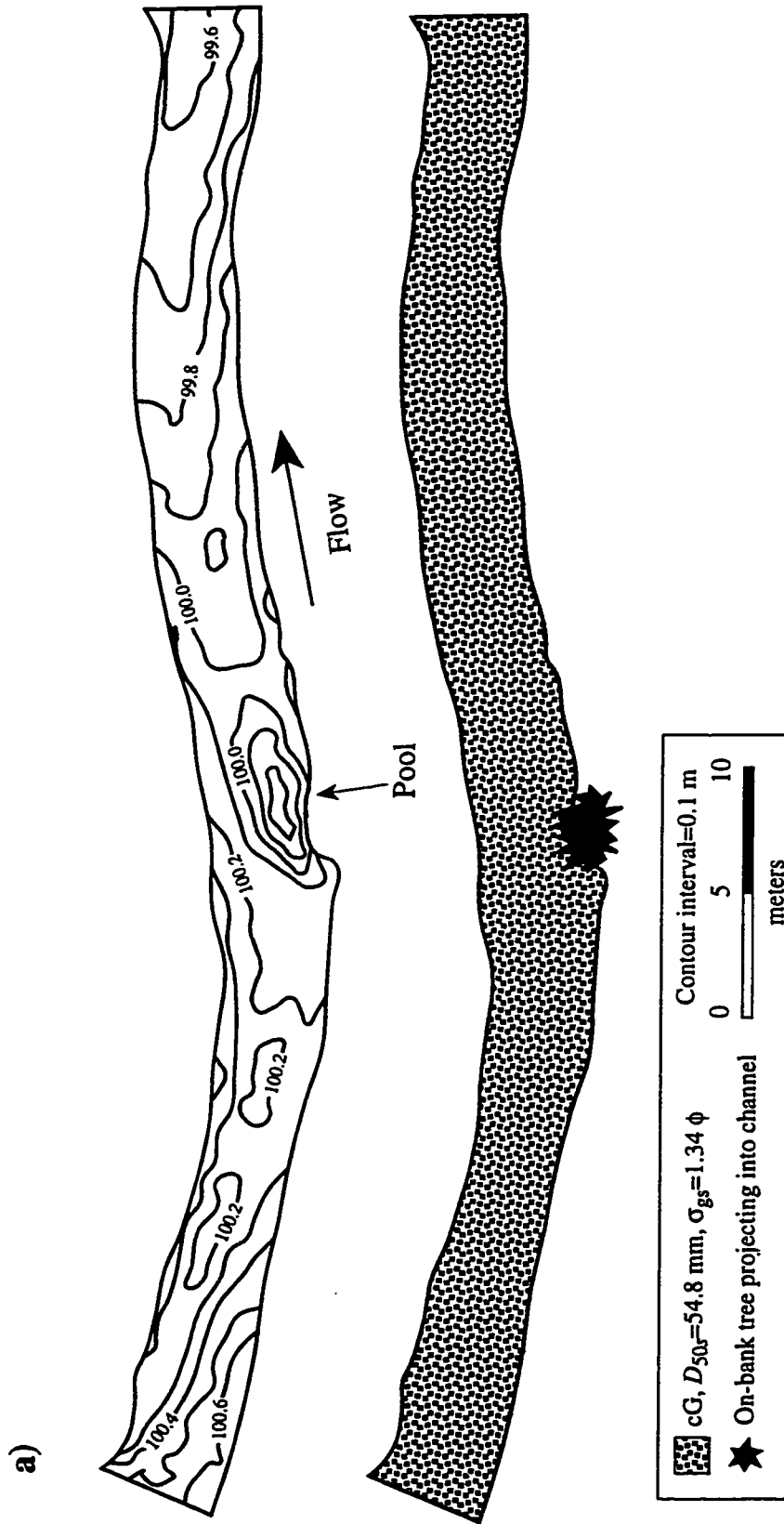


Figure 1.5: Typical topographic and textural maps of the three channel morphologies investigated: a) plane-bed (Hoko River 2), b) wood-poor pool-riffle (Hoko River 1), and c) wood-rich pool-riffle (Mill Creek). See Table 1.3 for texture definitions.

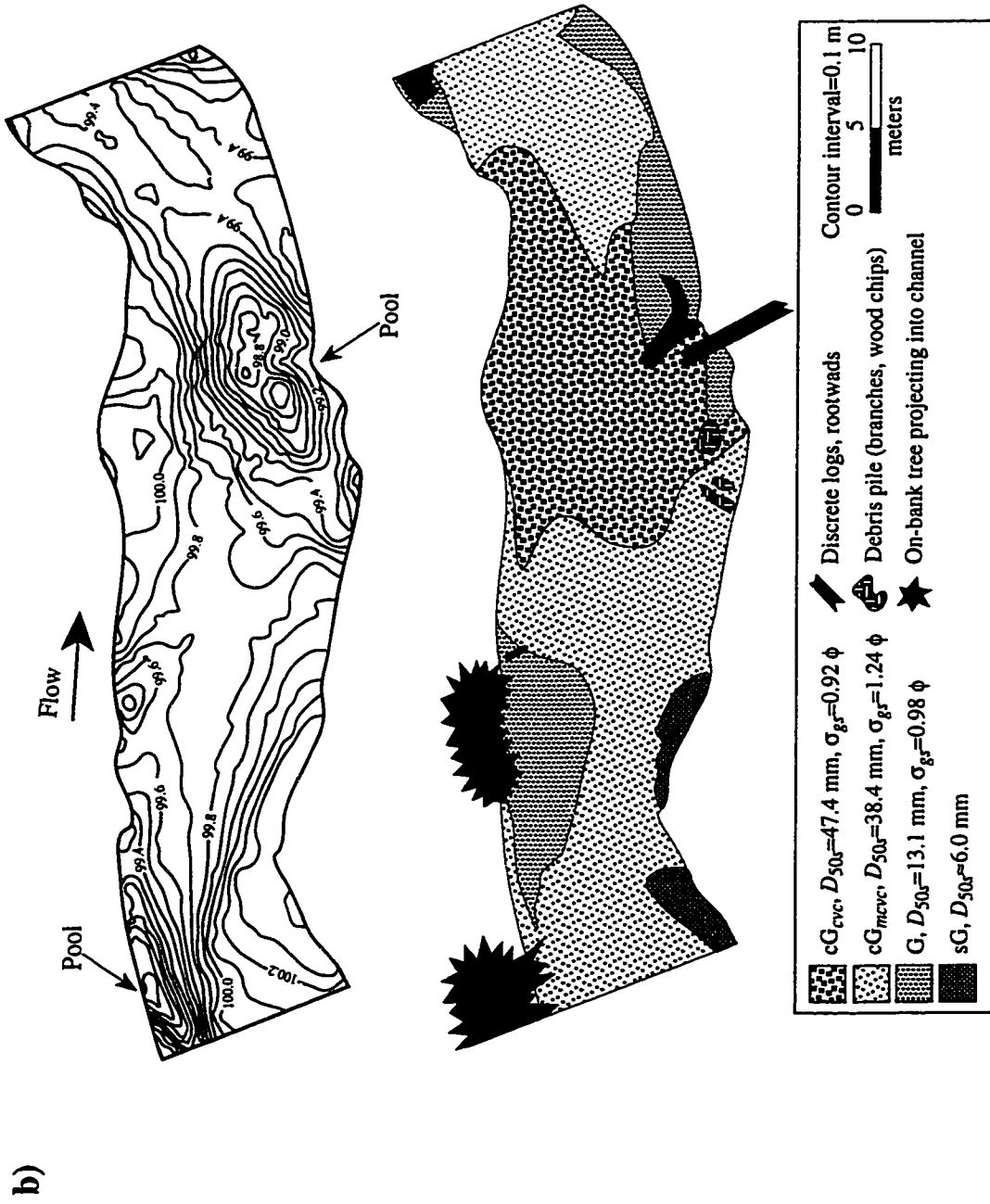


Figure 1.5 (continued)

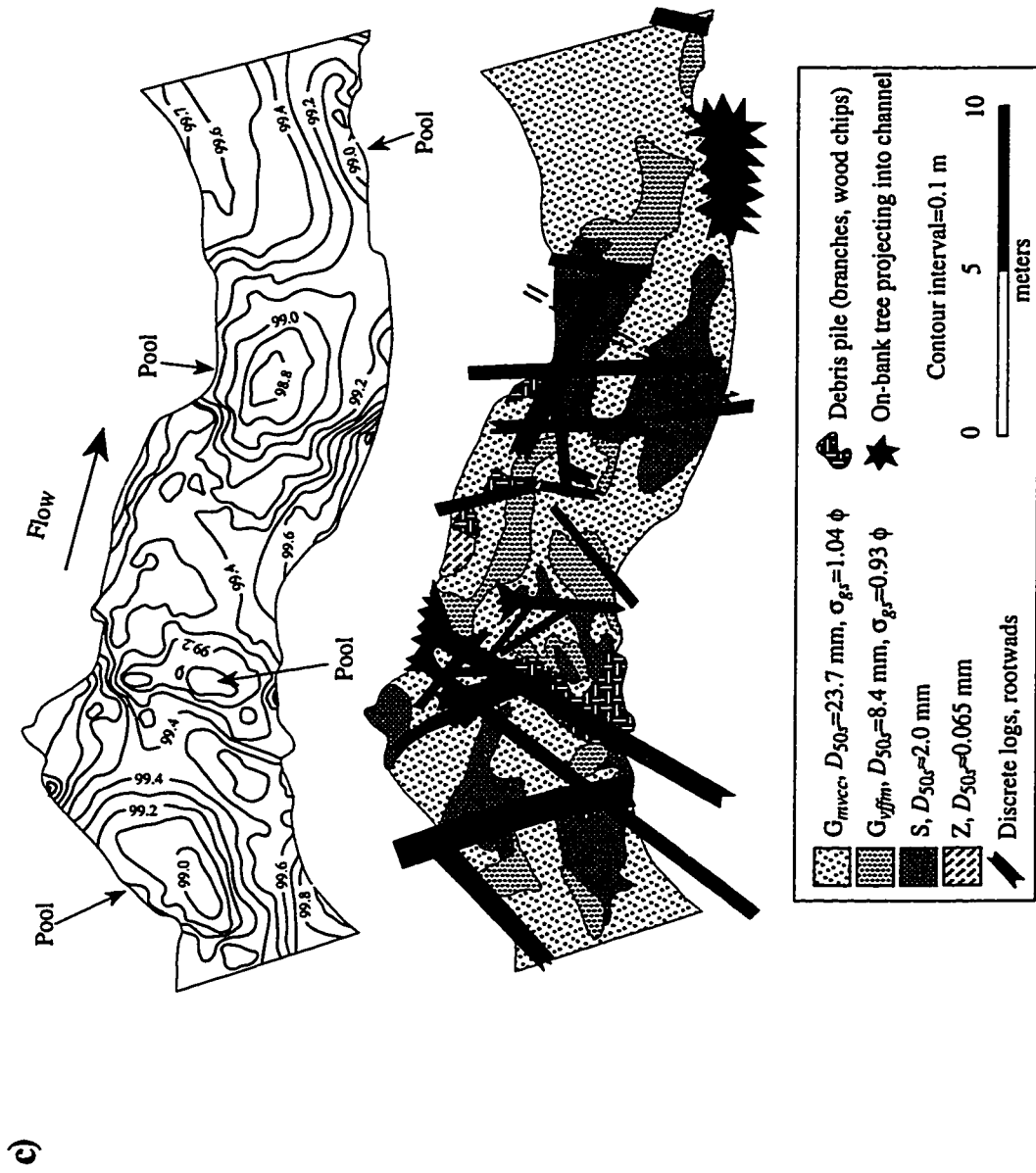


Figure 1.5 (continued)

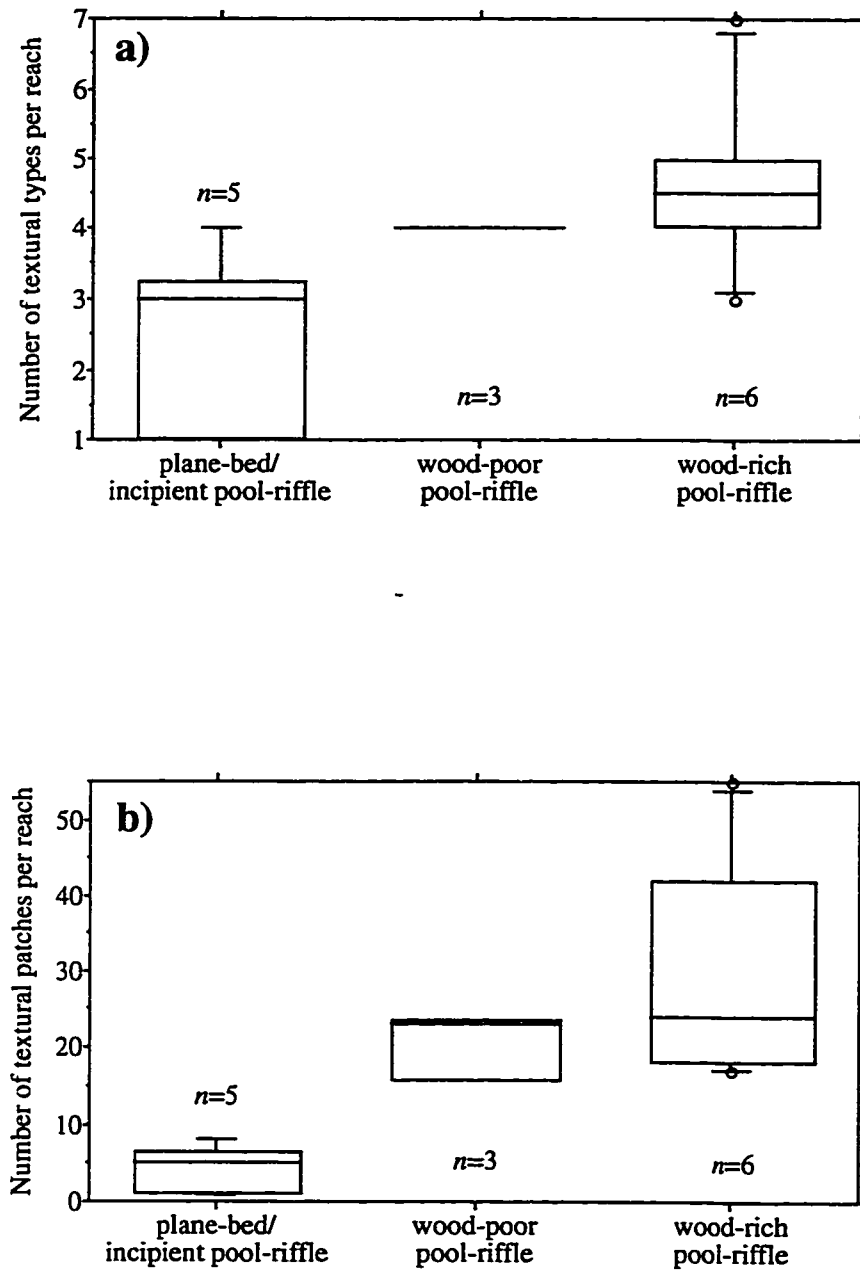


Figure 1.6: Box plots of the number of a) textural types (i.e., facies types) and b) textural patches per reach for the Olympic study sites. The line within each box is the median value of the distribution, box ends are the inner and outer quartiles, whiskers are the inner and outer tenths, and circles are the extrema. n is the number of observations per distribution.

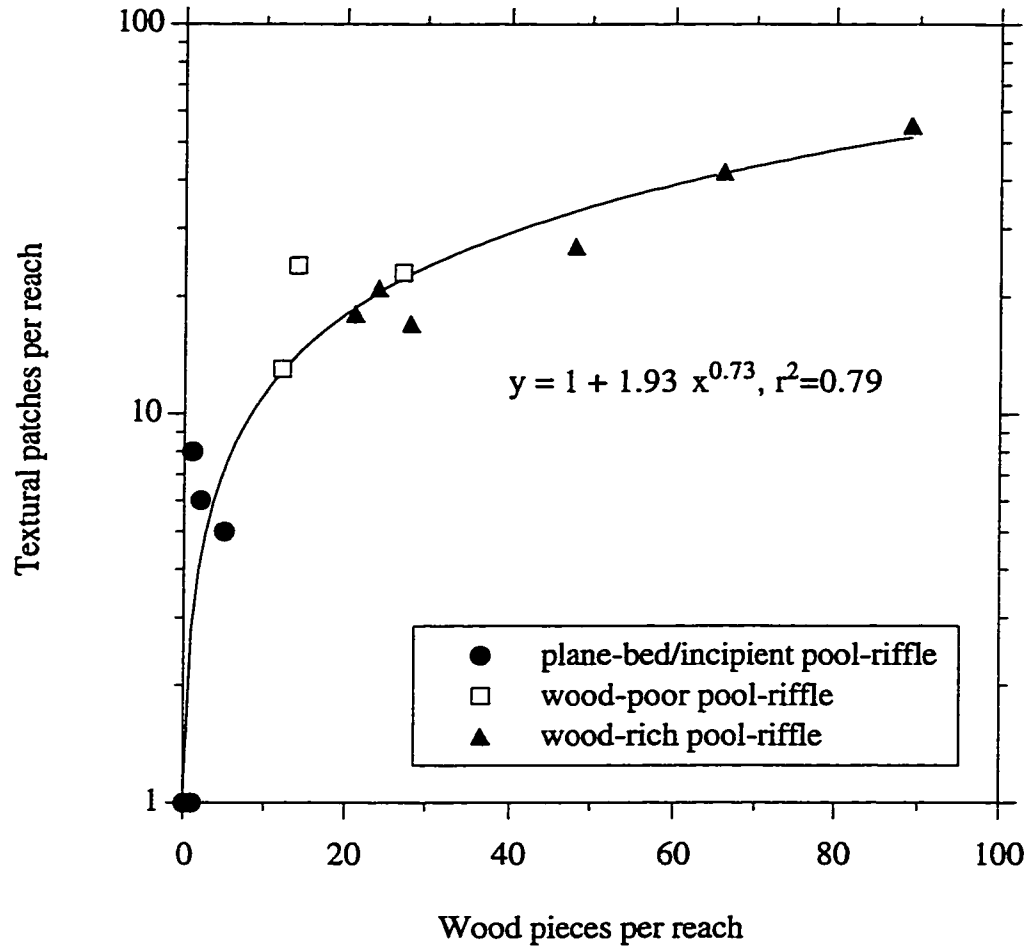


Figure 1.7: Textural patch frequency as a function of wood frequency at the Olympic study sites. The fitted curve is forced to one patch in plane-bed reaches with zero pieces of wood.

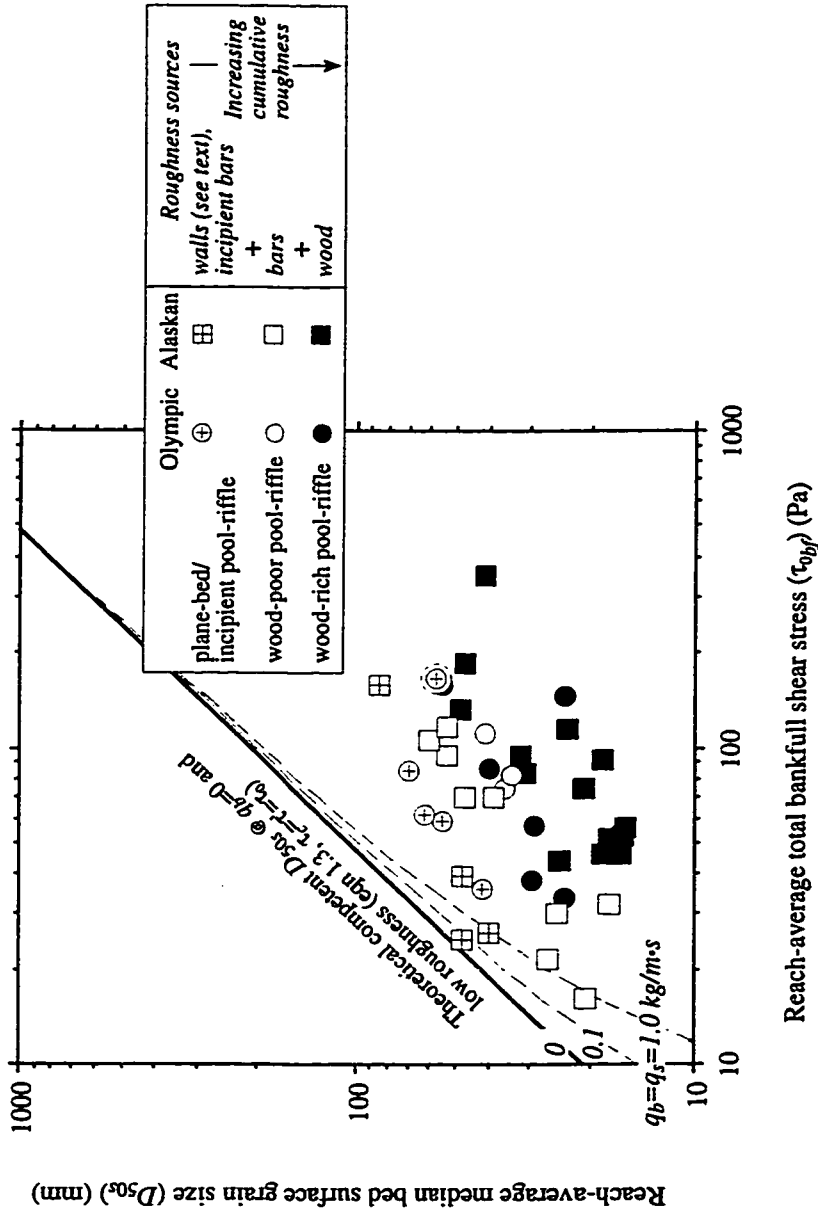


Figure 1.8: Reach-average bed surface grain size (D_{50s}) versus total bankfull boundary shear stress (τ_{0bf}), stratified by channel type. The channel types studied represent a general cumulative addition of wall, bar, and wood roughness, resulting in a progressive decrease in bed shear stress (eqn 1.2) and corresponding textural fining. The solid and dashed lines are predictions of the theoretical competent median grain size for low roughness (eqn 1.3, $\tau_c = \tau_0$) and bed load sediment supplies of 0, 0.1, and 1.0 kg/m·s, respectively (see text). Circled point is a plane-bed channel recently impacted by sediment input from a debris flow.

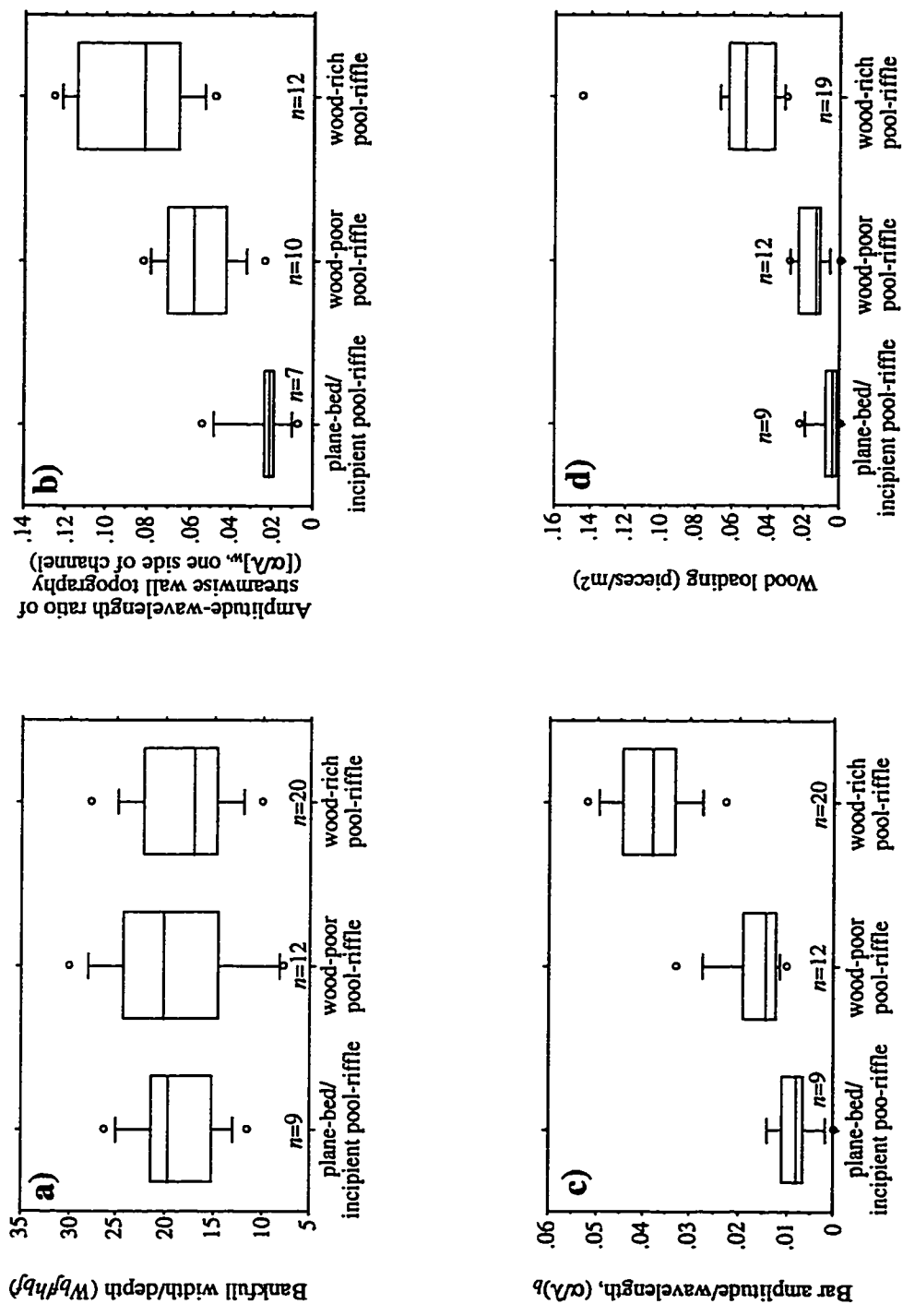


Figure 1.9: Box plots of reach-average a) width-to-depth ratio, b) amplitude-wavelength ratio of streamwise wall topography (one side of channel), c) amplitude-wavelength ratio of bar topography and d) wood loading. See Fig. 1.6 caption for box plot definition. Values used for these plots are listed in Table 1.1.

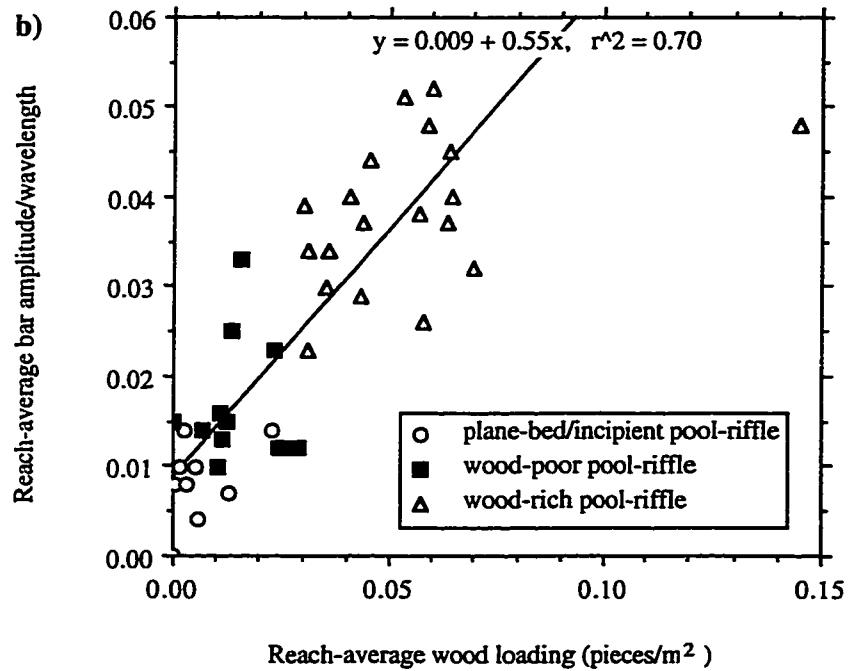
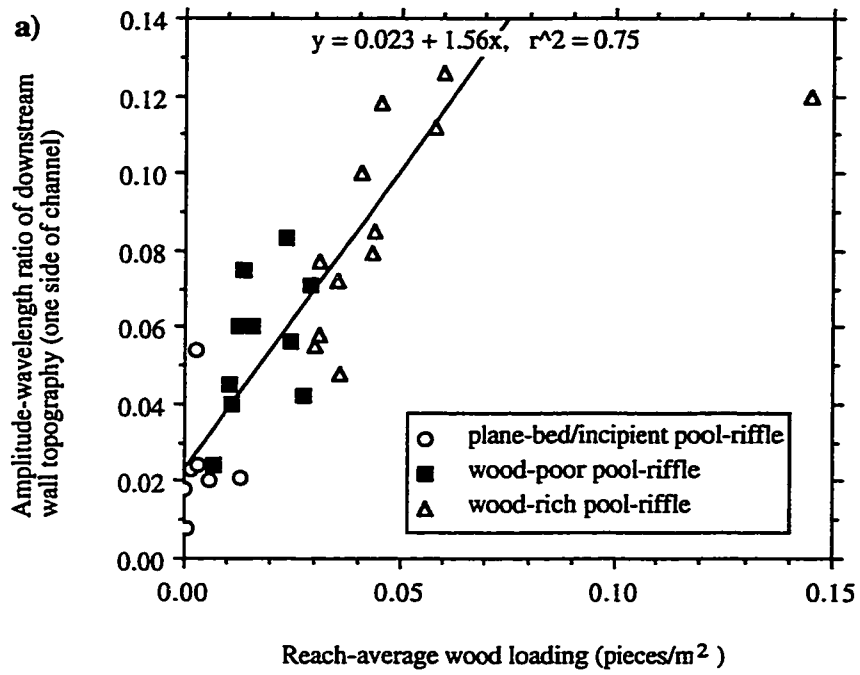


Figure 1.10: Amplitude-wavelength ratio of a) wall topography and b) bar topography as functions of wood loading. Mill Creek (far right point) is excluded from the curve fits.

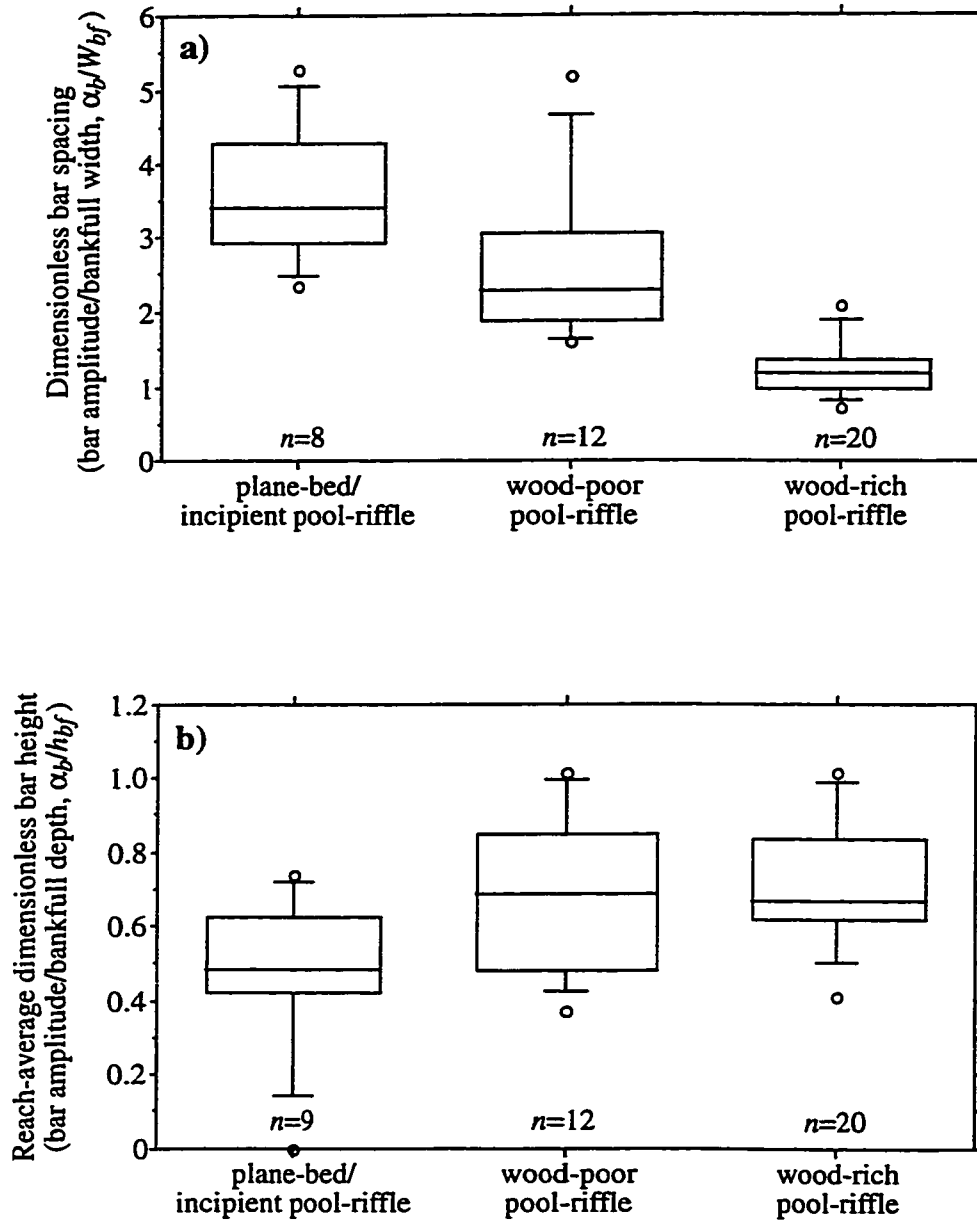


Figure 1.11: Box plots of reach-average, dimensionless bar wavelength and amplitude. See Fig. 1.6 caption for box plot definition.

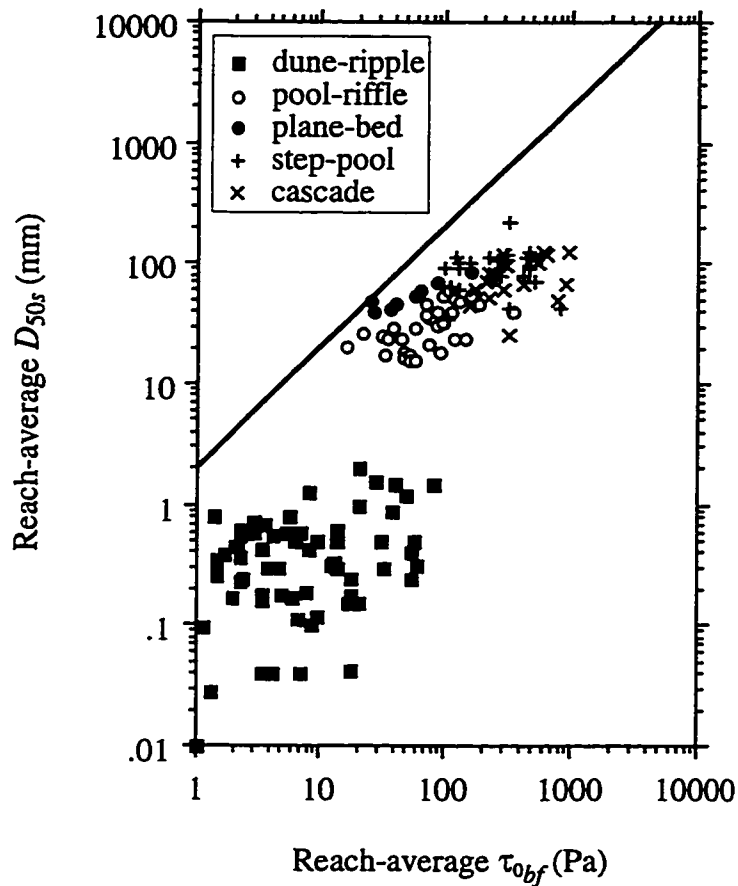


Figure 1.12: Median bed surface grain size versus total bankfull shear stress, stratified by reach morphology [sensu Montgomery and Buffington, 1997]. The solid line is the predicted competent D_{50s} (see Fig. 1.8 caption). Data sources are: dune-ripple [Simons and Albertson, 1963; Chitale, 1970; Williams, 1978; Higginson and Johnston, 1988]; plane-bed and pool-riffle [current study]; step-pool and cascade [D. R. Montgomery, unpublished].

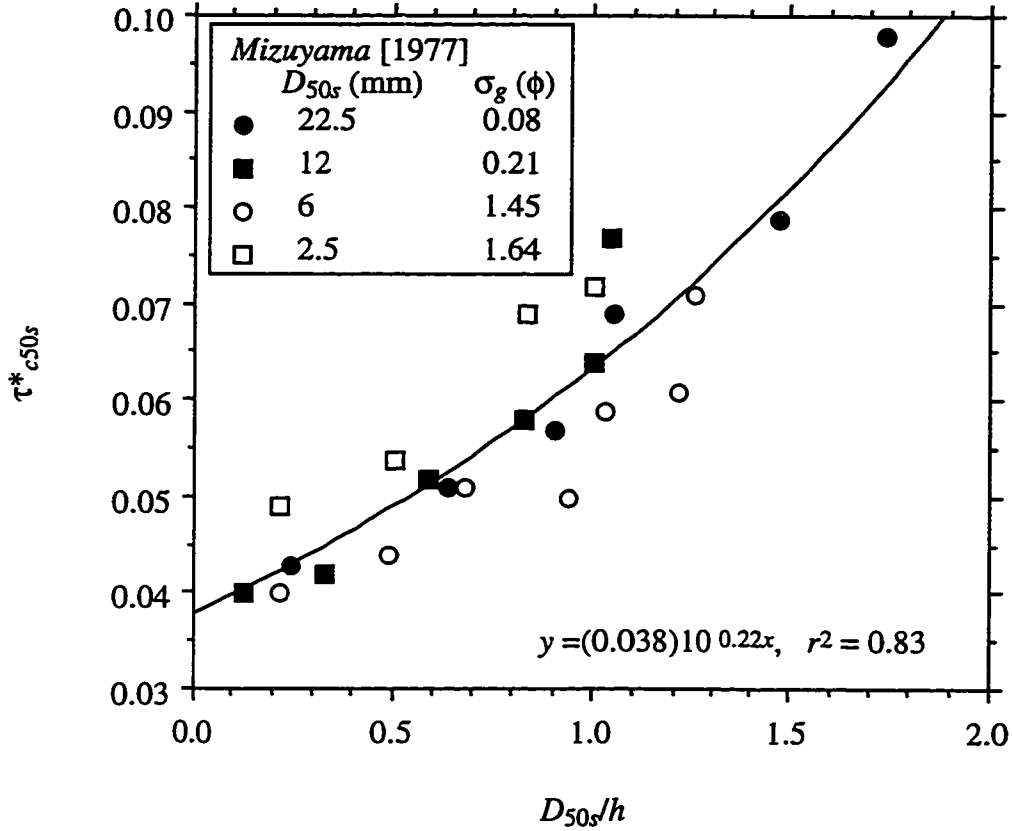


Figure 1.13: Apparent dimensionless critical shear stress as a function of relative roughness (D_{50s}/h). Here, we use a modified Shields equation [Bathurst et al., 1983] that accounts for downslope gravitational forces and intergranular friction angle ($\tau^*_{c50s} = \tau_{c50s} / [(\rho_s - \rho)gD_{50s}(\cos\theta \tan\Phi_{50} - \sin\theta)]$, where θ is the channel slope angle (0.6 - 11.3°) and Φ_{50} is the median friction angle for D_{50s}). For the 6 mm and 2.5 mm experiments, Φ_{50} is calculated from Buffington et al.'s [1992] equation 7, while for the nearly uniform 22.5 mm and 12 mm experiments we assume $\Phi_{50} \approx 45^\circ$ [Miller and Byrne, 1966]. τ_{c50s} is based on extrapolation to zero particle motion and is corrected for wall effects using the Einstein [1934; 1942] approach [Mizuyama, 1977]. The 22.5 mm and 12 mm values are median grain sizes of laboratory mixtures, which are approximately equal to D_{50s} due to the use of well-sorted mixtures.

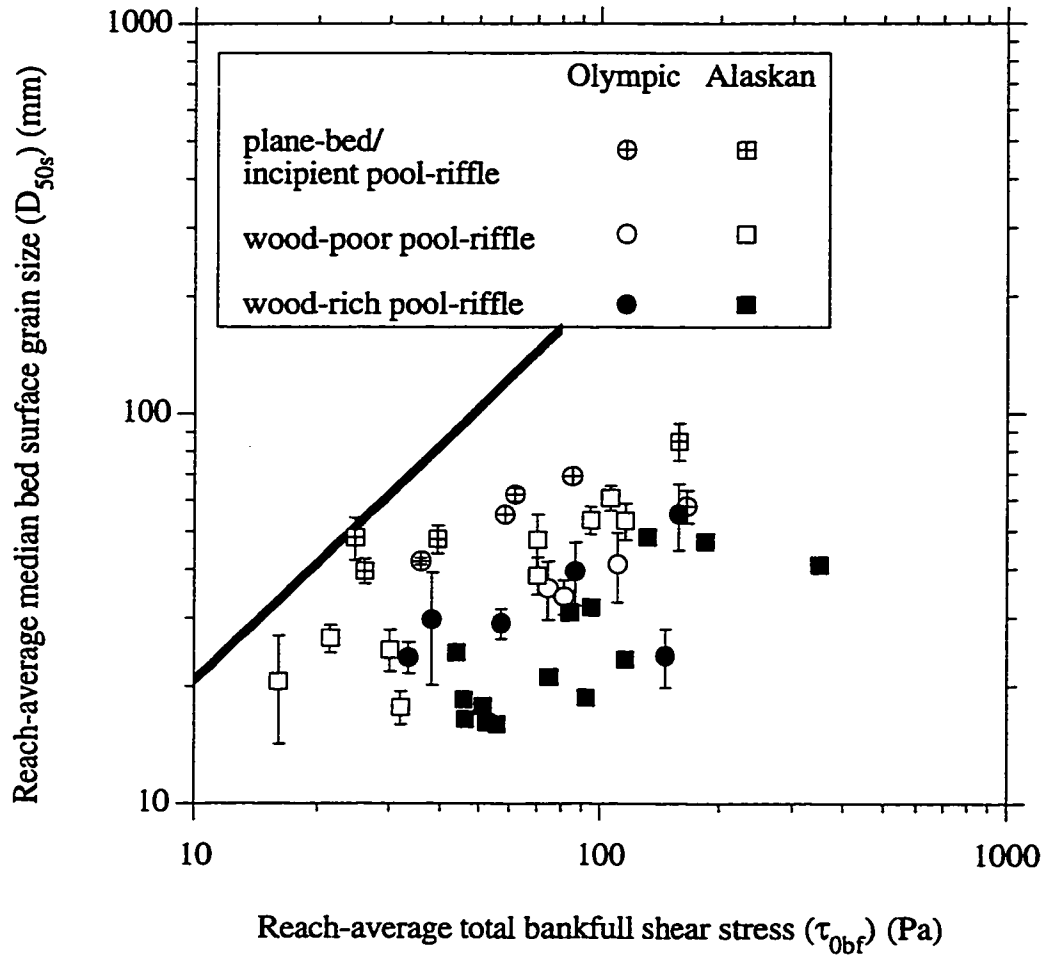


Figure 1.14: Figure 1.8 redrawn, showing standard errors of reach-average values of D_{50s} . Where error bars are not shown the error is smaller than the symbol size. Standard errors of D_{50s} are also listed in Table 1.1.

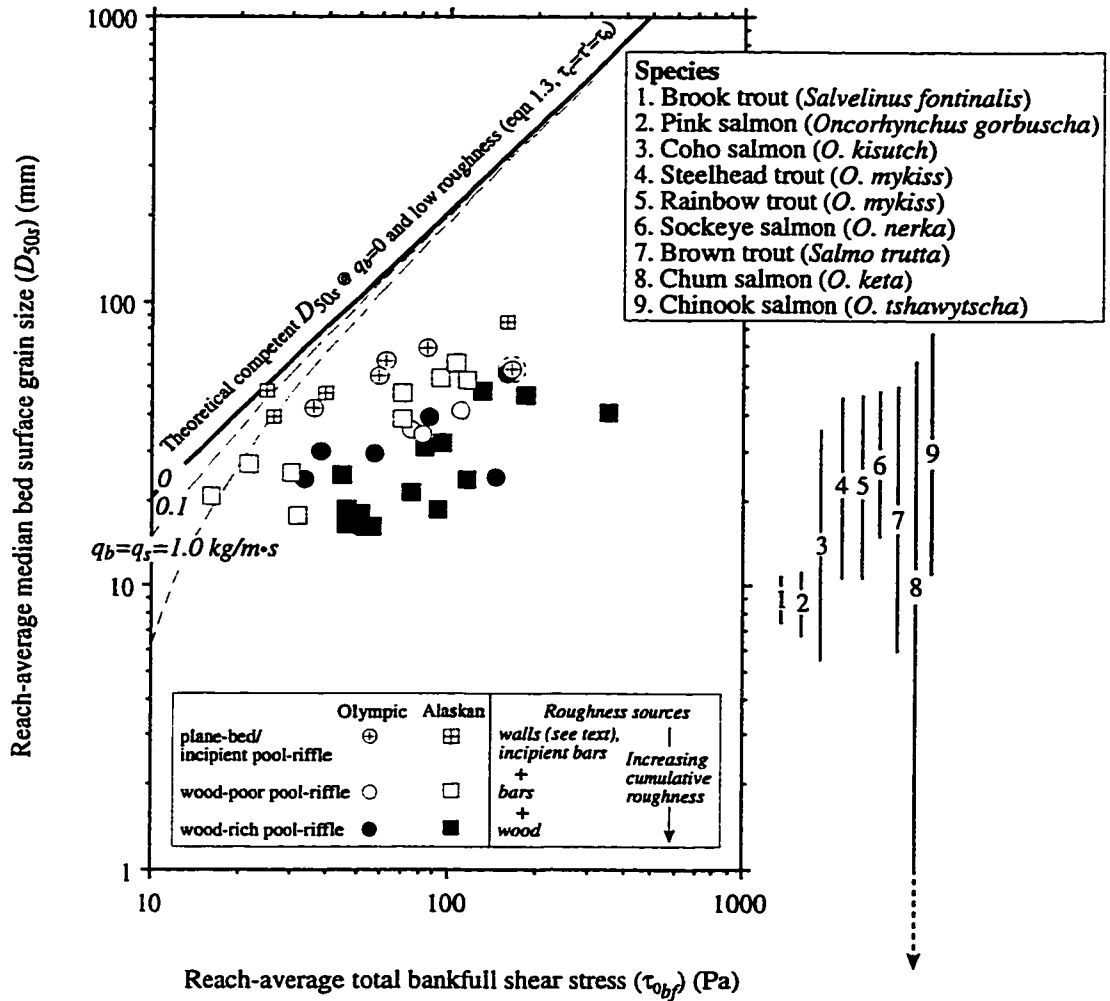


Figure 1.15: Comparison of median grain sizes preferred by spawning salmonids and those found in channels with wall, bar, and wood roughness. The spawning gravel median grain sizes are compiled from Kondolf and Wolman [1993] and are typically based on McNeil-type sampling [McNeil and Ahnell, 1960] that combines surface and subsurface material. Furthermore, these samples are typically underweight [sensu Church et al., 1987] and, in some cases, truncated at arbitrary upper grain sizes [Kondolf and Wolman, 1993]. Consequently, the reported ranges of median spawning gravels likely contain considerable error and may be biased toward small sizes due to coarse-tail truncation and combining surface and subsurface material (the latter is typically finer than surface sizes).

Chapter 2: A Procedure For Classifying And Mapping Textural Facies In Gravel-Bed Rivers²

Overview

Textural patches (i.e., grain size facies) are commonly observed in gravel-bed channels and are of significance for both physical and biological processes at subreach scales. We present a standard method for classifying and mapping textural patches. A field test of our classification indicates that it affords reasonable statistical discrimination of bed-surface textures. Facies maps provide a natural template for stratifying other physical and biological measurements and produce a retrievable and versatile data base that can be used as a component of channel monitoring efforts.

Introduction

Bed surfaces of natural and laboratory gravel channels are frequently organized into distinct textural patches (i.e., facies) that are distinguished from one another by differences in grain size and sorting (Fig. 2.1) [Iseya and Ikeda, 1987; Dietrich et al., 1989; Ferguson et al., 1989; Kinerson, 1990; Wolcott and Church, 1990; Lisle and Madej, 1992; Lisle et al., 1993; Paola and Seal, 1995; Powell and Ashworth, 1995; Kondolf, 1997; Buffington and Montgomery, in review (b)]. Textural patches likely result from size-selective deposition or entrainment caused by spatial variations in shear stress, sediment supply, and lateral bed slope [Dietrich and Smith, 1984; Parker and Andrews, 1985; Dietrich et al., 1993]. Grain interactions, such as kinematic waves [Langbein and Leopold, 1968], intergranular friction angles [Miller and Byrne, 1966; Buffington et al., 1992], relative grain protrusion [Kirchner et al., 1990], and grain wake effects [Iseya and Ikeda, 1987; Naden and Brayshaw, 1987; Whiting et al., 1988], also may play a role in textural patch development.

Patchy bed surfaces affect physical and biological processes within a stream reach. For example, textural patches affect bed load transport rates by creating patch-specific

² Co-authored paper by John M. Buffington and David R. Montgomery, in review with *Water Resources Research*.

mobility thresholds that give rise to spatially non synchronous sediment motion and the appearance of size-selective transport [Lisle and Madej, 1992; Paola and Seal, 1995]. Textural patches also influence bed load transport rates by providing spatially variable surface roughness [Dietrich et al., 1989]; fine patches with low surface roughness are expressways for coarse grains, while coarse patches with high surface roughness trap fine particles in downstream grain wakes [Iseya and Ikeda, 1987; Whiting et al., 1988] or in deep intergranular pockets [Buffington et al., 1992]. Differential roughness of textural patches also influences local boundary shear stress [Naot, 1984]. Patchy bed surfaces and spatial variability of physical environments have direct biological implications [Townsend, 1989], as many aquatic animals prefer specific substrate sizes [Cummins and Lauff, 1969; Reice, 1980; Kondolf and Wolman, 1993] and particular hydraulic regimes for different life stages [Sullivan, 1986].

In addition to their physical and biological significance, textural patches provide a natural template for stratifying sediment sample sites. In facies stratified sampling, grain size characteristics of each texture are quantified through random or systematic (i.e., grid/transect) sampling within patches (Fig. 2.2a-b), and then weighted by patch area to determine reach-average grain size statistics [Kinerson, 1990; Wolcott and Church, 1990; Lisle and Madej, 1992; Kondolf, 1997; Buffington and Montgomery, in review (b)]. Facies stratification also allows statistical comparison of between patch differences in grain-size distribution and physical environment [Krumbein, 1953; 1960]. However, stratified sampling is a two-step process that requires a method of classifying bed-surface facies. Many investigators choose a simpler approach of unstratified random sampling (Fig. 2.2c) or unstratified systematic sampling (Fig. 2.2d). The ability of unstratified sampling to measure the true underlying sediment distribution depends on the areal coverage and density of sample sites, as well as the spatial distribution of textural patches (i.e., their size and frequency) [Smartt and Grainger, 1974; Wolcott and Church, 1990]; too few observations and too large a sampling interval will produce a poor representation of the true underlying sediment population. For example, Bevenger and King [1995] recently proposed a pebble count procedure [Wolman, 1954] in which grains are selected from a transect that zig-zags bank-to-bank downstream through a channel reach to produce a reach-average grain-size distribution. While well intended, the proposed sampling coverage of this procedure would be insufficient to give the correct areal weighting of

textures and their grain sizes in channels with complex spatial arrangements of textural patches, such as those of Figure 1b [Kondolf, 1997].

Although the occurrence of textural patches is fairly common in gravel-bed channels and is of significance to both physical and biological processes, there is no standard procedure for identifying and classifying bed-surface facies; a variety of approaches exist that vary in subjectivity and universality. Fisheries biologists commonly differentiate bed-surface textures visually [Platts et al., 1983; Shirazi and Seim, 1981; Shirazi et al., 1981], but do not have a formal textural classification scheme and rarely conduct accompanying grain size measurements of the bed surface. Although visual differentiation is the primary means of classifying bed-surface textures, accompanying grain size measurements are required to verify visual classification and reduce subjectivity [Kondolf and Li, 1992]. In contrast to visual identification, Crowder and Diplas [1997] recently proposed a grid sampling technique that uses a moving window comparison of mean grain size to locate textural boundaries. While more rigorous, the success of their approach depends on grid spacing (i.e., density of sample sites) and may be unnecessarily laborious in channels that have distinct textural boundaries that can be located more simply by visual inspection. Other methods of classifying textural patches are frequently site- or study-specific [Lisle and Madej, 1992; Paola and Seal, 1995]. In this paper, we present a standard procedure for classifying and mapping textural patches that combines visual identification and quantitative grain size measurement.

Classifying and Mapping Textural Patches

It is standard practice in the Earth sciences to use ternary diagrams for classifying chemical composition of minerals [Deer et al., 1982], mineral composition of rocks [Dietrich and Skinner, 1979; Williams et al., 1982] and grain size composition of sediments [Folk, 1954; Ritter, 1967]. Continuing this tradition, we propose a two-level ternary classification for textural patches (Fig. 2.3) that uses standard grain size divisions and names (Table 2.1). Ternary diagrams classify objects according to the relative abundance of three primary components. Each of our ternaries are divided into fifteen categories: six equal area central fields that represent different, possible relative abundances of three primary grain sizes, and nine edge classes that represent end member conditions with one or two dominant grain sizes, effectively reducing the system to a binary or unary classification. In constructing the ternaries, we assumed equal probability

of occurrence of different grain size mixtures (i.e., no inherent mixture bias). Consequently, the central six fields within each ternary are equal area and tri-symmetrical.

Level I of the classification is used to classify the relative abundance of the three primary grain size classes of a texture (i.e., silt, sand, gravel, cobble, or boulder) (Fig. 2.3). For example, if a textural patch is predominantly composed of sand, gravel, and cobble the fourth ternary of Figure 2.3 is used to classify the texture based on the relative abundance of these three primary size classes. A texture with 15% gravel, 25% sand, and 60% cobble would be classified as gsC, a gravelly, sandy cobble facies; the order of the adjectives (lower case letters of the classification) denotes the relative abundance of each of the major subordinate size classes [Folk, 1954]. In practice, the dominant size class of a texture is identified (cobble in the above example), and then one of five subcategories for that dominant size class is chosen based on the relative abundance of the two major subordinate size classes. For example in the sand-gravel-cobble ternary, the five subcategories for a cobble texture are: C=cobble (>90% cobble), sC=sandy cobble (predominantly cobble, with >5% sand and <5% gravel), gsC=gravelly, sandy cobble (predominantly cobble, with gravel and sand each >5%, but more sand than gravel), sgC=sandy, gravelly cobble (same as previous, but with more gravel than sand), and gC=gravelly cobble (predominantly cobble, with >5% gravel and <5% sand).

Using similar ternary diagrams, Level II of the classification further delineates the grain size composition of the dominant size class (Fig. 2.3). The purpose of the second level of the classification is to distinguish visually distinct textures that have the same Level I name. For example, two gravel textures (G, >90% relative abundance, Level I) might be distinguished as G_{fm} and G_c (fine to medium gravel versus uniformly coarse gravel) using the second level of the classification. Level II delineates boulder, cobble, and gravel subsizes only; fine-scale divisions of sand and silt classes are not differentiated here because most surface-based sampling techniques (e.g., pebble counts [Wolman, 1954]) cannot realistically resolve those fine-scale divisions, nor are such divisions readily discernible by visual inspection.

The above classification scheme is applied as follows to identify and map textural patches within a study area:

- 1) Conduct a preliminary reconnaissance of the stream reach, visually identifying textural patches according to Figure 2.3.

- 2) Map surface textural patches according to the names given in step (1). Discrete patches of a given textural type may occur several times within a reach, as illustrated in Figure 2.1.
- 3) Determine grain-size distributions for several patches of each facies type (see discussion below) and compare them with the visually estimated grain size components of step (1). If there is a discrepancy, reclassify according to the measured grain-size distributions.
- 4) (Optional) Group visually similar, but technically dissimilar, textures as equivalent for practical purposes (Fig. 2.4).

In Step 3 above, grain size analysis of a given textural patch should encompass the entire surface area of the patch. The number of measurements per patch and the number of patches measured per facies type depends on the desired level of precision [Mosely and Tindale, 1985; Church et al., 1987; Rice and Church, 1996]. Choice of surface sampling technique (i.e., pebble count [Wolman, 1954], areal adhesion [Fripp and Diplas, 1993], photo-sieving [Ibbeken and Schleyer, 1986], etc.), as well as the strategy by which the technique is applied to a patch (i.e., random versus systematic sampling, Fig. 2.2a-b), may also influence sample precision and requisite size. Smartt and Grainger [1974] report that random sampling is more accurate, while Wolcott and Church [1990] demonstrate that systematic (i.e., grid/transect) sampling is superior. However, both investigations emphasize that the performance of each sampling strategy is influenced by the size and frequency of the objects being sampled and the areal coverage of the sampling effort (i.e., density of observations).

While there are a variety of surface sampling techniques to choose from, not all yield equivalent results [Leopold, 1970; Kellerhals and Bray, 1971; Potter, 1979; Church et al., 1987; Diplas and Sutherland, 1988]. Of the methods available, systematic (i.e., grid/transect) pebble counts [Wolman, 1954] are particularly attractive because they are easy to perform, relatively cheap (not much time and labor investment), and can be directly compared with subsurface samples sieved by weight [Kellerhals and Bray, 1971; Church et al., 1987; Diplas and Sutherland, 1988]. To minimize methodological differences between

pebble counts and sieved samples, a gravelometer (square grain size template [e.g., Hey and Thorne, 1983; Church et al., 1987]) should be used when conducting pebble counts.

Some bed surfaces exhibit continuous spatial gradients of grain size and sorting that make it difficult to identify discrete textural boundaries. Consequently, it may be necessary, in some cases, to classify and map bed surfaces as gradational from one textural composition to another. Regardless of whether bed surfaces are composed of punctuated (i.e., discrete) facies or gradational textures, our procedure for classifying and mapping bed surfaces will reduce subjectivity and observer bias.

Field Test

Demonstration of textural similarity within classification categories, as well as textural difference between categories, is required for acceptance of facies classification as a reliable means of quantifying textural variation within and between channel reaches. Our proposed textural classification distinguishes bed-surface facies based on differences in both grain size and sorting. Consequently, we test our classification by comparing grain-size distribution means and variances within and between textural categories. In particular, we test for within-group similarity of both grain size mean and variance, and between-group difference of one of these quantities. Because our classification distinguishes textures based on differences in either grain size or sorting, a difference of one of those quantities will suffice to demonstrate between-texture difference. For example, textures are distinguishable if they have different variances despite similar means (Fig. 2.5a), or vice versa (Fig. 2.5b). We choose to examine mean grain size (rather than some percentile of the grain-size distribution) because of the availability of statistical tests for sample means, and because the mean grain size is often similar to the median size (a commonly reported index value used in numerous sediment transport and hydrologic formulæ).

We also test whether more detailed classification schemes improve one's ability to discriminate statistically different textures. Specifically, we explore the potential compromise between classification simplicity and accuracy. To address this issue, we compare the statistical accuracy of our proposed classification to that of a simplified version (less categories per ternary), as well as to that of a complicated one (more categories per ternary). We further investigate the issue of simplicity versus accuracy by examining whether a Level I+II classification significantly improves one's ability to discriminate statistically different textures compared to that of a Level I classification alone.

We examined the above questions using 86 bed-surface textures sampled in 17 gravel-bed rivers in northwestern Washington and southeastern Alaska; the study sites are located in forested mountain drainage basins and are further described by Buffington and Montgomery [in review (b)]. Surface grain-size distributions of each texture were determined from patch-spanning, random pebble counts that sampled 100+ grains [Wolman, 1954]. All of the sampled textures plot in the sand-gravel-cobble ternary, with gravel being the most common size class (Fig. 2.6). Mean and median grain sizes of the sampled textures have flat-lying (platykurtic) distributions, predominantly composed of fine to very coarse gravel (Fig. 2.7). In contrast, the distribution of grain size standard deviations is peaked (leptokurtic), with most patches composed of moderately well sorted to poorly sorted sediment (Fig. 2.7). For this analysis, we are interested in the relative accuracy of different classification schemes, and assume that the pebble counts, themselves, are sufficiently accurate.

The sampled bed-surface textures were grouped with nine classification schemes: three Level I classifications, with ternaries divided into 15, 27, and 39 categories, respectively, (Fig. 2.3 and 2.8), three corresponding Level I+II classifications, and three Level I+II classifications using the above Level I ternaries combined with a unary Level II classification (i.e., one that describes only the primary component of the dominant size class; e.g., G_{fmc} and G_{cvc} textures would be classified as G_c and G_{vc} in a unary Level I+II scheme). The twenty seven-category and thirty nine-category ternaries (Fig. 2.8) represent successive halving of the central six fields of the basic fifteen-category ternary (Fig. 2.3). We use a short hand representation for each of these classifications by indicating in parentheses the number of textural categories per ternary (e.g. I (15) + II (1) is a fifteen-category Level I classification combined with a unary Level II classification).

Sample means were compared within and between classification categories using two-tailed, t-tests, assuming unequal and unknown variance

$$t_0 = \frac{\bar{x}_1 - \bar{x}_2}{\sqrt{\frac{s_1^2}{n_1} + \frac{s_2^2}{n_2}}} \quad (2.1)$$

where t_0 is Student's [1908] test statistic, \bar{x} is sample mean, s^2 is sample variance, and n is sample size. Sample variances were compared within and between categories using two-tailed F-tests

$$f_0 = \frac{s_1^2}{s_2^2} \quad (2.2)$$

where f_0 is Fisher's [1928] test statistic. For each of the nine candidate classifications, we conducted 3655 t-tests and F-tests, comparing each sample to all of the others. Results are summarized in Table 2.2, with the first two columns presenting results for sample means alone, and the second two columns presenting results for sample means and variances together. Our analysis demonstrates that Level I classifications do not perform as well as Level I+II classifications in terms of grouping statistically similar textures. For a Level I classification of our data, only 23-25% of within-group sample means are similar, and only 14-15% of both sample means and variances are similar. However, within-group similarity doubles when Level I classifications are embellished with a unary Level II classification, and nearly triples when a full, fifteen to thirty nine-category, Level I+II classification is used (Table 2.2). Although statistical similarity of within-group textures increases from Level I to Level I+II, there is little difference amongst the fifteen through thirty nine-category classification schemes. For example, there is only a 6% difference in the within-group similarity of means between the fifteen-category and thirty nine-category Level I+II classifications (71% vs. 77%, Table 2.2). Our analysis also demonstrates that the classification schemes examined here discriminate mean grain size of textures better than mean and variance together. For example, 59% of within-group means are statistically similar for a fifteen-category Level I+II classification of our data, while only 41% of both within-group means and variances are similar (Table 2.2). In contrast to the within-group comparisons, between-group comparisons show a slight decrease in accuracy from Level I to Level I+II, but are relatively insensitive to the type of textural classification used (Table 2.2).

We compared the combined t-test and F-test results of each classification (last two columns of Table 2.2) to one another to assess which classification schemes provide statistically significant improvements over the others. The t-tests and F-tests describe binomial distributions of significant versus non-significant observations, allowing comparison of the reported percentiles (Table 2.2) via one-tailed z-tests

$$z_0 = \frac{\hat{p}_1 - \hat{p}_2}{\sqrt{p(1-p)\left(\frac{1}{n_1} + \frac{1}{n_2}\right)}} \quad (2.3)$$

where z_0 is the test statistic, \hat{p} is the proportion of interest, and p is the pooled proportion defined as $(x_1+x_2)/(n_1+n_2)$ where x is the number of observations out of n that define \hat{p} . Results of these comparisons are presented in Table 2.3, with $P \leq 0.05$ representing a significant change in percent accuracy of classification. The first nine entries of Table 2.3 assess the significance of increasing the number of textural categories per ternary (i.e., 15, 27, 39) for a given type of classification (i.e., I, I+II(1), I+II), and demonstrate that, for our data, there is no statistical difference between the fifteen-category, twenty seven-category, and thirty nine-category classifications. The last six entries of Table 2.3 assess the significance of increasing the number of Levels used per classification (i.e., I vs. I+II for a given number of textural categories per ternary). These data demonstrate that within-group similarity is significantly improved by greater classification detail, while between-group difference is either unchanged (Table 2.3, tenth through twelfth entries) or significantly degraded (Table 2.3, last three entries; see also Table 2.2).

Our analysis shows that Level I classification is a poor discriminator of statistically significant differences in mean grain size and variance of bed-surface textures. However, discriminatory power is significantly improved with a Level I+II classification. Of the Level I+II classifications examined, the fifteen through thirty nine-category classifications are more accurate than the unary one (Table 2.2). But, there is no statistical difference in classification accuracy amongst the fifteen through thirty nine-category schemes (Table 2.2). Consequently, the simpler, fifteen-category, Level I+II classification (as proposed) is recommended. We emphasize, however, that the results of this analysis are specific to our particular data set, the generality of which remains to be tested.

Our analysis shows that Level I classification is a poor discriminator of statistically significant differences in mean grain size and variance of bed-surface textures. However, discriminatory power is significantly improved with a Level I+II classification. Of the Level I+II classifications examined, the fifteen through thirty nine-category classifications are more accurate than the unary one (Table 2.2). But, there is no statistical difference in classification accuracy amongst the fifteen through thirty nine-category schemes (Table 2.2). Consequently, the simpler, fifteen-category, Level I+II classification (as proposed)

is recommended. It is emphasized, however, that the results of this analysis are specific to this particular data set, the generality of which remains to be tested.

Discussion and Conclusion

Textural patches represent spatial differences in physical environments within a stream reach and provide a natural, easily discernible, stratification for sampling both physical and biological conditions. For example, surface and subsurface median grain sizes of textural patches (D_{50s} and D_{50ss} , respectively) are roughly correlated with one another in forest channels of western Washington (Fig. 2.9); coarser surface textures have correspondingly coarser subsurfaces (see figure caption for methodology). Consequently, classification and mapping of surface facies produces a useful template for locating and stratifying subsurface sample sites. Between patch differences in grain size, sorting, shear stress, and sediment supply also create a practical template for stratifying biological measurements, such as species preference for spawning, feeding, and resting sites. For example, the 24 mm patches of Fig. 2.1b should appeal most to spawning steelhead or chum salmon, while the 8 mm patches should appeal most to spawning brook trout [Kondolf and Wolman, 1993]. However, facies-stratification is only one of many ways to stratify sample sites within a stream reach. Depending on the study goals and the hypotheses to be tested, it may be more desirable to stratify physical and biological measurements by factors such as flow depth, velocity, or channel unit morphology (i.e., types of pools, bars, riffles, and steps [Church, 1992; Wood-Smith and Buffington, 1996]).

Classification and mapping of textural patches provides an important and versatile data base, in itself, regardless of whether such maps are used to structure further facies-stratified sampling. Textural mapping yields an easily understood visual record of channel conditions (particularly when combined with topographic and morphologic maps (Fig. 2.1)) from which a variety of data can be derived, such as subreach spawning habitat availability (a function of grain size and sorting [Kondolf and Wolman, 1993]), patterns of sediment transport and dispersal [Dietrich and Smith, 1984], and textural response to sediment supply [Dietrich et al., 1993] and hydraulic roughness (i.e., bars, wood, etc.) [Buffington and Montgomery, in review (b)]. Combined textural, topographic, and morphologic mapping produces a retrievable data base that allows one to associate channel

processes and morphologic response, and is a defensible means of monitoring channel characteristics.

Our classification provides a standard method for identifying textural patches and conducting facies-stratified sediment sampling. While this method of sampling can be quite time consuming and laborious in channels with complex textural distributions (Fig. 2.1b), it produces an accurate areal weighting of grain sizes. Unstratified sampling strategies (Fig. 2.2c-d) are less time consuming and less costly alternatives for sampling sediments within a stream reach, but are abstractions of the underlying, natural facies and may yield inaccurate results if there is insufficient areal coverage and density of sample sites. Furthermore, the underlying facies stratification and all of its uses, as discussed above, are, in some cases, unretrievable from unstratified sampling. Consequently, important channel characteristics and process-insights may be hidden by economical, but abstract, unstratified sampling strategies. For example, textural mapping conducted in forest channels of western Washington demonstrates that the frequency and diversity of textural patches (and therefore potential diversity of aquatic habitat) is well correlated with the frequency of in-channel wood and its consequent form drag and forced shear stress divergence [Buffington and Montgomery, in review (b)]. This insight would not be evident without textural mapping and facies-stratified sampling.

The results of our field test indicate that statistically meaningful textural classification requires a Level I+II analysis (Tables 2.2-3); statistical differences in mean grain size and variance of bed-surface textures are poorly represented by a Level I classification alone. This result is not surprising given that the Level I size classes (silt, sand, gravel, cobble, and boulder) each include a broad range of possible grain sizes and sortings (0.2 to 0.5 logarithmic orders of magnitude each, Table 2.1), and are, therefore, best used for large-scale, regional quantification of bed-surface texture. However, mechanistic studies of subreach-scale physical and biological processes require quantification of patch-scale variations of bed-surface texture, and therefore use of a Level I+II—type classification. While a Level I+II classification is more laborious than a Level I classification, our analysis demonstrates that there is no statistical difference amongst the fifteen-category, twenty seven-category, or thirty nine-category textural classifications (Table 2.3, first nine entries). Consequently, the simpler, fifteen-category ternaries (as proposed) can be used without significant loss of classification accuracy.

Although the unary Level I+II classification also is an improvement over the Level I classification (Table 2.3), and is simpler to perform than the proposed, fifteen-category, Level I+II scheme, the unary classification is less accurate than the fifteen-category Level I+II classification (Table 2.2) and may mask subtleties of textural variation that can have important physical and biological implications. For example, two textural patches classified as medium gravel in a unary Level I+II scheme may have very different fine and coarse gravel contents, the distinction and quantification of which may be of prime interest to fisheries biologists charged with assessing spawning gravel quality. The fifteen-category, Level I+II classification provides more detail about the relative abundance of component size classes in gravel textures than is available from Level I and unary Level I+II—type classifications currently used by fisheries biologists [e.g., Shirazi and Seim, 1981; Platts et al., 1983]. Consequently, it may offer better quantification of the physical differences driving habitat quality and use of the channel by aquatic animals.

Although our data set samples 86 bed-surface textures from seventeen rivers, the sampled textures are dominantly different subcategories of gravel (Fig. 2.6). Furthermore, the samples tend to plot along the edges of the sand-gravel-cobble ternary, indicating that our textures are dominated by one to two major grain sizes, rather than three; only one texture plots in the central portion of the ternary. The data also demonstrate that when there are two dominant size classes, they tend to be closely related (i.e., sand and gravel, or gravel and cobble, but not sand and cobble), suggesting a hydrologic control on the grain size composition of patches. A similar hydrologic control on grain size is commonly observed at reach scales; there is a general downstream sequence of boulder-bed, cobble-bed, gravel-bed, and sand-bed morphologies that covaries with the downstream decline of channel slope and shear stress [e.g., Montgomery and Buffington, 1997]. If our data are generally representative, then most bed-surface textures may plot along the edges of the Level I grain size ternaries, making the number of commonly observed textural types less than the full suite of possible textures proposed in our classification. Despite the tendency for our data to congregate along the edges of the grain size ternary, our analysis indicates that further subdivision of the classification ternary is not warranted; the basic, fifteen-category, Level I+II classification discriminates significant differences in mean grain size and variance reasonably well. Furthermore, if generally representative, the concentration of the data along the ternary edges makes it clear that Level I classification, alone, does not offer much discrimination of statistically different bed-surface textures (Fig. 2.6).

We have not conducted an exhaustive test of textural classifications, nor do we attempt to present the optimal scheme for mapping bed-surface facies. Rather, our approach is a minimalistic one that uses as few textural categories as possible without compromising statistical accuracy of the classification, thereby producing an economical classification procedure. However, there are numerous ways to classify bed-surface facies, and other approaches or variants of our procedure may be useful depending on the specific study goals.

Table 2.1: Standard grain-size divisions and names*

Size		Name	
(ϕ) [†]	(mm)		
-12	4096	Very coarse	BOULDER
-11	2048		
-10	1024		
-9	512		
-8	256	Coarse	COBBLE
-7.5	181		
-7.0	128		
-6.5	90.5		
-6.0	64.0	Medium	GRAVEL
-5.5	45.3		
-5.0	32.0		
-4.5	22.6		
-4.0	16.0	Fine	
-3.5	11.3		
-3.0	8.00		
-2.5	5.66		
-2.0	4.00	Very fine	
-1.5	2.83		
-1.0	2.00		
$\frac{1}{2}$	$\frac{1}{2}$		
4.0	0.0625		
$\frac{1}{2}$	$\frac{1}{2}$	SILT	
8.0	0.0039		
		CLAY	

* Udden [1898; 1914]-Wentworth [1922] grain size scale adapted from Church *et al.* [1987]

† ϕ is the standard \log_2 unit of grain size measurement [Krumbein, 1936]. $\phi = -\log_2 D$, where D is grain size in mm.

Table 2.2: Statistical accuracy of textural classification

Classification type	Mean Grain Size*		Mean Grain Size and Variance†	
	Percent of within-group comparisons that are statistically similar	Percent of between-group comparisons that are statistically different	Percent of within-group comparisons that are statistically similar	Percent of between-group comparisons that are statistically different
Level I (15 categories)	25	91	15	98
Level I (27)	24	89	14	98
Level I (39)	23	89	14	98
Level I (15) + II (1)	53	91	29	98
Level I (27) + II (1)	52	90	28	98
Level I (39) + II (1)	52	90	30	98
Level I (15) + II (15)	71	88	41	97
Level I (27) + II (27)	76	88	44	96
Level I (39) + II (39)	77	88	47	96

* Texture mean grain sizes compared via two-tailed t-test, assuming unequal and unknown variance, and 0.05 significance.

† Texture mean grain sizes compared as per note *. Texture variances compared via two-tailed F-test, with 0.05 significance. Here, within-group similarity requires acceptance of both the t-test null hypothesis (equal means) and the F-test null hypothesis (equal variances), while between-group difference requires rejection of either null hypothesis.

Table 2.3: Statistical significance of greater classification detail

Classification comparison	<i>P-value*</i>	
	Within-groups	Between-groups
<i>More divisions per ternary</i>		
I (15) vs. I (27)	0.235	0.420
I (15) vs. I (39)	0.451	0.315
I (27) vs. I (39)	0.280	0.246
I (15) +II (1) vs. I (27) + II (1)	0.434	0.170
I (15) +II (1) vs. I (39) + II (1)	0.387	0.229
I (27) +II (1) vs. I (39) + II (1)	0.329	0.415
I (15) +II (15) vs. I (27) + II (27)	0.297	0.309
I (15) +II (15) vs. I (39) + II (39)	0.141	0.202
I (27) +II (27) vs. I (39) + II (39)	0.299	0.462
<i>More Levels per classification</i>		
I (15) vs. I (15) + II (1)	0.000	0.347
I (27) vs. I (27) + II (1)	0.000	0.068
I (39) vs. I (39) + II (39)	0.000	0.278
I (15)+II (1) vs. I (15) + II (15)	0.001	(0.000)
I (27)+II (1) vs. I (27) + II (27)	0.000	(0.001)
I (39)+II (1) vs. I (39) + II (15)	0.000	(0.000)

* The P-values reported here are for one-tailed z-tests (eqn. 2.3) of proportions reported in the last two columns of Table 2.2. P-values ≤ 0.05 and not in parentheses indicate that the latter classification is a significant improvement over the former in its ability to discriminate statistical differences in mean grain size and variance of bed surface textures. P-values ≤ 0.05 and in parenthesis indicate the latter classification significantly worsens discriminatory power relative to that of the former.

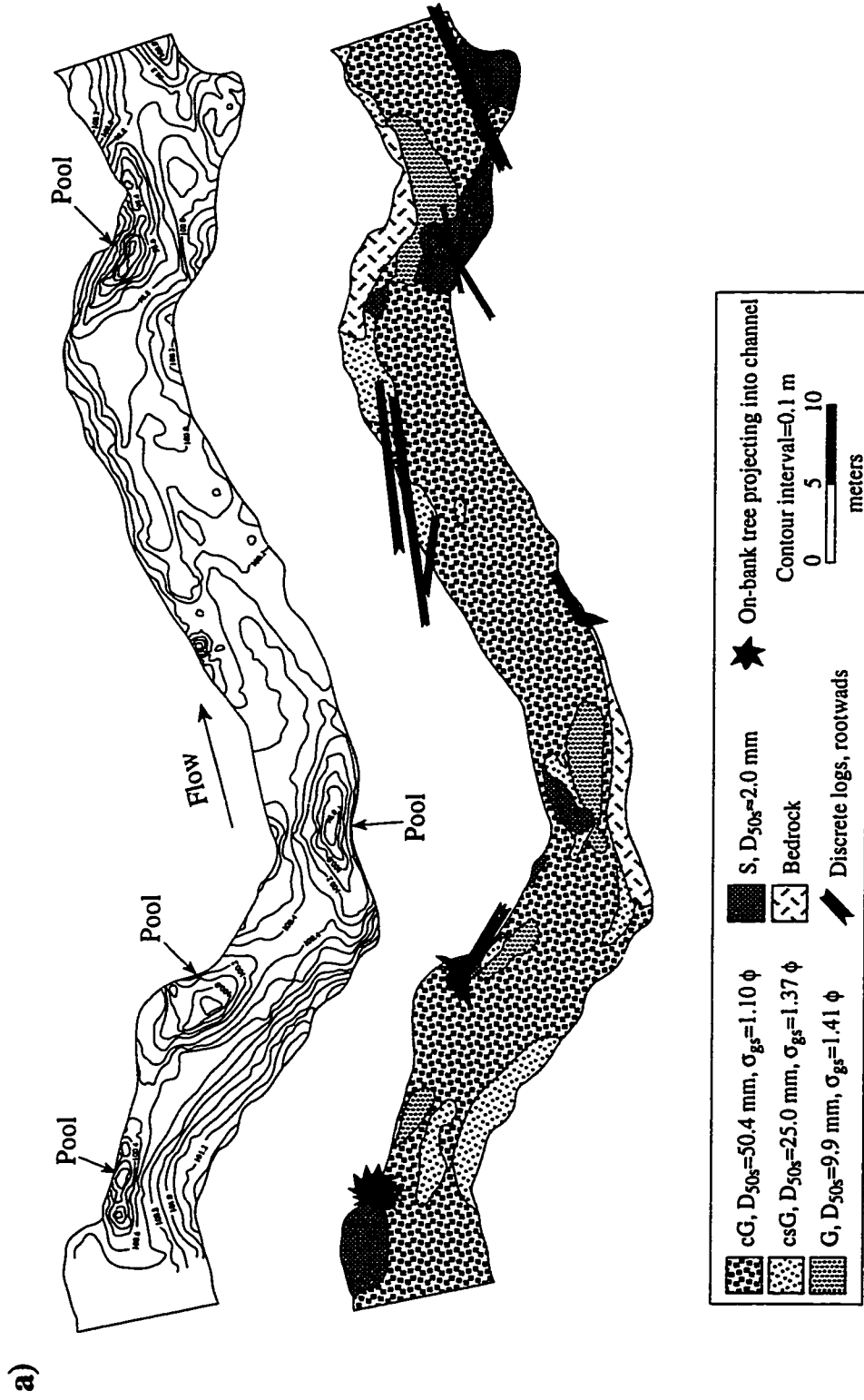


Figure 2.1: Textural and topographic maps of a) Skunk Creek and b) Mill Creek, forest pool-riffle channels of the Olympic Peninsula, western Washington, USA. Each facies type is named according to our textural classification (discussed later). D_{50s} is the median bed-surface grain size of a textural patch, and σ_{gs} is Folk's [1974] graphic standard deviation ($[\phi_{84}-\phi_{16}]/2$, where ϕ_{84} and ϕ_{16} are the \log_2 grain sizes [Krumbein, 1936] for which 16% and 84% of the surface grain sizes are finer.

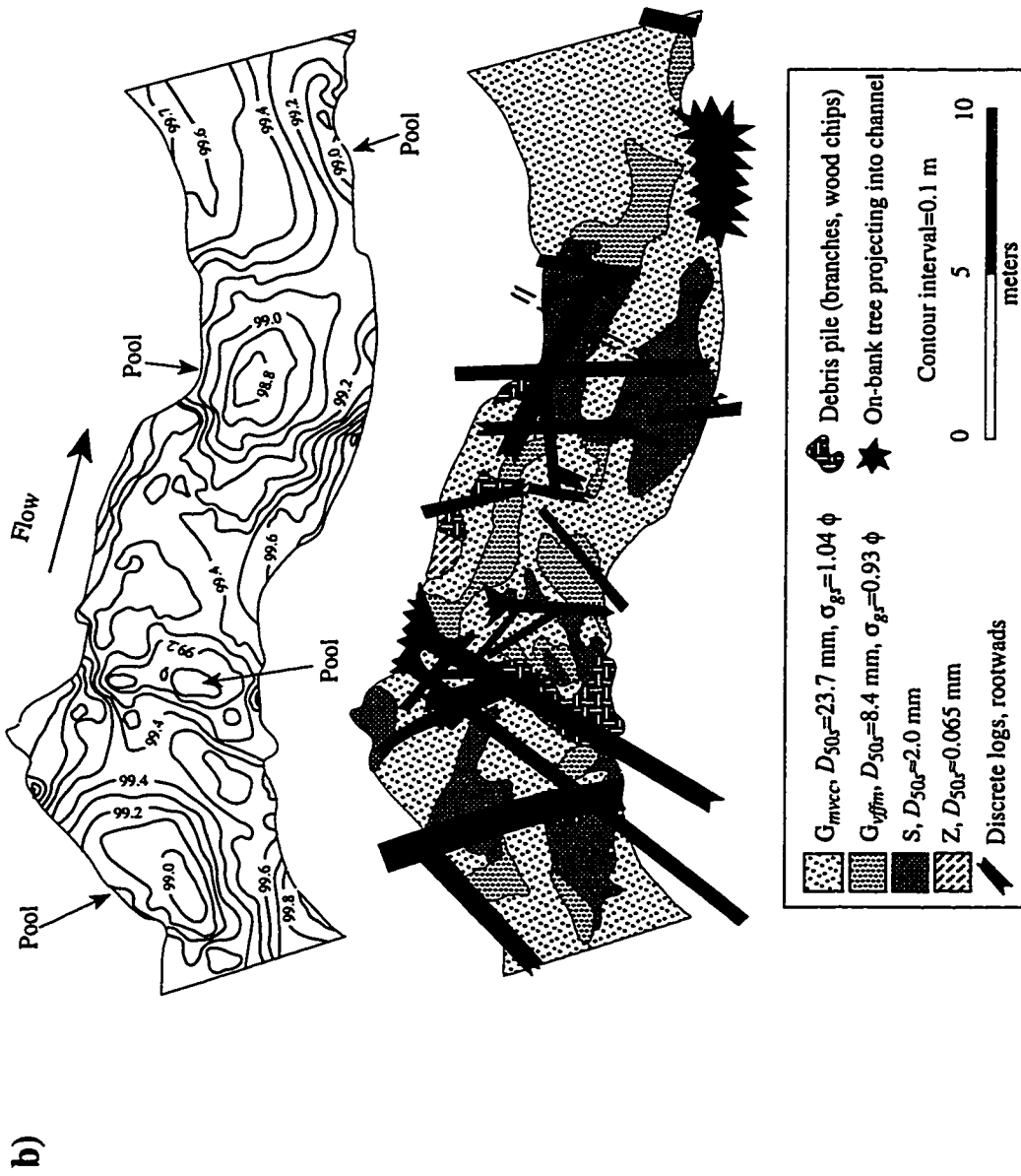


Figure 2.1 (continued)

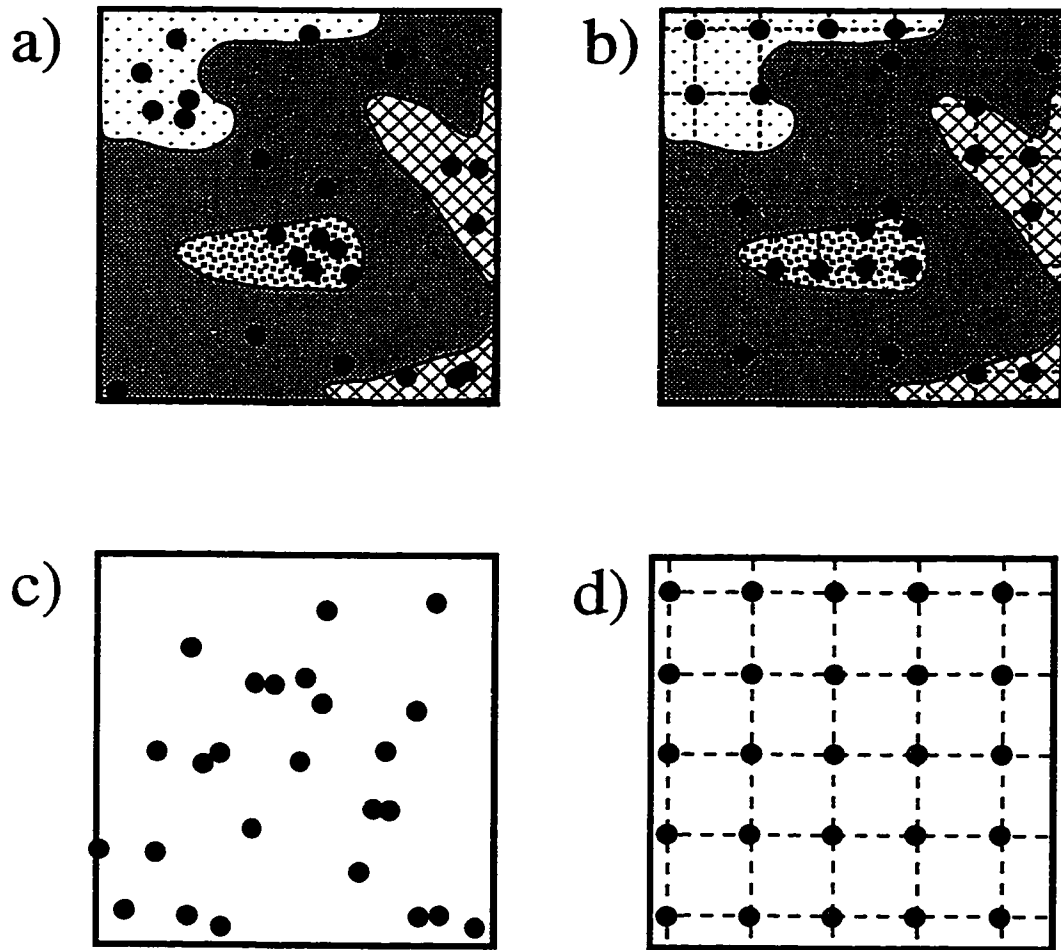


Figure 2.2: Cartoon illustrating basic strategies for sampling bed surface sediments in a stream reach: a) facies-stratified random, b) facies-stratified systematic (grid/transect), c) unstratified random, and d) unstratified systematic. Textural patches are indicated by different fill patterns, and sample locations are shown by black dots. In (b), the interval of sample sites within patches is scaled to individual patch area, with each patch having the same number of samples.

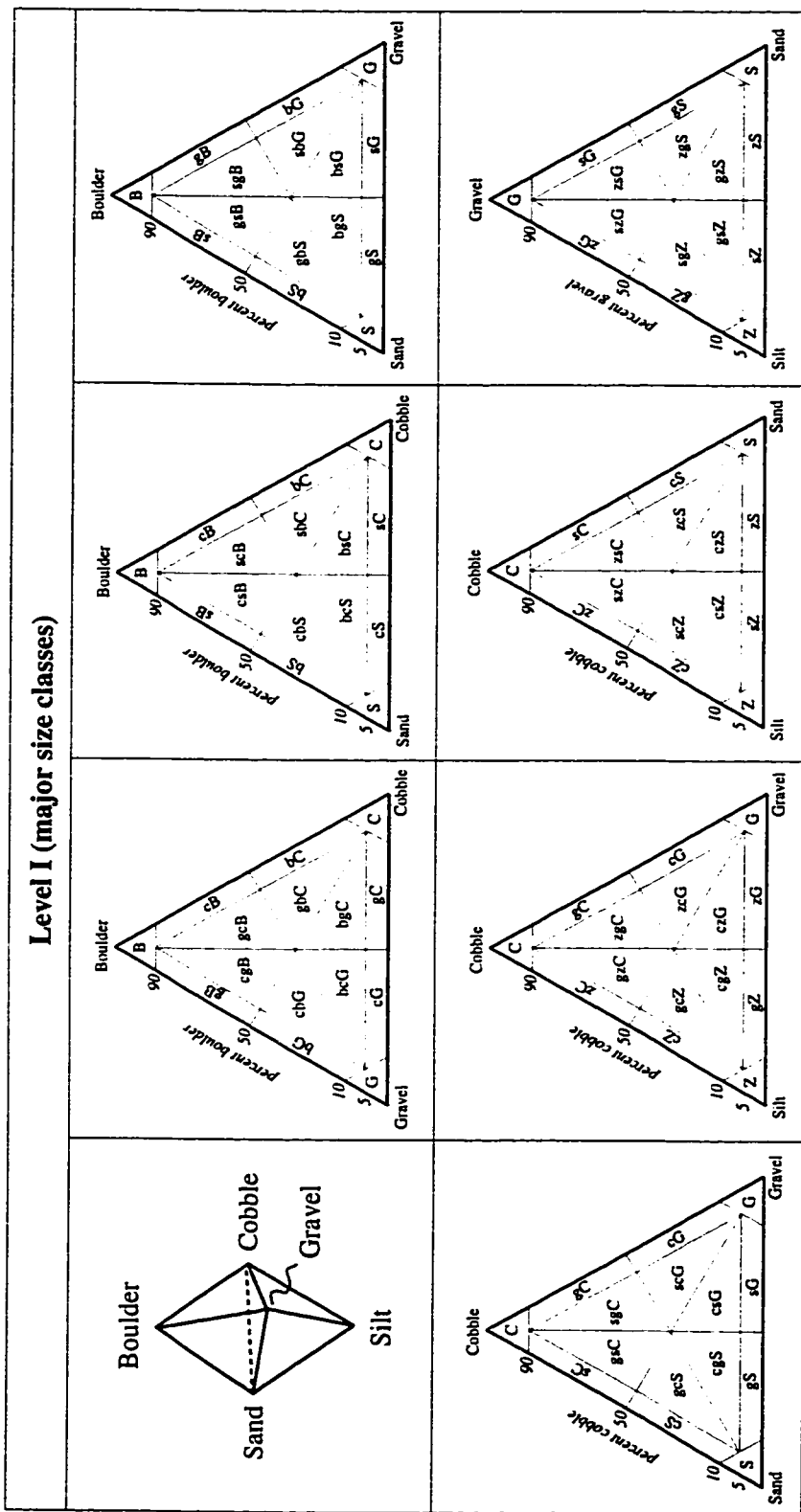


Figure 2.3: Two-level ternary classification for bed-surface facies. Level I decomposes the basic sextahedron of major size classes into seven ternary diagrams for classifying textures according to their relative abundance of three major size classes; standard grain size names and divisions are used (Table 2.1). Level II further delineates the grain size composition of the dominant size class (see figure text for symbol key and examples).

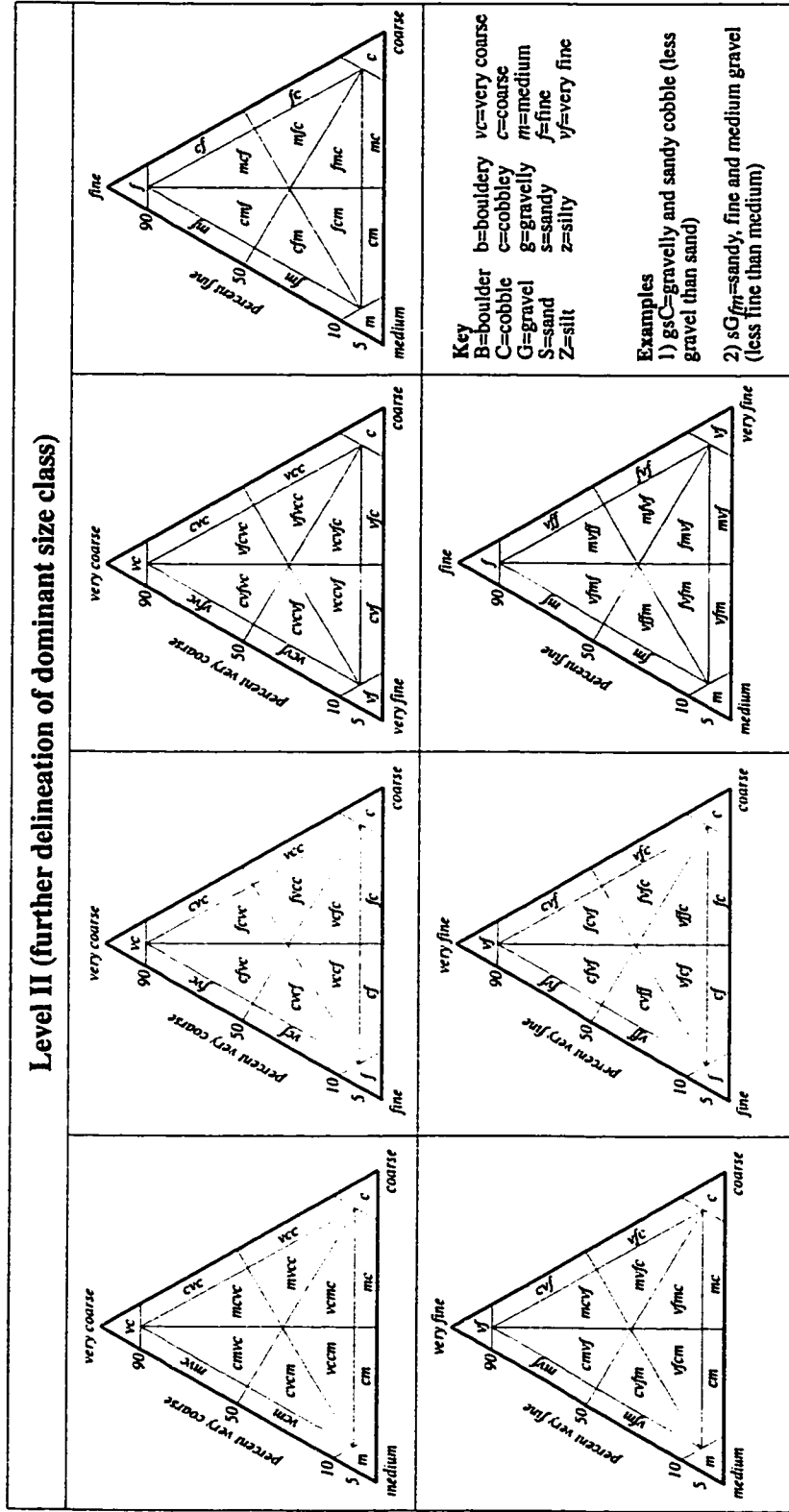


Figure 2.3 (continued)

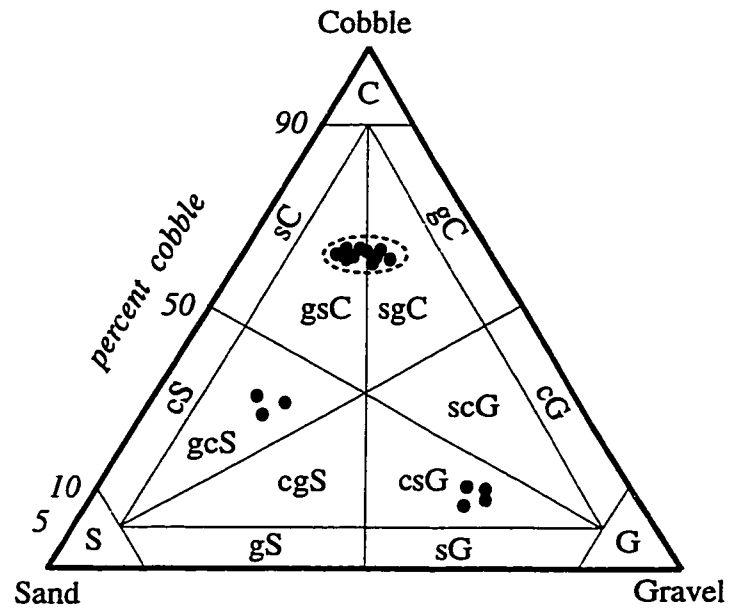


Figure 2.4: Technically dissimilar textures (sgC and gsC) grouped as functionally similar (circled points), but distinctly different from gcS and csG textures in the same reach.

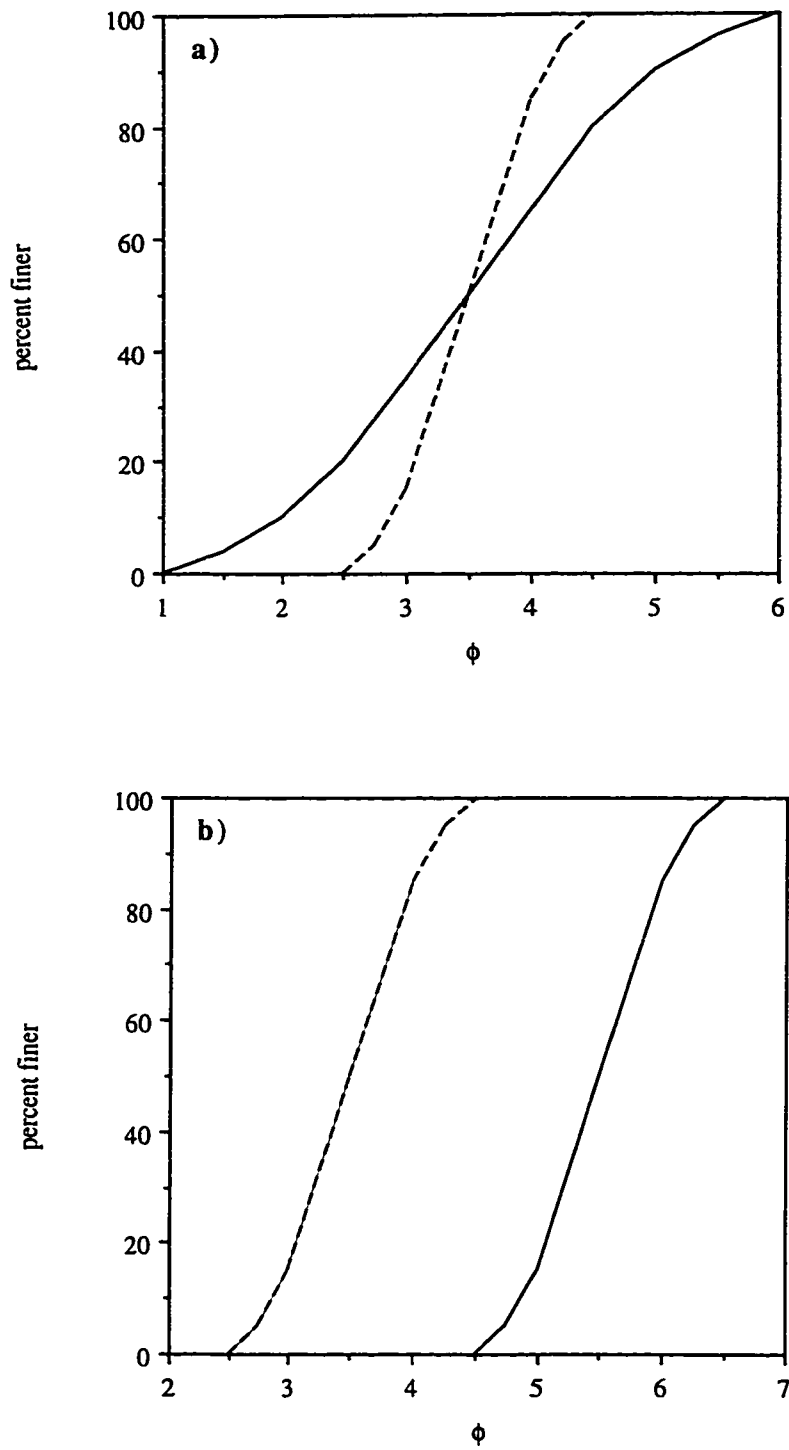


Figure 2.5: Cartoon illustrating bed-surface textures with a) similar means, but different variances, and b) different means, but similar variances.

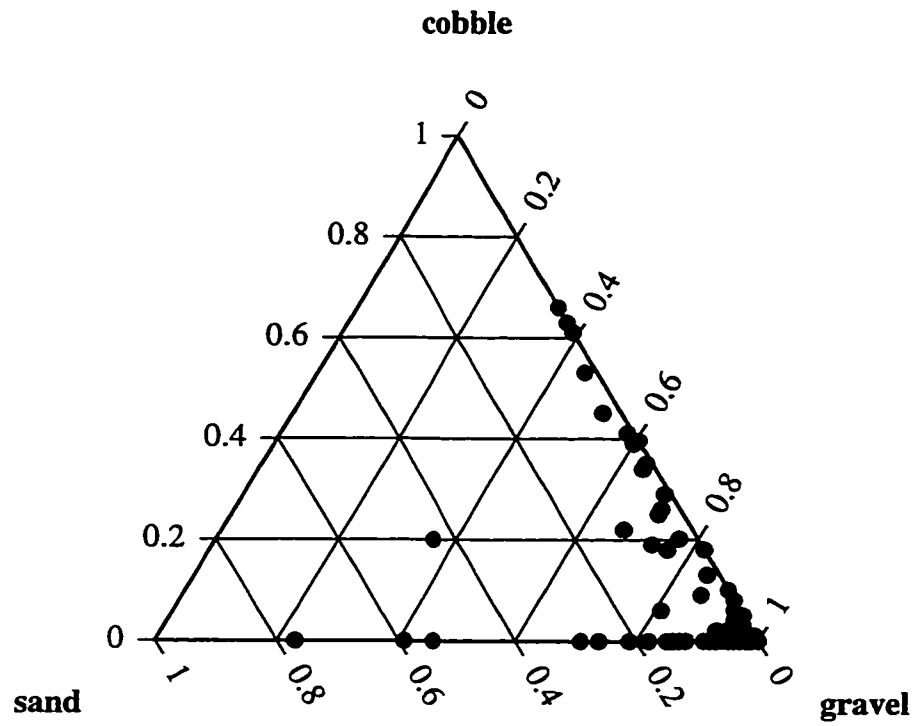


Figure 2.6: Level I grain size composition of textures sampled at our study sites.

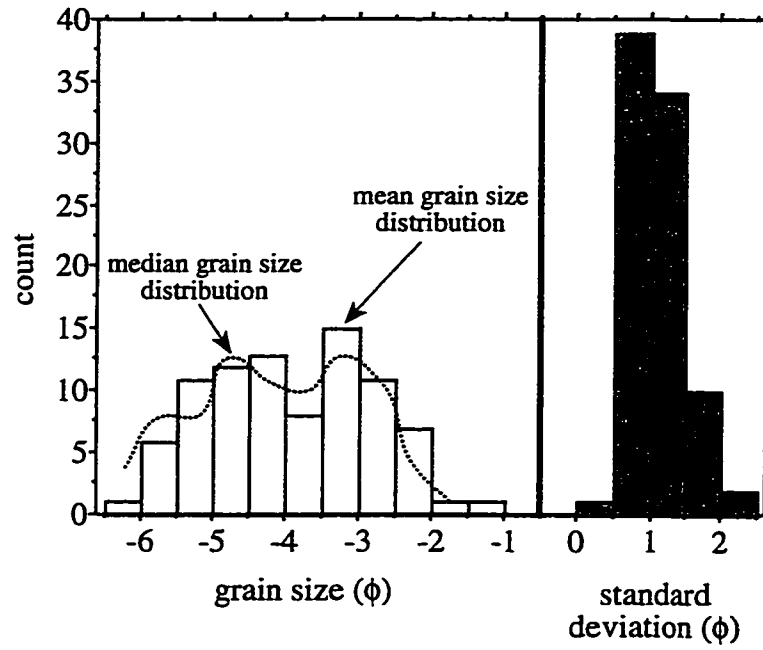


Figure 2.7: Distributions of grain size mean, median, and standard deviation for the sampled textures shown in Figure 2.6.

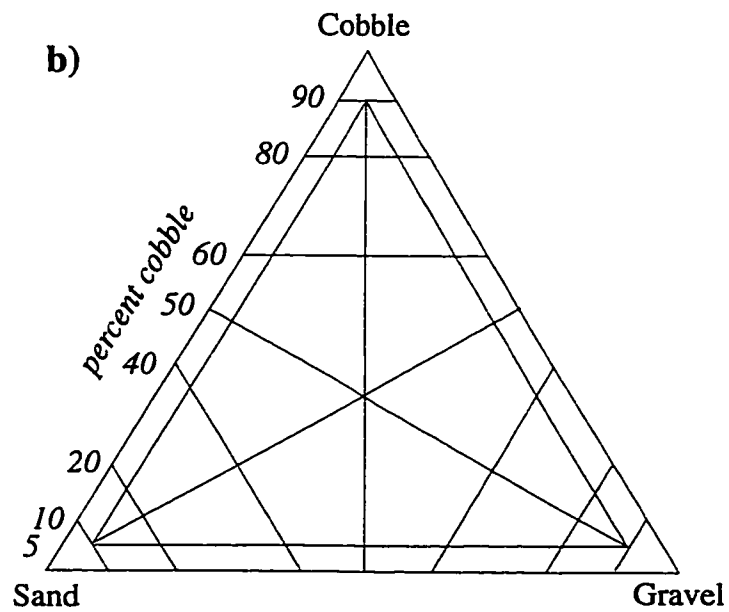
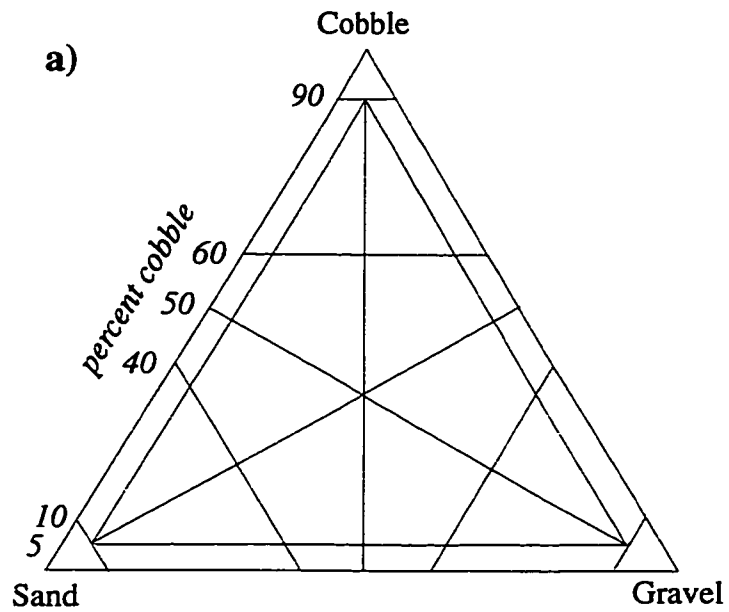


Figure 2.8: Modified classification ternaries, subdivided at a) the 60th percentile and b) the 60th and 80th percentiles. The modified ternaries increase the number of textural categories from 15 to 27 and 39, respectively.

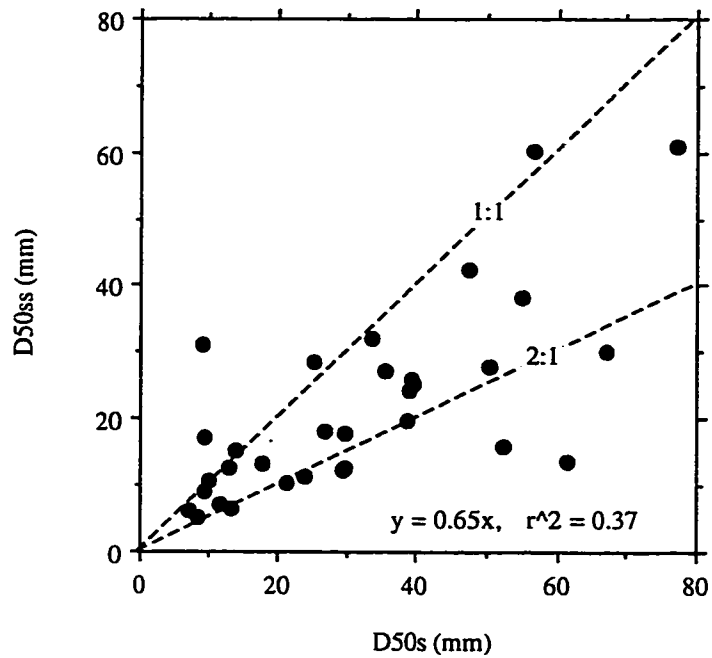


Figure 2.9: Comparison of surface (D_{50s}) and subsurface (D_{50ss}) median grain sizes of textural patches in forest channels of the Olympic Peninsula, western Washington, USA. Surface grain-size distributions were determined from patch-spanning, random, pebble counts [Wolman, 1954] of 100+ grains. Subsurface grain-size distributions were determined from sieved bulk samples, following the Church et al. [1987] sampling criterion (i.e., the largest grain is $\leq 1\%$ of the total sample weight). The reported linear regression is forced through zero.

Chapter 3: Hydraulic Roughness And Shear-Stress Partitioning In Forest Pool-Riffle Channels³

Overview

Sources and magnitudes of hydraulic roughness are quantified in two forest gravel-bed rivers. Total shear stress and hydraulic roughness are theoretically partitioned amongst resistance elements based on their physical characteristics. The accuracy of the partitioning model is assessed by comparing calculated reach-average flow velocities to those measured in the field with a salt-tracer technique. Results indicate that calculated reach-average velocities are within 7-8% of measured values, while calculated values of total roughness are within 7-9% of measured values. Observed values of reach-average median grain size at each site are in good agreement with those predicted from modeled bankfull bed stresses, indicating that bed-surface grain size of the sites is in quasi-equilibrium with bankfull channel hydraulics.

Introduction

The effects of hydraulic roughness on flow, sediment transport, and channel morphology have long been of interest to both civil engineers [Darcy and Bazin, 1865; Manning, 1891] and geomorphologists [Russel, 1907; Gilbert, 1914]. In particular, hydraulic roughness affects flow velocity and channel conveyance [Shields and Gippel, 1995], influences boundary shear stress and bedload transport [Einstein and Barbarossa, 1952; Dietrich et al. 1984], and contributes to the development of spatial gradients in bed shear stress that mold alluvial channels [Leighly, 1932]. There are many sources and scales of hydraulic roughness, such as skin friction caused by the channel bed and walls, form drag due to alluvial bed-forms or in-channel obstructions (lag boulders, wood debris, etc.), changes in momentum caused by large-scale channel curvature, and lateral diffusion of momentum caused by both the shape of the channel cross section and the proximity of

³ Co-authored paper by John M. Buffington and David R. Montgomery, in preparation for submission to *Water Resources Research*.

channel walls and their associated friction [Leighly, 1932; Parker 1978b; Houjou et al., 1990].

Here, we quantify sources and magnitudes of hydraulic roughness in two, forest, pool-riffle channels. We expand on the shear-stress partitioning models developed by Jim Smith and his colleagues [Smith and McLean, 1977; Dietrich et al., 1984; Nelson and Smith, 1989; Wiberg and Smith, 1989] to calculate reach-average shear stresses associated with different scales and types of roughness at our study sites. To assess the accuracy of our calculations, we compare our predicted values of reach-average velocity to those measured in the field.

Results of this analysis are used to investigate the correspondence between bed-surface grain size and bed shear stress as modified by hydraulic roughness. Buffington and Montgomery [in review (b)] recently suggested that imbalances between transport capacity and sediment supply in alluvial channels can be equilibrated, in part, through textural adjustment of the bed surface. Size-selective deposition or erosion of the bed alters bed skin-friction, boundary shear stress, and critical shear stresses for sediment traveling over the bed, contributing to the equilibration of sediment supply and bedload transport rate. In particular, the authors hypothesized that grain size should vary directly with hydraulic roughness and consequent boundary shear stress in channels with low sediment supply. Here, we further examine that hypothesis.

Study Site and Field Methods

We conducted extensive morphologic and hydrologic measurements in two gravel-bed channels (Bambi Creek and Trap Creek) located on Chichagoff Island, southeastern Alaska (Fig. 3.1). The channels flow through old growth forests of Sitka spruce (*Picea sitchensis*) and western hemlock (*Tsuga heterophylla*) and are located in a small cirque valley that drains into Trap Bay and Tenakee Inlet. Bambi Creek is a small (4.7 m wide) pool-riffle channel that had all in-channel wood removed during experiments conducted by the US Forest Service to examine channel response to altered wood loading [Sidle, 1988; Smith et al., 1993a, b; Wood-Smith and Buffington, 1996]. The channel has a slope of 0.01, a bed composed of rounded granitic grains with a median size (D_{50}) of 23 mm, and a well-formed alternate bar sequence with a pool spacing of three channel widths. The slope and bed-surface grain size of Trap Creek (0.008 and 16 mm) are similar to that of Bambi Creek, but Trap Creek is considerably wider (12.9 m), has a bed composed of angular

limestone grains, and has a very high loading of old growth wood debris (0.05 pieces/m², roughly eight pieces of wood per square channel width).

At each study site, we 1) identified sources of hydraulic roughness, 2) measured their physical characteristics for use in predicting magnitudes of hydraulic roughness and consequent flow velocity, and 3) conducted a series of velocity measurements to assess the accuracy of our predicted values of channel roughness and flow velocity.

During summer low flow, we constructed detailed maps of channel topography, bed-surface texture, and wood loading in reaches that were roughly twenty channel widths long. Topography and wood characteristics were surveyed with a digital theodolite. Bed-surface grain sizes were mapped as textural patches [Buffington and Montgomery, in review (a)] and sampled by patch-spanning random pebble counts [Wolman, 1954] of 100+ grains. These measurements made during the summer field season were used to determine physical characteristics (i.e., size, frequency, and orientation) of channel roughness elements.

In the fall, we measured reach-average hydraulic velocity during a series of rainstorms at each study site. Reach-average velocity was determined from a standard salt-tracer technique [Church 1974; Day 1977]. For these measurements, a slug of salt water was introduced at a certain distance upstream and the passage of the salt wave was recorded at the study site by measuring conductivity at both the upstream and downstream ends of the reach. Each conductivity meter was anchored on a vertical rod placed in the channel thalweg and data was logged remotely at five-second intervals.

The mean travel time (t_m) for each concentration curve was determined from Day's [1977] approximation

$$t_m = t_r + 0.63 t_c \quad (3.1)$$

where t_r is the time coordinate for which the rising limb of the concentration curve attains one half its peak value ($C_p/2$) and t_c is the time period between t_r and t_f (the falling limb complement of t_r) (Fig. 3.2). Reach-average velocity (\bar{u}) was calculated as reach length (L) divided by the difference between the upstream and downstream mean travel times (t_{m1} and t_{m2} , respectively)

$$\bar{u} = L / (t_{m1} - t_{m2}) \quad (3.2)$$

The salt-tracer technique requires that the salt is thoroughly mixed throughout the flow by the time it reaches the measurement sites. The mixing length (l_m) was estimated from the Yotsukura and Cobb [1972] equation

$$l_m = \frac{0.25 \bar{u} W^2}{u^* h} \quad (3.3)$$

where W and h are the flow width and depth, respectively, and u^* is the shear velocity ($u^* \equiv \sqrt{\tau/\rho}$, where τ is the boundary shear stress and ρ is the fluid density). To provide a maximum estimate of l_m for the flows likely to be encountered, we used bankfull values of W , u^* , and h determined from channel surveys upstream of the study sites. Calculation of l_m also requires an estimate of the upstream flow velocity. We calculated a maximum velocity (and therefore a maximum mixing length) for the channel reaches upstream of the study sites by assuming a wide, plane-bed morphology, allowing approximation of the reach-average velocity from the law of the wall [Keulegan, 1938]

$$\langle u \rangle = \frac{u^*}{\kappa} \left\langle \ln \left(\frac{z}{z_0} \right) \right\rangle = \frac{u^*}{\kappa} \frac{\int \ln \left(\frac{z}{z_0} \right) dz}{\int dz} = \frac{u^*}{\kappa} \left[\ln \left(\frac{z}{z_0} \right) - 1 \right] \quad (3.4)$$

where terms in pointed brackets are vertical averages ($\langle u \rangle = \bar{u}$ for a wide plane-bed channel), κ is von Karaman's constant ($\kappa=0.407$), z is flow depth, and z_0 is a characteristic roughness length-scale, which, for our assumed plane-bed morphology, we define as that of the grain skin friction ($z_0 = z_{0sf} \approx 0.1 D_{84}$ [Whiting and Dietrich, 1990], where D_{84} is the surface grain size for which 84% of the sizes are smaller); all values in (3.4) are reach averages. Use of z_{0sf} , rather than the total roughness length scale (z_{0T} , which includes all sources of roughness, not just grain skin friction) overestimates the actual reach velocity, providing a maximum estimate of l_m . Calculated values of l_m for Bambi Creek and Trap Creek are 306 m and 1040 m, respectively. Salt slugs were introduced to the channel at these distances upstream of the study sites.

During the velocity experiments, water-surface elevations were recorded at fixed channel cross-sections placed at intervals of one channel width. These measurements were

used to determine reach-average values of flow width, depth, and water-surface slope during each discharge event.

Hydraulic Roughness and Shear-stress Partitioning

Sources of roughness

We identified six sources of hydraulic roughness at our study sites: 1) skin friction due to bed-surface grains; 2) form drag caused by channel bars; 3) form drag due to in-channel wood; 4) form drag resulting from wave-like undulations of downstream channel width; 5) cross-sectional diffusion of fluid momentum caused by the combined effects of cross-section shape, proximity of channel walls (so-called 'width-depth effects'), and differences between roughness scales of the channel bed and walls [Leighly, 1932; Parker, 1978b; Hey, 1979; Houjou et al. 1990]; and 6) changes in fluid momentum caused by plan-form curvature (i.e., channel sinuosity). Each of these scales of roughness are illustrated in Figure 3.3. Panel A shows grain skin friction, bar form-drag, and wood form-drag at various positions within the flow (discussed further below). Panel B illustrates form drag caused by wall undulations. Panel C shows cross-sectional scales of roughness, including cross section form, proximity of walls, and differences between wall and bed skin friction (different stipple patterns). These three types of cross-sectional resistance influence isovel structure, which, in turn, affects the isovel-perpendicular rays that define the area of flow and consequent boundary shear stress affecting a given portion of the channel perimeter (Fig. 3.3c) [Leighly, 1932; Houjou et al., 1990]. Panel D shows hydraulic resistance associated with plan-form channel sinuosity.

The model

The hydraulic roughness and consequent shear stress associated with each of these roughness elements was quantified using the approach outlined by Nelson and Smith [1989]. Their method is based on boundary-layer theory and involves the cumulative addition of successive scales of channel roughness as one moves up through the flow column from the channel bed to the water surface (Fig 3.4).

The total, reach-average, boundary shear stress of the channel (τ_0) is linearly partitioned into shear stress components representing each of the above six sources of hydraulic roughness

$$\tau_0 = \tau_{sf} + \tau_b + \tau_l + \tau_w + \tau_x + \tau_s \quad (3.5)$$

where the right-hand stresses are, respectively, those due to grain skin friction (τ_{sf}), bar form-drag (τ_b), wood drag (predominantly logs) (τ_l), wall form-drag (downstream undulations of channel width) (τ_w), the combined effects of cross-sectional shape, proximity of walls, and difference between bed and wall roughness-scales (τ_x), and channel sinuosity (τ_s). Each scale of roughness and its consequent shear stress is influenced by the presence of other roughness elements in the channel. Therefore, the shear stress components of equation (3.5) are expressed as functions of one another and solved simultaneously.

The total, reach-average, boundary shear stress is defined as a depth-slope product

$$\tau_0 = \rho g h S \quad (3.6)$$

where g is the gravitational constant and S is the water-surface slope. Form drag (F_D) caused by flow obstructions (in this case, bars, wood, and wall undulations) is expressed as

$$F_{D_i} = \frac{1}{2} \rho C_{D_i} \langle u_r \rangle^2 A_{x_i} \quad (3.7)$$

where C_D is the drag coefficient, u_r is the far-field reference velocity (vertically averaged over the height of the obstruction), A_x is the flow-perpendicular area of the obstruction, and the subscript i indicates values for an obstruction of interest. The corresponding shear stress resulting from an obstruction of interest (τ_i) is

$$\tau_i = \frac{1}{2} \rho C_{D_i} \langle u_r \rangle^2 \frac{A_{x_i}}{A_{b_i}} \quad (3.8)$$

where A_b is the horizontally-projected area of the obstruction. The reference velocity is the far-field velocity in the absence of the obstruction of interest and is calculated from the law of the wall expressed in terms of the next smallest scale of roughness

$$u_r = \frac{\sqrt{\tau_r/\rho}}{\kappa} \ln \left(\frac{z}{z_{0r}} \right) \quad (3.9)$$

where τ_r and z_{0r} are the reference values of shear stress and roughness length-scale. For example, in a two-component system of grain and bar roughness, the reference velocity for calculating bar form-drag is that characterized by skin friction alone (the velocity that would occur in the absence of bars) with $\tau_r = \tau_{sf}$ and $z_{0r} = z_{0sf}$. Similarly, for a three-component system of grain, bar, and wood roughness (each representing successive scales of resistance), the wood form-drag would be calculated with $\tau_r = \tau_{sf} + \tau_b$ and $z_{0r} = z_{0sf+b}$, where the latter term is the roughness-scale due to the combined effects of skin friction and bar form-drag; note that because shear stresses are linearly additive here (eqn 5), roughness length-scales are logarithmically additive, hence the use of a single roughness term with multiple subscripts to represent combined roughness elements (i.e., $z_{0r} = z_{0sf+b} \neq z_{0sf} + z_{0b}$). Inserting (3.9) in (3.8) yields

$$\tau_i = \frac{\tau_r}{2\kappa^2} C_{Di} \left\langle \ln \left(\frac{z_i}{z_{0r}} \right) \right\rangle^2 \frac{A_{xi}}{A_{bi}} \quad (3.10)$$

where the logarithmic velocity profile is vertically averaged over the height of the obstruction (z_i).

The reference-velocity approach results in a segmented vertical-velocity profile [e.g., Smith and McLean, 1977; Middleton and Sourthard, 1984; Robert et al., 1992], where each segment represents the cumulative addition of successive roughness length-scales (Fig. 3.5). For example, the lowest segment may represent grain resistance only, followed by a segment representing the combined effects of grain and bed-form resistance, and so forth. Roughness length-scales for a segment of interest (z_{0i}) can be calculated from the adjoining reference-segment by matching the two profiles at the height of the obstruction of interest (z_i) [Nelson and Smith, 1989]

$$\frac{\sqrt{\tau_r/\rho}}{\kappa} \ln \left(\frac{z_i}{z_{0r}} \right) = \frac{\sqrt{\tau_i/\rho}}{\kappa} \ln \left(\frac{z_i}{z_{0i}} \right) \quad (3.11a)$$

$$\Rightarrow z_{0i} = z_i \left[\frac{z_i}{z_{0r}} \right]^{-\left(\frac{\tau_i}{\tau_r}\right)^{-0.5}} \quad (3.11b)$$

For example, in the two-component system of grain and bar resistance, the roughness due to the combined effects of skin friction and bar form-drag ($z_{0i} = z_{0sf+b}$) is calculated from (3.11b) with $z_i = z_b$ (the height of the bar), $z_{0r} = z_{0sf}$, $\tau_i = \tau_{sf} + \tau_b$, and $\tau_r = \tau_{sf}$.

In Bambi Creek, the progression of roughness elements in increasing order of scale is bed-surface skin friction (τ_{sf}), bars (τ_b), downstream wall-undulations (τ_w), cross-sectional form (τ_x) (including cross-section shape, width-depth ratio, and differences in roughness between the channel bed and walls), and channel sinuosity (τ_s). The corresponding shear stress equations are

$$\tau_{sf} = \tau_0 - \tau_b - \tau_w - \tau_x - \tau_s \quad (3.12a)$$

$$\tau_b = \frac{\tau_{sf}}{2\kappa^2} C_{Db} \left\langle \ln \left(\frac{z_b}{2 z_{0sf}} \right) \right\rangle^2 \frac{A_{xb}}{A_{bb}} = \frac{\tau_{sf}}{2\kappa^2} C_{Db} \frac{z_b}{2 \lambda_b} \left[\ln \left(\frac{z_b}{2 z_{0sf}} \right) - 1 \right]^2 \quad (3.12b)$$

$$\tau_w = \frac{\tau_{sf} + \tau_b}{2\kappa^2} C_{Dw} \left\langle \ln \left(\frac{z_w}{z_{0sf+b}} \right) \right\rangle^2 \frac{A_{xw}}{A_{bw}} K_w = \frac{\tau_{sf} + \tau_b}{2\kappa^2} C_{Dw} \cdot \frac{2 h \alpha_w}{W \lambda_w} \left[\ln \left(\frac{h}{z_{0sf+b}} \right) - 1 \right]^2 \quad (3.12c)$$

$$\tau_x = f \left(\frac{W}{h}, \frac{z_{0B}}{z_{0W}} \right) \tau_0 \quad (3.12d)$$

$$\tau_s = \frac{\tau_{sf} + \tau_b + \tau_w + \tau_x}{2\kappa^2} C_{Ds} \left\langle \ln \left(\frac{z_s}{z_{0sf+b+w+x}} \right) \right\rangle^2 \frac{A_{xs}}{A_{bs}} = \frac{\tau_{sf} + \tau_b + \tau_w + \tau_x}{2\kappa^2} C_{Ds} \frac{h}{L} \left[\ln \left(\frac{h}{z_{0sf+b+w+x}} \right) - 1 \right]^2 \quad (3.12e)$$

where in (3.12b) $C_{Db} = 0.84$ [Nelson and Smith, 1989], z_b is the bar height, $A_{xb} = z_b W / 2$ (that of a triangular wedge [Nelson and Smith, 1989]), W is the channel width, $A_{bb} = \lambda_b W$, and λ_b is the bar wavelength; in (3.12c) $C_{Dw} = 0.84$ (assuming that the drag of wall-form undulations is similar to that of bed-form undulations), z_w is the vertical height of wall undulations (equal to the total flow depth h), $A_{xw} = 2 \alpha_w z_w$, α_w is the horizontal amplitude of wall undulations along one side of the channel, $A_{bw} = 2 \lambda_w \alpha_w$, λ_w is the downstream

wavelength of wall undulations, and $K_w \equiv A_{b_w} / \lambda_w W$ is a correction factor introduced to distribute the drag of the wall undulations across the entire channel width, rather than just across A_{b_w} ; in (3.12d) τ_x is a function of channel width-depth ratio (W / h) and the ratio of bed to wall roughness (z_{0B} / z_{0W}), where the bed and wall roughnesses include the combined effects of all scales of roughness near the boundary (i.e., skin friction and bed form-drag) (discussed further below); in (3.12e) $C_{D_s} = \sum (W_{b_i} / r_{c_i})$ [Rouse, 1965; Shields and Gippel, 1995], W_{b_i} is the width of an individual bend of the river, r_{c_i} is the radius of curvature of that bend, z_s is the effective obstruction height associated with the resistance caused by plan-form sinuosity (set equal to the total flow depth, h , because sinuosity is a channel-scale roughness), $A_{x_s} = W h$ (where W is the reach-average channel width, as opposed to an individual bend width), $A_{b_s} = W L$, and L is reach length. Because the bars in Bambi Creek tend to be well-formed wedges, we follow the approach of Nelson and Smith [1989] and treat the cross-sectional area of the bars as a triangular obstruction.

In the above equations, form drag due to channel bars and downstream wall-undulations is predominantly a function of the height-wavelength ratio of the obstruction (z_b / λ_b and h / λ_w , respectively). Resistance caused by channel sinuosity is similarly a function of h / L , but also depends on the sum of W_{b_i} / r_{c_i} . The boundary shear stress along the channel walls (τ_x) depends on lateral momentum diffusion caused by cross-sectional shape, proximity of channel walls, and relative magnitudes of wall and bed roughness [Leighly, 1932; Parker, 1978b; Hey, 1979; Houjou et al. 1990]. Here, we treat τ_x as a cross-sectional-scale resistance, greater in scale than bar-form drag, but smaller in scale than plan-form sinuosity. We approximate the magnitude of τ_x using the results of Houjou et al. [1990], which are based on an eddy-diffusion model that calculates the velocity-field of the channel cross-section using a finite difference approach, and allows determination of the isovel-perpendicular flow area and consequent shear stresses associated with the channel walls versus the channel bed (Fig. 3.3c). Their calculations model flow in a rectangular channel and investigate the effects of W / h and z_{0B} / z_{0W} on bed stress. They find that W / h is the primary influence, while z_{0B} / z_{0W} is a secondary effect that is progressively less important at values of $W / h > 20$. From their results, we estimate τ_x as a fixed proportion of τ_0 that depends on channel W / h and z_{0B} / z_{0W} . Because the bed and walls of Bambi Creek are both characterized by similar scales of roughness (skin friction plus undulating topographic form-drag), we assume that a first-order estimate of the relative roughness of the bed and walls is $z_{0B} / z_{0W} = 1$. Houjou et

al.'s results indicate that for $W / h = 22.6$ (that of Bambi Creek) and $z_{0B} / z_{0W} = 1$, $\tau_x \approx 0.08 \tau_0$. This value of τ_x is likely an underestimate because it is based on a rectangular channel form and does not consider the effects of specific channel shape. However, because Bambi Creek has a large value of W / h , τ_x is a minor component of the overall shear stress, so errors associated with the assumption of a rectangular channel and $z_{0B} / z_{0W} = 1$ likely have a minimal effect on the overall analysis. In practice, many investigators conclude that cross-sectional resistance effects can be neglected for channels with $W / h > 20$ [Hey, 1979; Knight, 1981; Flinham and Carling, 1988].

The roughness length-scales corresponding with the shear stress equations of (3.12a-e) are

$$z_{0sf} = 0.1 D_{84} \quad (3.13a)$$

$$z_{0sf+b} = \frac{z_b}{2} \left[\frac{z_b / 2}{z_{0sf}} \right] - \left(\frac{\tau_{sf} + \tau_b}{\tau_{sf}} \right)^{-0.5} \quad (3.13b)$$

$$z_{0sf+b+w} = z_w \left[\frac{z_w}{z_{0sf+b}} \right] - \left(\frac{\tau_{sf} + \tau_b + \tau_w}{\tau_{sf} + \tau_b} \right)^{-0.5} \quad (3.13c)$$

$$z_{0sf+b+w+x} = z_x \left[\frac{z_x}{z_{0sf+b+w}} \right] - \left(\frac{\tau_{sf} + \tau_b + \tau_w + \tau_x}{\tau_{sf} + \tau_b + \tau_w} \right)^{-0.5} \quad (3.13d)$$

$$z_{0sf+b+w+x+s} = z_s \left[\frac{z_s}{z_{0sf+b+w+x}} \right] - \left(\frac{\tau_{sf} + \tau_b + \tau_w + \tau_x + \tau_s}{\tau_{sf} + \tau_b + \tau_w + \tau_x} \right)^{-0.5} \quad (3.13e)$$

where z_w , z_x , and z_s are all set equal to the total flow height, h , because these roughness elements are channel-scale features whose heights all extend to the water surface, which is the physical limit of boundary layer growth (see discussion by Nelson and Smith [1989], p. 85). The system of equations defined by (3.12a-e) and (3.13a-e) is solved iteratively and simultaneously until a stable solution is obtained. Here, the equations are solved for reach-average stresses using reach-average values everywhere.

The system of equations for Trap Creek is similar, but includes the effects of wood obstructions. Wood debris in Trap Creek is predominantly logs and occurs at a variety of locations within the flow column (at the bed, mid flow, at the water surface, etc.) and is of

assorted sizes (lengths of <1-21 m, and diameters of 0.1-1.0 m). Consequently, the logs cannot be assigned a fixed roughness-scale and position relative to the other channel-roughness elements. Therefore, we divided the logs into three spatial categories for purposes of conducting the stress-partitioning calculations (Fig. 3.3a): 1) logs that are positioned at or below the average bar height (τ_{11}); 2) logs that straddle the average bar height (τ_{12}); and 3) logs that are above the average bar height (τ_{13}). The resulting system of shear stress equations for Trap Creek is

$$\tau_{sf} = \tau_0 - \tau_{11} - \tau_b - \tau_{12} - \tau_{13} - \tau_w - \tau_x - \tau_s \quad (3.14a)$$

$$\tau_{11} = \frac{\tau_{sf}}{2\kappa^2} C_{D1} \left[\frac{\int_{hb1}^{ht1} \ln\left(\frac{z}{z_{0sf}}\right) dz}{\int_{hb1}^{ht1} dz} \right]^2 \frac{A_{x11}}{A_{b11}} K_{11} \quad (3.14b)$$

$$\tau_b = \frac{\tau_{sf} + \tau_{11}}{2\kappa^2} C_{Db} \left\langle \ln\left(\frac{z_b}{z_{0sf+11}}\right) \right\rangle^2 \frac{A_{xb}}{A_{bb}} = \frac{\tau_{sf} + \tau_{11}}{2\kappa^2} C_{Db} \frac{z_b}{\lambda_b} \left[\ln\left(\frac{z_b}{z_{0sf+11}}\right) - 1 \right]^2 \quad (3.14c)$$

$$\tau_{12} = \left[\frac{(\tau_{sf} + \tau_{11}) \int_{hb2}^{z_b} \ln\left(\frac{z}{z_{0sf+11}}\right) dz + (\tau_{sf} + \tau_{11} + \tau_b) \int_{z_b}^{ht2} \ln\left(\frac{z}{z_{0sf+11+b}}\right) dz}{\int_{hb2}^{ht2} dz} \right]^2 \cdot$$

$$\frac{C_{D1}}{2\kappa^2} \frac{A_{x12}}{A_{b12}} K_{12} \quad (3.14d)$$

$$\tau_{l3} = \frac{\tau_{sf} + \tau_{l1} + \tau_b + \tau_{l2}}{2\kappa^2} C_{D1} \left[\frac{\int_{hb3}^{ht3} \ln \left(\frac{z}{z_{0sf+l1+b+l2}} \right) dz}{\int_{hb3}^{ht3} dz} \right]^2 \frac{A_{x13}}{A_{b13}} K_{13} \quad (3.14e)$$

$$\begin{aligned} \tau_w &= \frac{\tau_{sf} + \tau_{l1} + \tau_b + \tau_{l2} + \tau_{l3}}{2\kappa^2} C_{Dw} \left\langle \ln \left(\frac{z_w}{z_{0sf+l1+b+l2+l3}} \right) \right\rangle^2 \frac{A_{xw}}{A_{bw}} K_w \\ &= \frac{\tau_{sf} + \tau_{l1} + \tau_b + \tau_{l2} + \tau_{l3}}{2\kappa^2} C_{Dw} \frac{2}{W} \frac{h}{\lambda_w} \alpha_w \left[\ln \left(\frac{h}{z_{0sf+l1+b+l2+l3}} \right) - 1 \right]^2 \end{aligned} \quad (3.14f)$$

$$\tau_x = f \left(\frac{W}{h}, \frac{z_{0B}}{z_{0W}} \right) \tau_0 \quad (3.14g)$$

$$\begin{aligned} \tau_s &= \frac{\tau_{sf} + \tau_{l1} + \tau_b + \tau_{l2} + \tau_{l3} + \tau_w + \tau_x}{2\kappa^2} C_{Ds} \left\langle \ln \left(\frac{z_s}{z_{0sf+l1+b+l2+l3+w+x}} \right) \right\rangle^2 \frac{A_{xs}}{A_{bs}} \\ &= \frac{\tau_{sf} + \tau_{l1} + \tau_b + \tau_{l2} + \tau_{l3} + \tau_w + \tau_x}{2\kappa^2} C_{Ds} \frac{h}{L} \left[\ln \left(\frac{h}{z_{0sf+l1+b+l2+l3+w+x}} \right) - 1 \right]^2 \end{aligned} \quad (3.14h)$$

where C_{D1} is the drag-coefficient for logs, approximated as that of a circular cylinder. C_{D1} varies as a function of both Reynolds number and attack angle of the flow [e.g., Hoerner, 1965], but is typically between 0.83-1.2 for the flows and log orientations encountered in

the current investigation. Many of the logs are suspended above the bed surface for part or all of their length. Consequently, the reference velocities for the logs are vertically-averaged across the bottoms and tops of the logs (h_b , h_t). Because the logs are often pitched at an angle with respect to horizontal, h_b and h_t are averages along the log lengths. Furthermore, because the logs are discrete obstructions that do not provide continuous coverage of the channel bed, an area correction-factor is introduced in equations (3.14b, d-e) (K_{11} , K_{12} , and K_{13}) that effectively averages the calculated stresses over the bed surface of the reach. The K values are defined as $\sum A_{bi} / (WL)$ for each of the three log categories. Because logs in the second height-category (τ_{12}) straddle the average bar height, equation (3.14d) is divided into two parts; the first term in the square brackets is for a reference velocity below the average bar height, while the second term is for a reference velocity above the average bar height. As with Bambi Creek, we assume in (3.14g) that the first-order estimate of z_{0B} / z_{0W} is 1, which combined with the Trap Creek value of W / h (17.6) indicates that $\tau_x \approx 0.09 \tau_0$ at this study site. Unlike Bambi Creek, the bars in Trap Creek are irregular in form and cannot be treated as triangular wedges. Consequently, A_{xb} is defined as $z_b W$, where z_b is a cross-sectionally and longitudinally averaged value of bedform bumpiness.

The roughness length-scale for skin friction in Trap Creek is defined by (3.13a), while the length-scales corresponding with (3.14b-h) are, respectively,

$$z_{0sf+l_1} = h_{t1} \left[\frac{h_{t1}}{z_{0sf}} \right] - \left(\frac{\tau_{sf} + \tau_{11}}{\tau_{sf}} \right)^{-0.5} \quad (3.15a)$$

$$z_{0sf+l_1+b} = z_b \left[\frac{z_b}{z_{0sf+l_1}} \right] - \left(\frac{\tau_{sf} + \tau_{11} + \tau_b}{\tau_{sf} + \tau_{11}} \right)^{-0.5} \quad (3.15b)$$

$$z_{0sf+l_1+b+l_2} = h_{t2} \left[\frac{h_{t2}}{z_{0sf+l_1+b}} \right] - \left(\frac{\tau_{sf} + \tau_{11} + \tau_b + \tau_{12}}{\tau_{sf} + \tau_{11} + \tau_b} \right)^{-0.5} \quad (3.15c)$$

$$z_{0sf+l_1+b+l_2+l_3} = h_{t3} \left[\frac{h_{t3}}{z_{0sf+l_1+b+l_2}} \right] - \left(\frac{\tau_{sf} + \tau_{11} + \tau_b + \tau_{12} + \tau_{13}}{\tau_{sf} + \tau_{11} + \tau_b + \tau_{12}} \right)^{-0.5} \quad (3.15d)$$

$$z_{0sf+l_1+b+l_2+l_3+w} = z_w \left[\frac{z_w}{z_{0sf+l_1+b+l_2+l_3}} \right] - \left(\frac{\tau_{sf} + \tau_1 + \tau_b + \tau_2 + \tau_3 + \tau_w}{\tau_{sf} + \tau_1 + \tau_b + \tau_2 + \tau_3} \right)^{-0.5} \quad (3.15e)$$

$$z_{0sf+l_1+b+l_2+l_3+w+x} = z_x \left[\frac{z_x}{z_{0sf+l_1+b+l_2+l_3+w}} \right] - \left(\frac{\tau_{sf} + \tau_1 + \tau_b + \tau_2 + \tau_3 + \tau_w + \tau_x}{\tau_{sf} + \tau_1 + \tau_b + \tau_2 + \tau_3 + \tau_w} \right)^{-0.5} \quad (3.15f)$$

$$z_{0sf+l_1+b+l_2+l_3+w+x+s} = z_s \left[\frac{z_s}{z_{0sf+l_1+b+l_2+l_3+w+x}} \right] - \left(\frac{\tau_{sf} + \tau_1 + \tau_b + \tau_2 + \tau_3 + \tau_w + \tau_x + \tau_s}{\tau_{sf} + \tau_1 + \tau_b + \tau_2 + \tau_3 + \tau_w + \tau_x} \right)^{-0.5} \quad (3.15g)$$

Test of the model

The accuracy of the above calculations for Bambi Creek and Trap Creek is assessed by comparing field measurements of reach-average velocity determined from salt-tracers (\bar{u}) with those predicted from the stress-partitioning calculations. The predicted total velocity (u_T) is defined from the law of the wall using reach-average bankfull values

$$u_T = \frac{\sqrt{\tau_0/\rho}}{\kappa} \ln \left(\frac{h}{z_{0T}} \right) \quad (3.16)$$

and is vertically averaged ($\langle u_T \rangle$) to provide a reach-average velocity equivalent to the salt-tracer velocity (\bar{u}), which is both a cross-sectional and longitudinal average velocity

$$\langle u_T \rangle = \frac{\sqrt{\tau_0/\rho}}{\kappa} \left\langle \ln \left(\frac{h}{z_{0T}} \right) \right\rangle = \frac{\sqrt{\tau_0/\rho}}{\kappa} \left[\ln \left(\frac{h}{z_{0T}} \right) - 1 \right] \quad (3.17)$$

z_{0T} is the total channel roughness. In the above stress-partitioning model, z_{0T} for Bambi Creek and Trap Creek is defined by equations (3.13e) and (3.15g) [Nelson and Smith, 1989], which can be written more simply as

$$z_{0T} = h \left[\frac{h}{z_{0sf+b+w+x+s}} \right] - \left(\frac{\tau_0}{\tau_{sf} + \tau_b + \tau_w + \tau_x + \tau_s} \right)^{-0.5} \quad (3.18a)$$

$$z_{0T} = h \left[\frac{h}{Z_{0sf+l_1+b+l_2+l_3+w+x+s}} \right] - \left(\frac{\tau_0}{\tau_{sf} + \tau_1 + \tau_b + \tau_2 + \tau_3 + \tau_w + \tau_x + \tau_s} \right)^{-0.5} \quad (3.18b)$$

Results and Discussion

Channel characteristics

Maps of channel topography and wood debris at each study site are shown in Figure 3.6. Bambi Creek exhibits a well-formed, regular, sequence of alternate bars, while pool-and-bar topography of in Trap Creek tends to be irregular and forced by local pieces of wood debris. The wood loading in Trap Creek is quite high, with considerable variability of log orientations and groupings. Logs in Trap Creek tend to form individual, frequently-spaced obstructions, rather than accumulating in debris jams. Many of the wood pieces fall into the channel during windstorms or from local undercutting of the bank and are large enough to resist downstream transport. Dendrochronologic studies of the wood debris in Trap Creek demonstrate that some pieces have been in place for over 100 years, but that there is an overall exponential decline of debris ages, suggesting either that the debris is fairly mobile, or that age-indicators (typically nurse trees) are frequently scoured off of the debris during high-flow events [Buffington and Wood-Smith, in prep.].

Physical characteristics of both the channel and the roughness elements are summarized in Table 3.1. All values presented are reach averages. Many of these parameters show considerable variability, as indicated by the reported standard deviations. Figure 3.7 illustrates the observed ranges of channel width and depth, while Figure 3.8 demonstrates the variability of bar-form amplitude and wave-length. Similarly, Figure 3.9 shows the wave-like changes in downstream channel width that result in wall form-drag.

Measured reach-average velocity

As expected, reach-average velocity at both study sites increases non linearly with stage (Fig. 3.10). The increasing velocity reflects the 'drowning out' of boundary roughness elements (skin friction and topographic form-drag) as the flow rises and moves away from the channel perimeter. The data demonstrate that at Trap Creek, reach-average velocities level-off more rapidly with increasing stage than at Bambi Creek. This may

reflect the difference in wood loading between the two sites. Because wood-debris occurs at a variety of heights within Trap Creek, the flow continuously interacts with it and is not able to 'drown out' this roughness feature.

A sample of the salt concentration curves used to determine reach-average velocity is shown in Figure 3.2. As observed in other studies [Calkin and Dunne, 1970; Church, 1972; Day, 1977], the concentration curves are left-skewed with long declining limbs. The falling limbs of the concentration curves at Trap Creek tended to be longer than those of Bambi Creek due to backwater effects caused by wood obstructions, resulting in temporary storage of portions of the salt-tracer. We initially attempted to measure surface-velocities with plastic fishing bobs, but found that most of the bobs were trapped by wood-forced eddies and were not able to travel more than several tens of meters downstream. The concentration curves tend to become more peaked and narrow with rising stage due to faster travel times of the salt water.

Shear-stress partitioning

Shear-stress calculations for each site are summarized in Table 3.2 and Figure 3.11 and represent reach-average bankfull conditions. In Bambi Creek, the dominant shear stress components are those due to skin friction (τ_{sf}) and bars (τ_b), each comprising roughly similar proportions of the total bankfull boundary shear stress (43-35%, respectively). Although the shear-stress component due to bars is a large proportion of the total stress in Bambi Creek, it is consistent with other field studies which indicate that bar resistance in sand-bed and gravel-bed channels can comprise between 10 to 75% of the total roughness [Parker and Peterson, 1980; Prestegard, 1983; Dietrich et al., 1984; Hey, 1988]. Wall topography (τ_w), cross-sectional form (τ_x), and channel sinuosity (τ_s) are smaller, roughly-equal portions of the total boundary shear stress in Bambi Creek. As expected, the dominant shear stress component in Trap Creek is that due to logs (58% of the total boundary shear stress), while bar roughness is a secondary source of resistance (17% of τ_0). In contrast to Bambi Creek, skin friction is a fairly small component of the total boundary shear stress (9%) and is comparable to resistance caused by wall undulations, cross-sectional form, and channel sinuosity (2-9%) (Table 3.2, Fig. 3.11).

As expected, the roughness length scales increase away from the bed with cumulative addition of roughness elements, and generally parallel the relative magnitudes of the shear stress components (Table 3.2). Despite similar values of grain size, slope, width-

to-depth, channel sinuosity, and amplitude-wavelength ratio of bar forms, the predicted total roughness of Trap Creek is an order of magnitude larger than that of Bambi Creek (Table 3.2) due to differences in wood loading between the two study sites.

Reach-average velocity

Measured and calculated reach-average velocities agree favorably at the two study sites (Table 3.3), verifying the stress-partitioning model and its results. In Bambi Creek, measured and calculated velocities are within 7% of one another, while at Trap Creek they are within 8%. These results are quite encouraging, given the approximate nature of both the measurements and the calculations. The corresponding measured and calculated total roughness length-scales (z_{0T}) are within 9% of one another at Bambi Creek, and within 7% at Trap Creek. The observed errors between measured and calculated roughness length-scales are comparable to those found by Shields and Gippel [1995] in a similar stress-partitioning study of the Obion River (Tennessee, USA) and Tumut River (New South Wales, Australia).

Velocity profiles corrected for roughness elements identified in this study are compared to uncorrected profiles (i.e., those based on skin friction only) (Fig. 3.12). Differences between the profiles underscore the need for roughness-correction before calculating values such as channel conveyance or bed load transport rate in hydraulically-complex forest channels like Bambi Creek and Trap Creek. The approach presented here provides a reliable means of making such corrections. However, because the input parameters of the stress-partitioning model are reach-averages with considerable subreach variability (Table 3.1), the values of shear stress and channel velocity calculated here should be viewed as first-order estimates. More detailed, higher-order analyses would involve calculating stresses on a local obstruction-by-obstruction basis and summing these values through the reach, similar to the approach employed by Wiberg and Smith [1991] for determining particle form-drag in coarse-grained channels. Correction for wake effects (modeled as a velocity defect that recovers exponentially with distance downstream of an obstruction) also may provide insight into the effects of different log architectures (i.e., single-spaced versus clustered pieces of wood).

Grain-size Response to Hydraulic Roughness

Surface grain size of gravel-bed channels is responsive to both bed shear stress (as modified by hydraulic roughness elements) and bed load sediment supply [Buffington and Montgomery, in review (b)]. Using the results of the stress-partitioning calculations we investigated the influence of hydraulic roughness on reach-average bed-surface grain size. In particular, we examined the correspondence between calculated bed stresses and observed grain sizes. Calculated bed stresses were used to predict a competent bed-surface grain size, which was compared with observed values. Grain sizes smaller than the competent size indicate either a limited sediment caliber or a high sediment supply rate [Buffington and Montgomery, in review (b)].

The competent, median, bed-surface grain size for the calculated bankfull bed stress can be determined from the Shields [1936] equation for incipient motion

$$\tau^*_{c50} = \frac{\tau_{c50}}{(\rho_s - \rho) g D_{50}} \quad (3.19a)$$

$$\Rightarrow D_{50} = \frac{\tau_{c50}}{(\rho_s - \rho) g \tau^*_{c50}} \quad (3.19b)$$

where τ^*_{c50} is the dimensionless critical shear stress for the median surface grain size (D_{50}) and τ_{c50} is the corresponding dimensional critical shear stress. Here, we set τ^*_{c50} equal to 0.03 (a conservative value for visually-based studies of initial motion [Buffington and Montgomery, 1997]) and τ_{c50} equal to the calculated value of τ_{sf} . Observed and calculated values of reach-average D_{50} are reasonably similar to one another (Table 3.4), indicating that bed-surface grain size is in near-equilibrium with the applied bankfull bed stress (τ_{sf}). This result suggests that the study sites are not limited by sediment caliber and have relatively low sediment supplies [Buffington and Montgomery, in review (b)].

Conclusion

Our investigation focuses on roughness elements of hydraulically-complex forest gravel-bed rivers. We find that reach-average hydraulic roughness and flow velocity can be successfully predicted from the stress-partitioning model used here. This result is quite encouraging, and may help to dispel the common belief that the complexity of forest channels hinders meaningful investigation of these environments.

We also find that the observed reach-average bed-surface grain size is in good agreement with that predicted for the calculated bed stress, indicating that bed-surface grain size is in quasi-equilibrium with channel hydraulics at our study sites. This equilibrium occurs despite the 'flashy' hydrology of our study basins, suggesting that bed-surface grain size may adjust rapidly to imposed hydrology. Because bed-surface grain size can be responsive to both channel roughness and sediment supply [Buffington and Montgomery, in review (b)], the ability to accurately calculate bed shear stress (as presented here by the partitioning model) is important in order to separate grain size response to hydraulic roughness from that due to variations in sediment supply. However, we emphasize that our calculations are based on reach-averages and are therefore of an approximate nature. In detail, local bed-surface grain size, hydraulic resistance, and sediment supply may be very different than the reach-average values [e.g., Buffington and Montgomery, in review (b)]. This detail and local variability of channel conditions may be of primary interest to aquatic biologists. Nevertheless, the stress-partitioning approach presented here can be applied to smaller-scale, subreach investigations, as well.

Table 3.1: Reach-average physical characteristics of the channels and their hydraulic roughness elements

	Bambi Creek	Trap Creek
<u>Bankfull channel geometry</u>		
width, W (m) [§]	4.72 ± 1.47	12.88 ± 2.66
depth, h (m) [§]	0.26 ± 0.07	0.80 ± 0.13
water-surface slope (m/m)	0.0108	0.0077
length, L (m)	79	250
<u>Skin friction</u>		
D_{84} (mm)	$39 \pm 1.11 \phi$	30
<u>Bar form-drag</u>		
height, z_b (m) [†]	0.60 ± 0.16	0.58 ± 0.26
wavelength, λ_b (m)	10.58 ± 3.79	14.18 ± 7.73
height-wavelength ratio, z_b / λ_b	0.06	0.04
<u>Wall form-drag*</u>		
horizontal amplitude, α_w (m)	2.34 ± 0.89	3.79 ± 3.11
downstream wavelength, λ_w (m)	33.78 ± 16.4	31.6 ± 8.09
wall (flow) height-wavelength ratio, h / λ_w	0.01	0.03
<u>Log form-drag</u>		
<i>category 1, $h_t \leq z_b$</i>		
top height, h_t (m)		0.25 ± 0.14
bottom height, h_b (m)		0.06 ± 0.09
area correction factor, K		0.04
drag coefficient, C_{D1}		1.02 ± 0.13
<i>category 2, $h_b < z_b < h_t$</i>		
h_t (m)		0.74 ± 0.13
h_b (m)		0.35 ± 0.17
K		0.03
drag coefficient, C_{D1}		1.04 ± 0.10
<i>category 3, h_b and $h_t > z_b$</i>		
h_t (m)		0.94 ± 0.16 (limited to $h = 0.80$)
h_b (m)		0.73 ± 0.16
K		0.02
drag coefficient, C_{D1}		1.01 ± 0.11

Table 3.1 (continued)

	Bambi Creek	Trap Creek
<u>Cross-sectional form drag</u>		
width-depth ratio, W / h^\ddagger	22.6	17.6
relative bed/wall roughness, z_{0B} / z_{0B}	1	1
<u>Channel sinuosity</u>		
	2.3	2.1

[§] reported values are restricted to the area over the channel bed.

[†] In Bambi Creek z_b is the reach-average maximum bar height, while in Trap Creek z_b is the cross-sectionally and longitudinally averaged bar height (see text). Values of $z_b / 2$ used in equations (3.12b) and (3.13b) are limited to $h = 0.26$ in Bambi Creek.

* reported characteristics are for each side of the channel.

[‡] because the channel banks are often sloped, rather than vertical, the width-depth ratio reported here is for an average of the bed width (i.e., width of the bank bottoms) and bankfull top-width.

Table 3.2: Calculated shear stress components and roughness length-scales

	<u>Bambi Creek</u>	<u>Trap Creek</u>
<i>Shear stress (Pa)</i>		
τ_{sf}	11.8 (43.3)*	5.7 (9.5)
τ_{l_1}	na	10.6 (17.5)
τ_b	9.6 (35.1)	10.3 (17.0)
τ_{l_2}	na	9.0 (14.8)
τ_{l_3}	na	15.5 (25.6)
τ_w	1.8 (6.6)	2.8 (4.6)
τ_x	2.1 (7.8)	5.4 (8.9)
τ_s	1.9 (7.1)	1.3 (2.1)
τ_0	27.2	60.5
<i>Roughness length (m)</i>		
Z_{0sf}	0.0039	0.003
Z_{0sf+l_1}	na	0.018
Z_{0sf+l_1+b}	0.012	0.039
$Z_{0sf+l_1+b+l_2}$	na	0.058
$Z_{0sf+l_1+b+l_2+l_3}$	na	0.089
$Z_{0sf+l_1+b+l_2+l_3+w}$	0.013	0.094
$Z_{0sf+l_1+b+l_2+l_3+w+x}$	0.015	0.104
$Z_{0sf+l_1+b+l_2+l_3+w+x+s}$ (Z_{0T})	0.016	0.106

* values in parentheses are proportions of the total shear stress.

Table 3.3: Comparison of measured and calculated reach-average flow velocities and total channel roughness

	<u>Bambi Creek</u>	<u>Trap Creek</u>
measured velocity (m/s)	0.67	0.57
calculated velocity (m/s)	0.71	0.62
% error	+7.0	+7.9
measured total roughness (m)	0.018	0.115
calculated total roughness (m)	0.016	0.106
% error	-8.5	-7.2

Table 3.4: Comparison of measured and calculated reach-average median bed-surface grain size

	<u>Bambi Creek</u>	<u>Trap Creek</u>
measured D_{50} (ϕ)*	-4.52	-4.00
calculated D_{50} (ϕ)	-4.58	-3.58
% error	+1.4	-10

* is the standard \log_2 unit of grain size measurement [Krumbein, 1936].

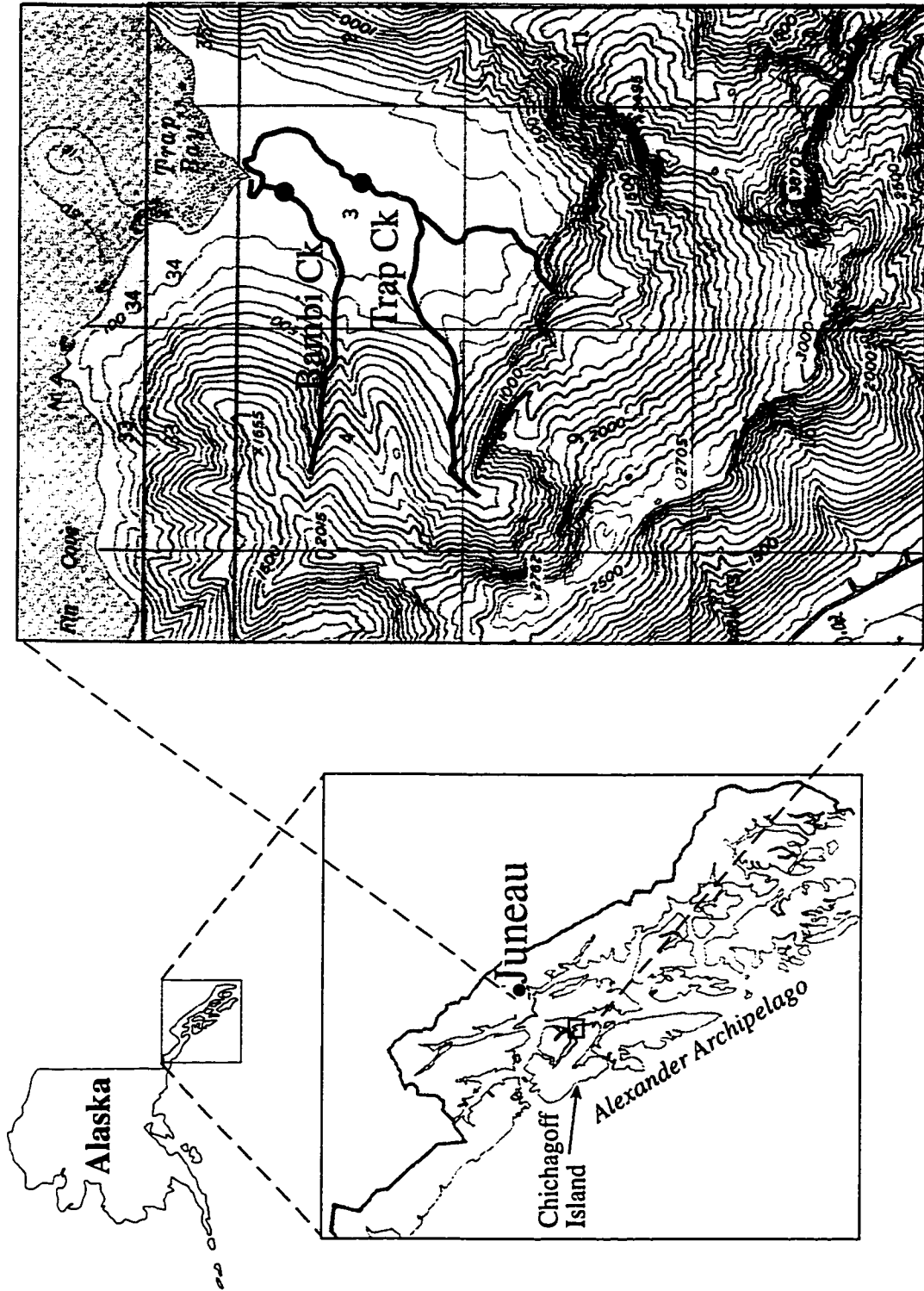


Figure 3.1: Location of study sites.

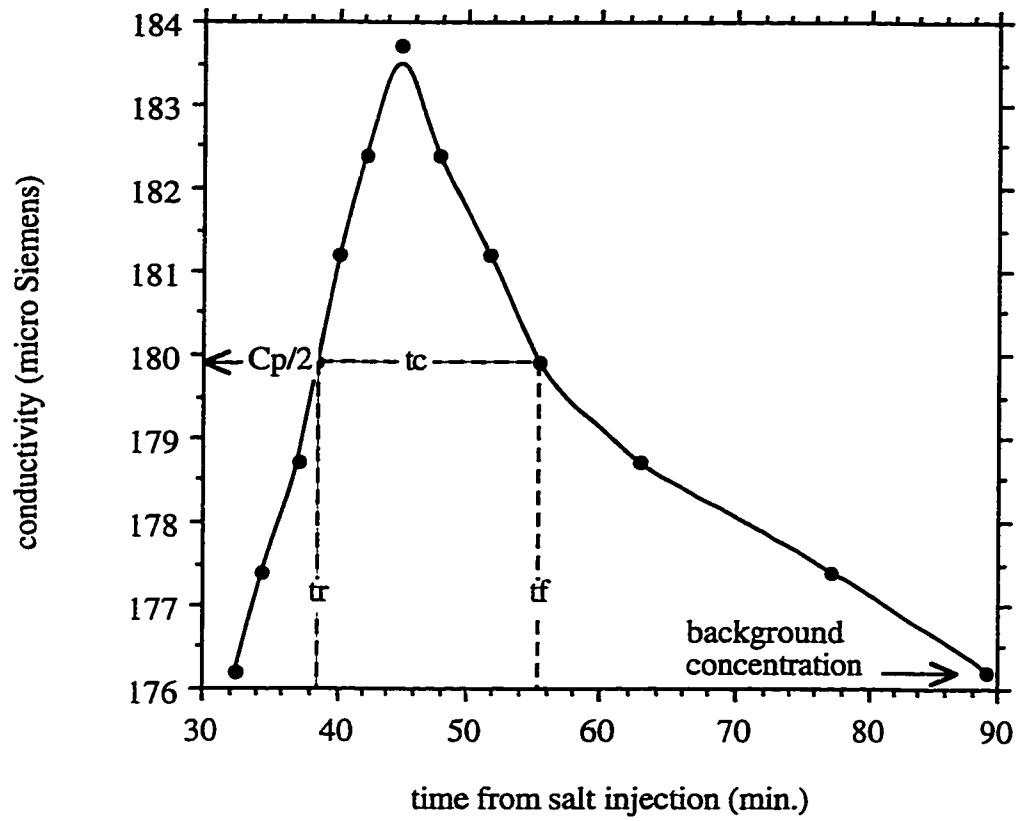


Figure 3.2: Salt-concentration curve from Trap Creek. See text for symbol definitions

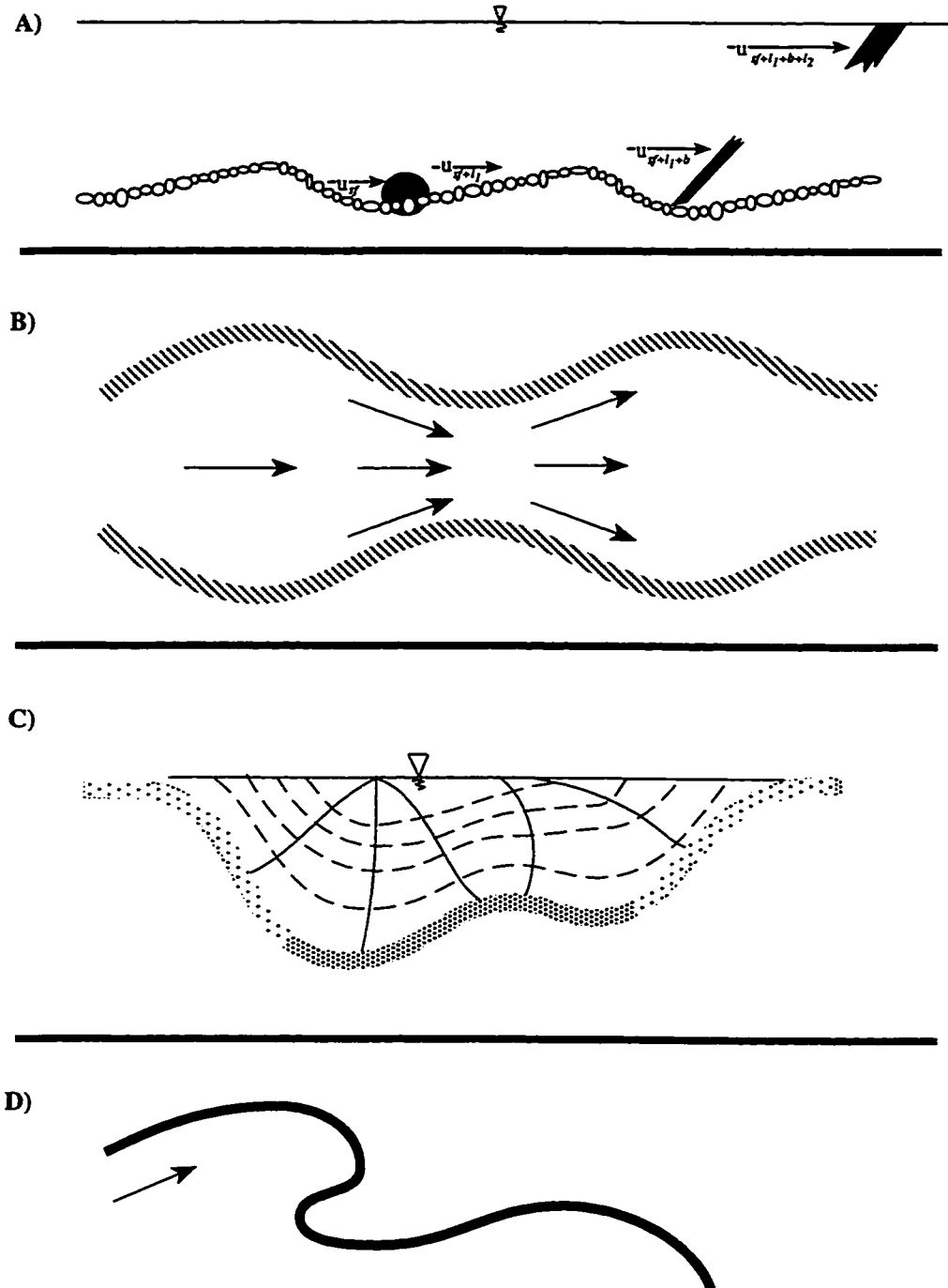


Figure 3.3: Cartoon of successive scales of roughness identified at the study sites.

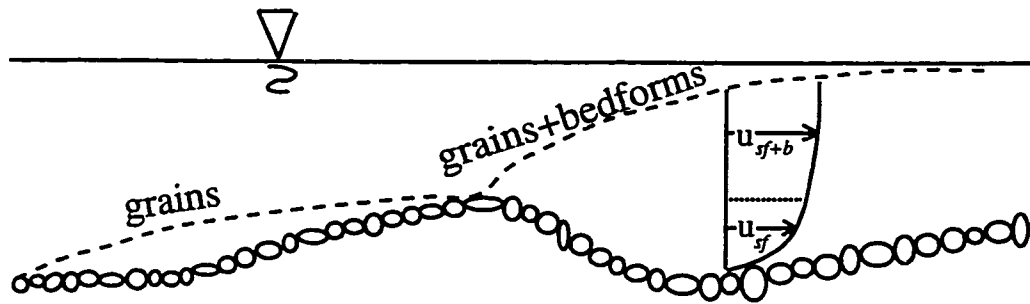


Figure 3.4: Cartoon of boundary layers and successive addition of roughness length-scales in a two-component system of grain skin-friction and bar from-drag.

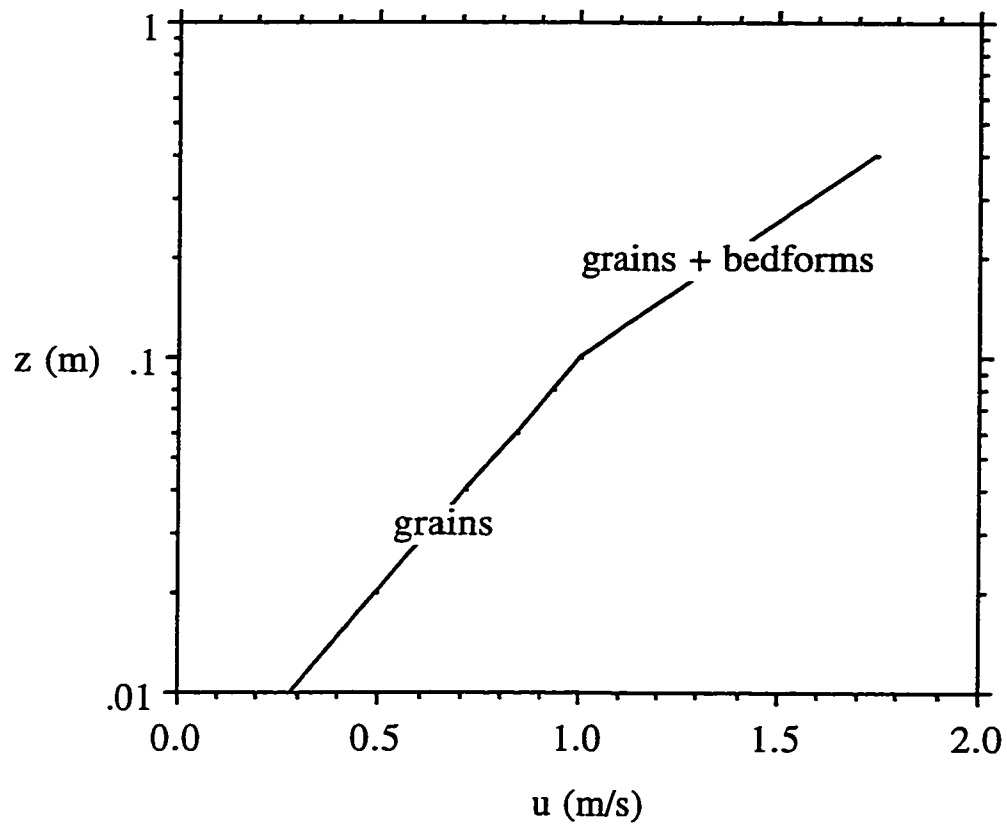


Figure 3.5: Cartoon of a segmented velocity profile in a two-component system of grain and bar-form roughness. The portion of the profile near the bed is influenced by grain skin-friction, while that away from the bed and above the height of the bars is influenced by the combined effects of skin friction and bar form-drag.

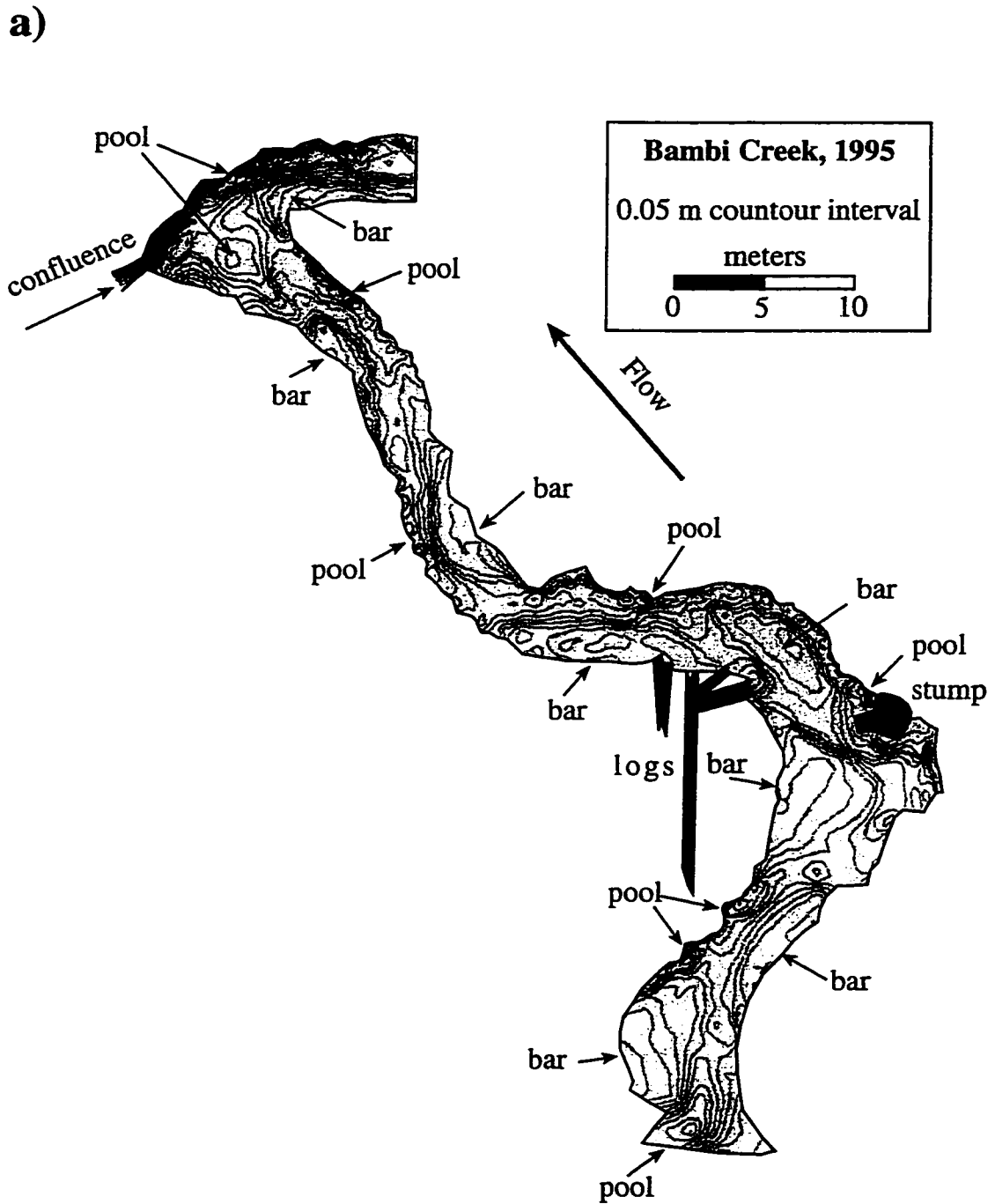


Figure 3.6: Study-site maps of channel topography and wood debris for a) Bambi Creek and b) Trap Creek.

b)

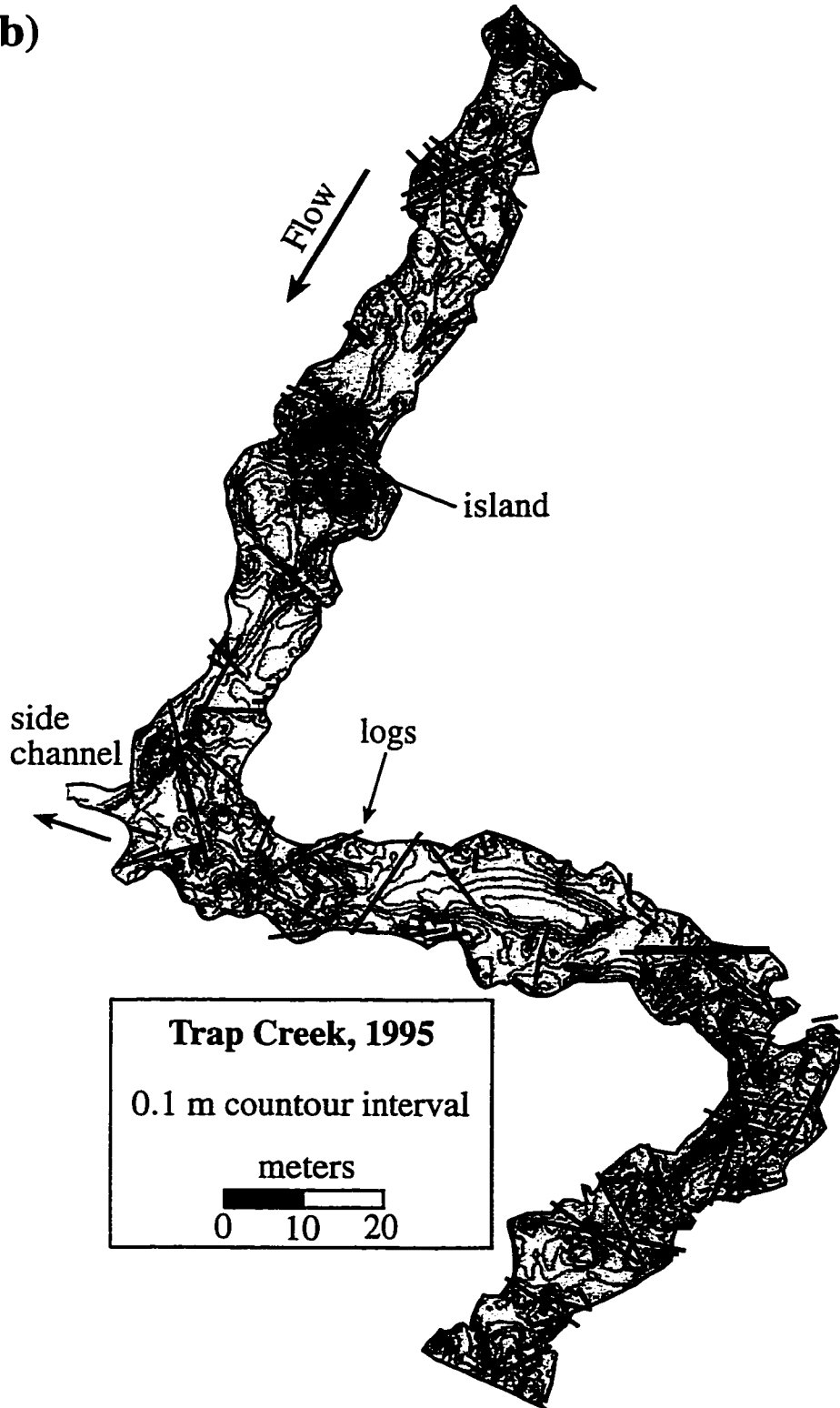


Figure 3.6 (continued)

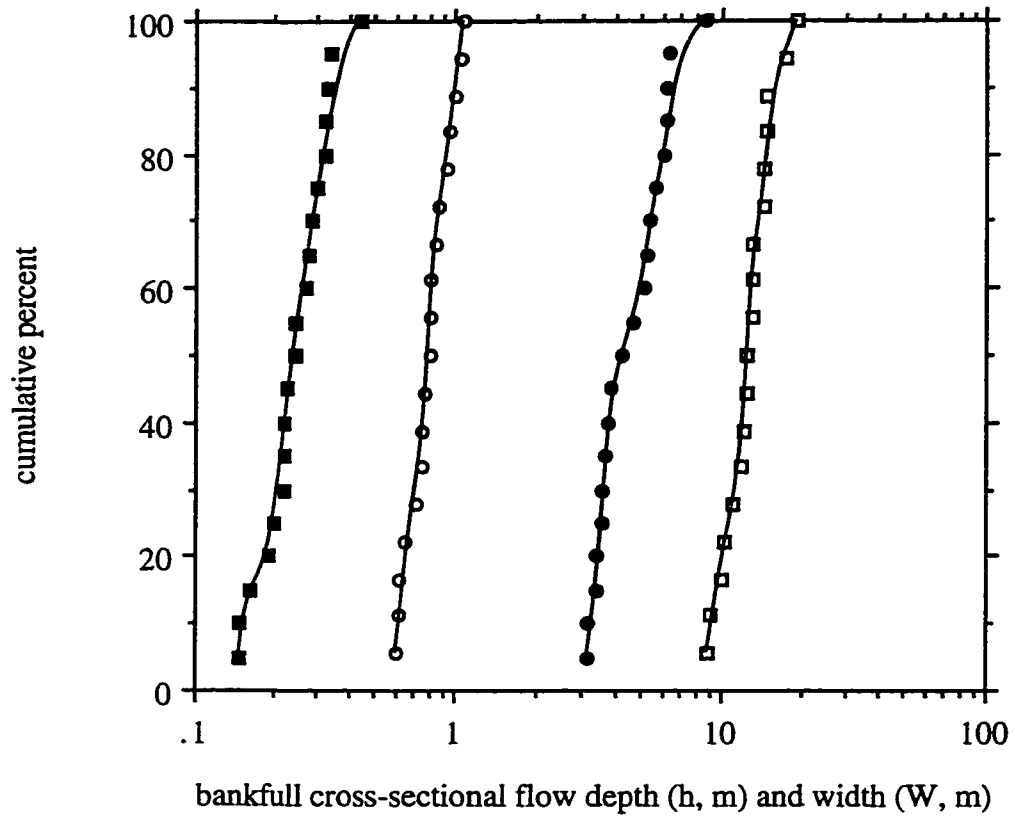


Figure 3.7: Variation of cross-sectional values of bankfull channel width (W , circles) and depth (h , squares) at Bambi Creek (solid symbols) and Trap Creek (open symbols).

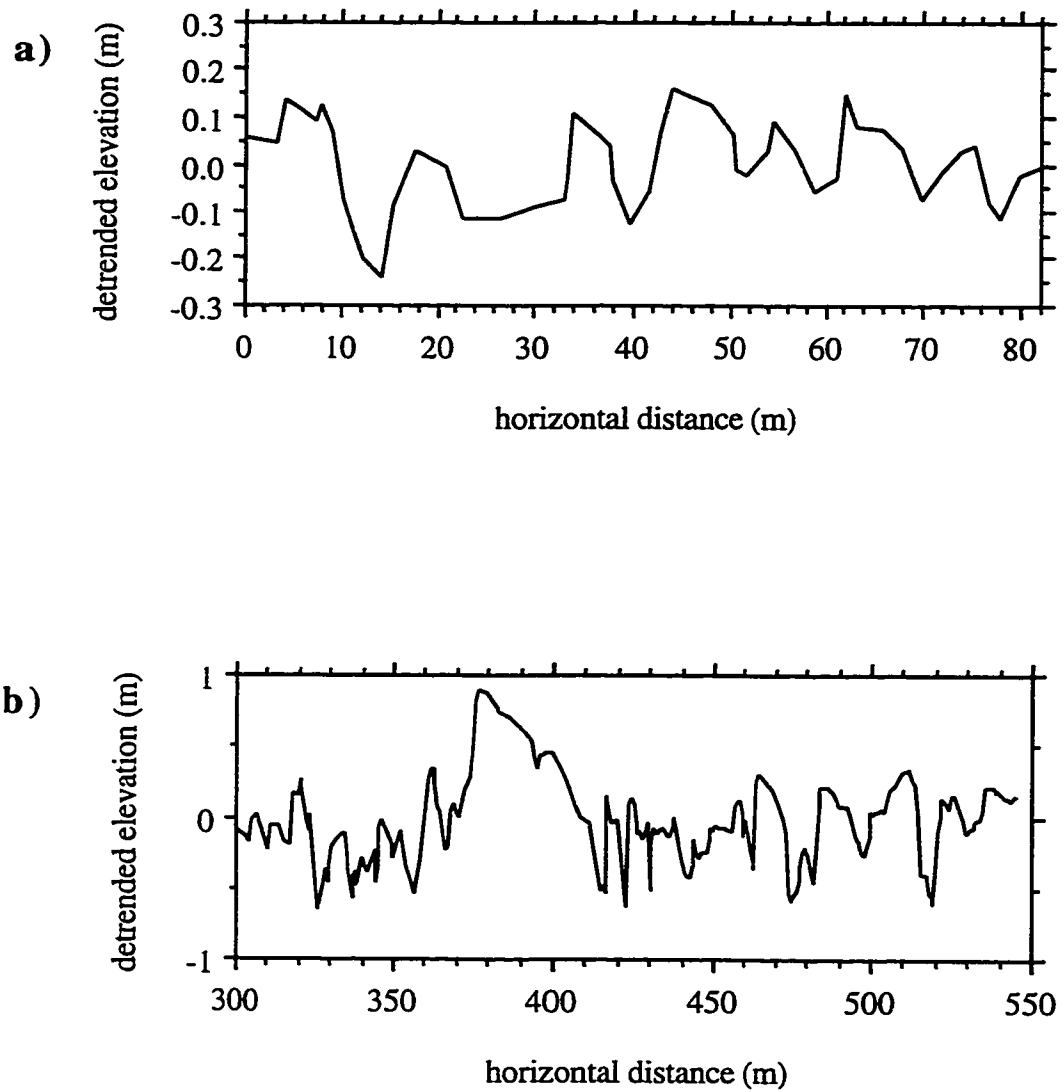


Figure 3.8: Detrended bed-surface profiles of a) Bambi Creek and b) Trap Creek

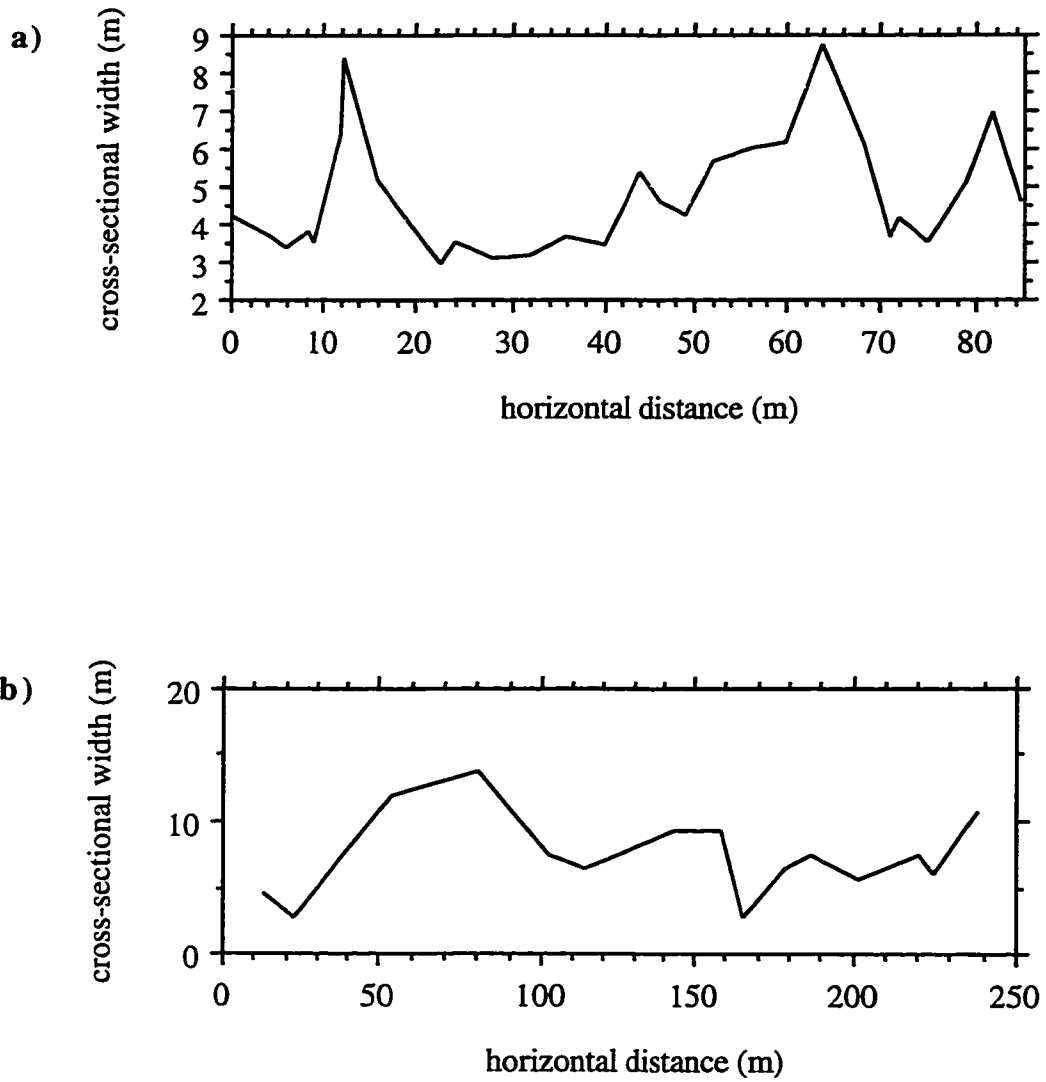


Figure 3.9: Profiles of downstream width undulations at a) Bambi Creek and b) Trap Creek.

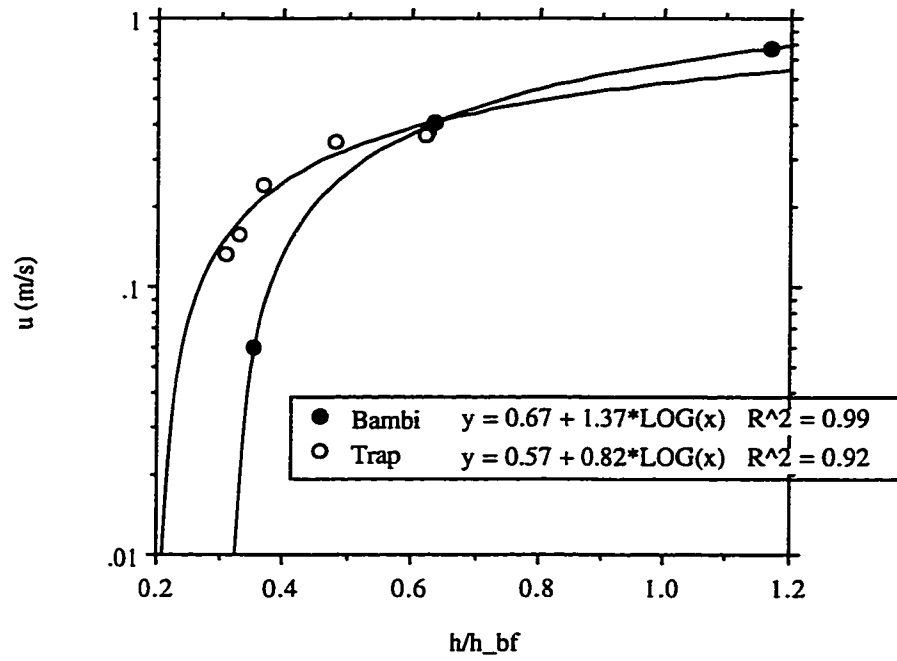


Figure 3.10: Reach-average flow velocity as a function of relative flow depth (h / h_{bf}).

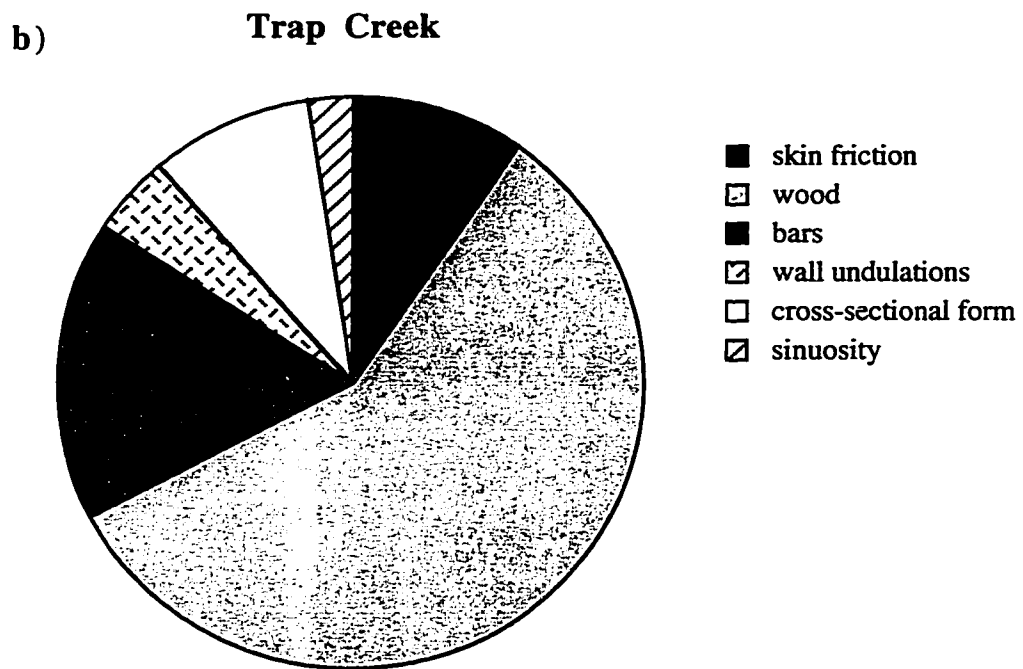
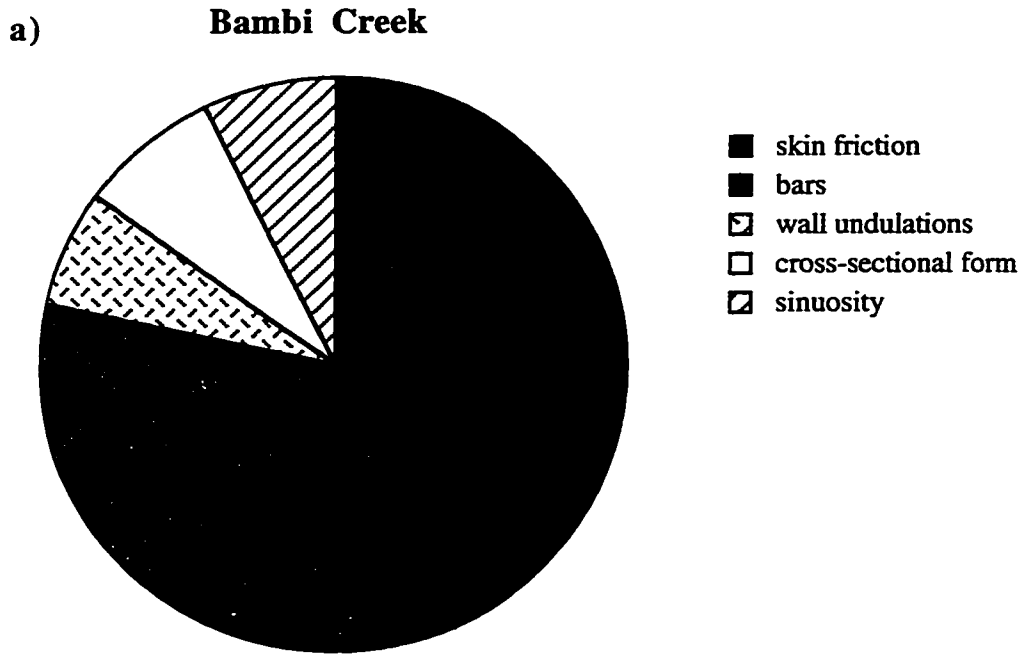


Figure 3.11: Pie charts illustrating the proportion of the total, reach-average, bankfull boundary shear stress represented by each shear-stress component in a) Bambi Creek and b) Trap Creek.

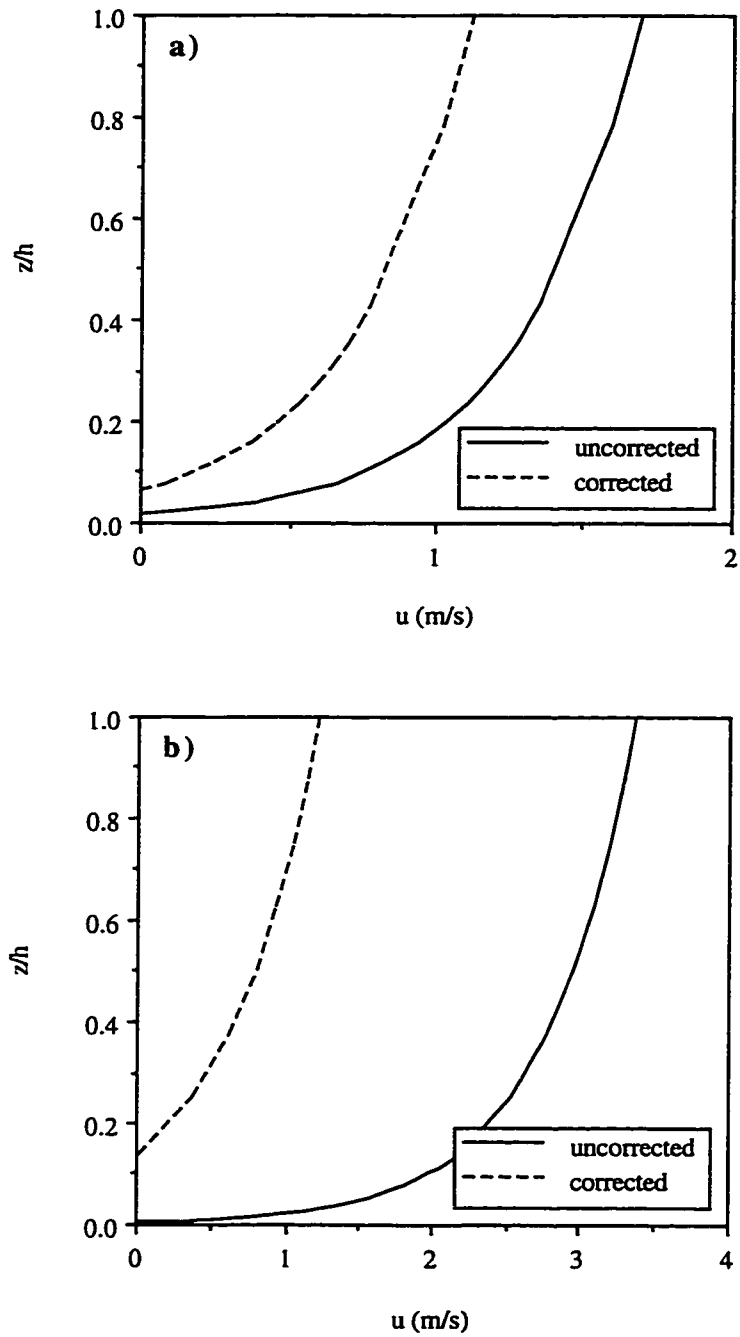


Figure 3.12: Comparison of roughness-corrected velocity profile to that assuming skin friction only in a) Bambi Creek and b) Trap Creek.

Chapter 4: Watershed-Scale Availability Of Salmonid Spawning Habitat As Influenced By Hydraulic Roughness⁴

Overview

A general framework is proposed for assessing hydraulic controls on bed-surface grain size and consequent potential availability of salmonid spawning gravels. Reach-scale predictions of bankfull shear stress and median bed-surface grain size (D_{50}) are integrated via digital elevation models (DEMs) into basin-scale assessments of the availability of spawning habitat in three mountain drainage basins of western Washington, USA. In particular, we investigate the potential effects of bar and wood roughness on bed shear stress, competent D_{50} , and spawning-gravel availability. Results from each watershed are strikingly similar despite differences in basin geology, geomorphic history, and watershed size. Approximately 85% of the total stream length in each study basin is inhospitable for spawning due to slopes $> 4\%$ and associated boulder-bed channel morphologies that are not typically used by anadromous salmonids. Model predictions indicate that spawning-gravel availability is limited to mainstem reaches of each watershed. Of these reaches, only 0-6% are predicted to host spawning gravels when channels are modeled as hydraulically-simple plane-bed reaches. However, an additional 41-73% of this stream length can be opened to spawning if characterized by a pool-riffle morphology and textural fining caused by bar resistance. Another 25-53% may be suitable for spawning if characterized by a wood-forced pool-riffle morphology and textural fining due to the combined effects of bar and wood roughness. Our predictions indicate that bar roughness is important for production of spawning gravels in lower mainstem reaches, while wood roughness may be required for spawning-gravel production in steeper, upper mainstem channels. Wood loss and consequent textural coarsening can deplete one quarter to one half of the potentially-usable spawning area at our study sites.

⁴ Co-authored paper by John M. Buffington, David R. Montgomery, and Harvey M. Greenberg, in preparation for submission to *Canadian Journal of Fisheries and Aquatic Science*.

Introduction

Channel characteristics such as temperature, depth, velocity, percent fines and intra-gravel flow affect selection of salmonid spawning sites [Bjornn and Reiser, 1991], but perhaps the most important characteristic is the physical size of the gravel in which an adult salmonid can excavate a redd. As a family, salmonids prefer to spawn in sediments ranging in size from small gravel to cobble [Kondolf and Wolman, 1993]. The availability of preferred sediment sizes depends on two geomorphic factors: 1) the bed shear stress and competence of the channel as modified by hydraulic roughness elements, and 2) the caliber and rate of sediment input both from upstream sediment sources and channel-margin sources. In this paper, we assess the influence of hydraulic roughness on bed-surface grain size and spawning habitat availability.

Bed-surface sediment of coarse-grained rivers is responsive to the presence of hydraulic roughness elements, such as frictional resistance caused channel walls or form drag caused by channel bars, wood, and boulders [Buffington and Montgomery, in review (b)]. Hydraulic roughness reduces the effective bed shear stress (τ'), which can be expressed as the total boundary shear stress (τ_0) minus roughness-associated stresses other than grain resistance (τ'' , τ''' , etc.)

$$\tau' = \tau_0 - \tau'' - \tau''' - \dots - \tau_n \quad (4.1)$$

The bed stress is that which acts on the grains and is responsible for sediment transport. A simple expression for bed load transport is

$$q_b = k (\tau' - \tau_c)^n \quad (4.2)$$

where q_b is the bed load transport rate, τ_c is the critical shear stress for grain movement, and k and n are empirical values. Roughness elements alter τ' (equation 4.1) and therefore alter the transport capacity of the channel (equation 4.2), which may lead to size-selective erosion or deposition of sediment, resulting in altered bed-surface texture.

Field studies demonstrate that bed-surface texture of forest gravel-bed rivers varies with hydraulic roughness and consequent bed stress [Buffington and Montgomery, in review (b)]. Figure 4.1 shows that reach-average, median bed-surface grain size (D_{50}) of forest channels systematically decreases with greater channel roughness. In this figure,

textural response is evaluated relative to a theoretical prediction of the competent median grain size (i.e., largest mobile D_{50}) for bankfull flow. The competent median grain size is determined from the Shields [1936] equation which is a force balance for assessing the onset of sediment motion in wide, planar channels (i.e., ones with low hydraulic resistance) and is defined as

$$\tau^*_{c50} = \frac{\tau_{c50}}{(\rho_s - \rho) g D_{50}} \quad (4.3)$$

where τ_{c50} is the critical shear stress for movement of D_{50} , ρ and ρ_s are the fluid and sediment densities (set equal to 1000 kg/m^3 and 2650 kg/m^3 , respectively), g is the gravitational acceleration, and τ^*_{c50} is the dimensionless critical shear stress for D_{50} (an empirical parameter set equal to 0.03, a conservative value for visually-based studies of incipient motion [Buffington and Montgomery, 1997]). Rearranging equation (4.3) allows theoretical prediction of the competent D_{50} for a given bed shear stress ($\tau' \equiv \tau_{c50}$)

$$D_{50} = \frac{\tau'}{(\rho_s - \rho) g \tau^*_{c50}} \quad (4.4)$$

Here, we predict the competent D_{50} for a bed shear stress approximated by the total bankfull boundary shear stress ($\tau' \approx \tau_0 = \rho g h S$, where h and S are channel depth and slope, respectively)

$$D_{50} = \frac{\rho g h S}{(\rho_s - \rho) g \tau^*_{c50}} \quad (4.5)$$

Use of the total boundary shear stress in equation (4.5) assumes the absence of hydraulic resistance other than grain skin friction (i.e., $\tau' \approx \tau_0$ in equation 4.1), and establishes a theoretical, end-member reference condition for low hydraulic roughness (i.e., for a wide, planar channel) [Buffington and Montgomery, in review (b)]. Moreover, because we define $\tau' \approx \tau_0$, equation (4.5) predicts the maximum competent D_{50} for bankfull flow. Actual occurrence of this theoretical value of D_{50} also depends on the sediment supply rate and caliber [Buffington and Montgomery, in review (b)].

Also shown in Figure 4.1 are typical ranges of median grain sizes preferred by different salmonid species for spawning [data from Kondolf and Wolman, 1993]. Comparison of these preferred median grain sizes with the observed textural response to bar and wood roughness indicates that hydraulic resistance can provide an important control on the availability of spawning gravels. In particular, hydraulic roughness that reduces bed shear stress and causes textural fining may create suitable spawning habitat in channels that would otherwise be too coarse for use by spawning salmonids.

Here, we examine the potential effect of hydraulic roughness on spawning habitat availability in several Pacific Northwest watersheds. We assess basin-scale availability of salmonid spawning gravel based on field observations and theoretical predictions coupled via digital elevation models (DEMs). Field relationships between channel depth and drainage area are combined with DEM river-slopes to predict reach-average bankfull shear stress and competent median bed-surface grain size using equation (4.5). Spawning habitat availability is assessed by comparing predicted values of D_{50} with those generally preferred by salmonids (Fig. 4.1). Empirical data obtained from forest pool-riffle channels (Fig. 4.1) are used to assess the potential effects of bar and wood roughness on bed shear stress, competent D_{50} , and potential spawning habitat availability compared to that predicted for a simple plane-bed morphology (i.e., equation 4.5).

Our analysis is purposefully general, investigating potential hydrologic controls on grain size and consequent extent of salmonid spawning habitat. Our intent is to provide a general framework for assessing potential availability of spawning habitat, on top of which basin-specific and species-specific issues can be overlain.

Study Sites

We examined potential spawning habitat availability in three mountain drainage basins of western Washington, USA: the Boulder River watershed, the Finney Creek basin, and the Willapa River watershed. The Boulder River (a tributary to the North Fork Stillaguamish River) and Finney Creek (a tributary to the Skagit River) are located near each other in the Cascade mountain range north of Seattle, while the Willapa River is located along the Pacific coast south of Seattle (Fig. 4.2). The drainage networks of the Boulder River and Finney Creek watersheds are characterized by a variety of alluvial channel types, ranging from lower-gradient plane-bed and pool-riffle channels to steeper-gradient step-pool and cascade channels [Montgomery and Buffington, 1997]. In contrast,

the channels of the Willapa basin are a mixture of alluvial and bedrock reaches, with many of the alluvial channels forced by large wood jams on slopes that otherwise would not support alluvial deposits [Massong, 1998].

These three basins were chosen because they represent a broad range of lithology, geologic history, and physical size. The Boulder River and Finney Creek are underlain by Cretaceous metamorphic rocks (folded and foliated phyllite, greenschist, and argillitic mélanges) and glacial sediments derived from Pleistocene ice-sheet advances [Tabor et al., 1988]. In contrast, the Willapa River is incised into Tertiary marine sediments (sandstones, siltstones, and mudstones) and Eocene marine basalts [Massong, 1998]. The glacial histories of the basins also differ. Both the Boulder River watershed and the Finney Creek basin contain abundant ice-sheet deposits from Pleistocene glaciation, while the Willapa watershed escaped glaciation due to its position south of the Pleistocene ice-sheet advance. The physical size of the study basins also differs. The drainage area of the Boulder River watershed (63 km²) is roughly half the size the Finney Creek basin (128 km²), which is, in turn, more than five times smaller than the Willapa River watershed (679 km²). These three basins also were selected because of the availability of high-quality digital elevation data (10 m grid-cell resolution), as well as the availability of basin-specific relationships between drainage area and bankfull depth (necessary to drive the shear stress and grain size predictions).

Methods

Preferred spawning gravels —We used Kondolf and Wolman's [1993] data (Fig. 4.1) to define a general range of median grain sizes preferred by salmonids as a family. The range of median grain sizes usable for spawning was defined as 7–47 mm based on the upper and lower limits of the inner and outer quartiles (25th and 75th percentiles) of the reported median grain-size distributions; the quartiles are indicated by open circles on the grain-size distributions of Figure 4.1. Although salmonids can spawn in both smaller and larger median grain sizes than the selected range, these values represent a central tendency of sizes used by salmonids as a whole.

Usable plane-bed channels —Digital elevation models of each basin were coupled with equation (4.5) to predict the location of plane-bed channels with usable spawning gravels ($D_{50} = 7\text{--}47$ mm). DEMs with 10 m grid-cells were constructed from USGS 7.5' quadrangle contour-files for each study basin using ARC/INFO. For the Finney Creek

basin, channel segments were determined from the DEM. Following the approach suggested by Montgomery and Foufoula-Georgiou [1993], cells were classified as streams if the product of slope and contributing area squared exceeded 50,000 m². For both the Boulder and Willapa watersheds, stream segments were defined by the Washington State Department of Natural Resources hydrology coverage, which is based on channels occurring on the 7.5' topographic maps and supplementary inspection of aerial photographs. For all basins, the 40 ft contours were used to define channel-segment lengths. These segments were further divided at tributary confluences that occurred between contour intervals [Greenberg, 1997].

Assuming a plane-bed morphology throughout each basin, equation (4.5) was used to predict reach-average median grain size. Spawning habitat availability was assessed by comparing predicted values of D_{50} with those preferred by salmonids (7-47 mm). Because the study basins are typically quite steep with relatively shallow flow over the bed-surface grains, we modified equation (4.5) to correct for particle form-drag (so-called 'relative roughness' effects, D_{50}/h) which provides an additional source of hydraulic resistance that reduces τ' (equation 4.1) and therefore reduces the competent D_{50} (equation 4.5). Particle form-drag generally becomes a significant source of roughness for values of $D_{50}/h > 0.2$. Based on Mizuyama et al.'s [1977] data (see analysis by Buffington and Montgomery [in review (b)]) we suggest a relative roughness correction of the form

$$\tau^*_{c50}' = \tau^*_{c50} 10^{(0.22 D_{50} / h)} \quad (4.6)$$

where τ^*_{c50}' is the effective dimensionless critical shear stress. A general solution for equation (4.6) is found by re-writing equation (4.5) as a relative roughness, expressed as a function of the effective dimensionless critical shear stress

$$\frac{D_{50}}{h} = \frac{\rho S}{(\rho_s - \rho) \tau^*_{c50}'} \quad (4.7)$$

and iterating equations (4.6) and (4.7) for a given channel slope. For $\tau^*_{c50} = 0.03$, this procedure yields

$$\tau^*_{c50}' = 0.03 + 0.236 S \quad (4.8)$$

Equation (4.5), re-written in terms of the effective dimensionless critical shear stress, is therefore

$$D_{50} = \frac{\rho g h S}{(\rho_s - \rho) g (\tau_{c50}^* + 0.236 S)} \quad (4.9)$$

Prediction of D_{50} from equation (4.9) requires determination of channel slope and flow depth. Channel slope was determined from the constructed DEMs. Flow depth was determined from field relationships between bankfull depth (h) and drainage area (A) (Fig. 4.3). The depth-drainage area relationships are power functions of the form

$$h = \alpha A^\beta \quad (4.10)$$

where α and β are basin-specific empirical parameters reflecting climate, lithology, geologic history, and consequent architecture of the drainage network. Substituting this relationship into equation (4.9), yields the following general equation for grain-size prediction driven by DEM slopes and drainage areas

$$D_{50} = \frac{\rho (\alpha A^\beta) S}{(\rho_s - \rho) (\tau_{c50}^* + 0.236 S)} \quad (4.11)$$

Based on salmonid preference for gravel-bed and cobble-bed rivers, we limited our analysis of spawning habitat availability to channels with slopes between 0.1% and 4% (typical of plane-bed and pool-riffle morphologies [Montgomery and Buffington, 1997; 1998]). Alluvial channels with slopes greater than 4% tend to have boulder beds (step-pool and cascade morphologies) [Montgomery and Buffington, 1997; 1998] that are generally inhospitable for spawning salmonids. Although salmonids (particularly resident species) do spawn in gravel and cobble patches that occur in local backwater areas and low shear-stress environments in these steep channels [e.g., Kondolf, 1991], salmonids typically prefer lower-gradient plane-bed and pool-riffle channels.

Usable pool-riffle channels —For channel slopes of 0.1-4%, equation (4.9) indicates that median grain sizes in the range of 7-47 mm are predicted to occur in plane-

bed channels with $\tau' = \tau_0 = 3\text{-}23$ Pa. Inspection of Figure 4.1 shows that the range of usable spawning gravels (7-47 mm) also can occur in steeper channels with higher shear stresses if additional hydraulic roughness reduces both τ' and bed-surface grain size. In particular, Figure 4.1 indicates that textural fining caused by bar roughness allows pool-riffle channels to host spawning gravels at total shear stresses as large as 140 Pa (roughly five times greater than the upper shear stress for suitable spawning gravels in plane-bed reaches). Similarly, due to the combined effects of bar and wood roughness, spawning gravels can be found in wood-forced pool-riffle channels at total shear stresses as high as 440 Pa (Fig. 4.1). These data suggest that in addition to the usable plane-bed channels predicted from equation (4.11), channel segments with total shear stresses $>23\text{-}140$ Pa could host spawning gravels *if* characterized by a self-formed pool-riffle morphology and textural fining caused by channel bars. Similarly, channels with total shear stresses $>140\text{-}440$ Pa could be usable for spawning *if* characterized by a wood-forced pool-riffle morphology and textural fining resulting from the combined roughness of bars and wood.

Channel types —Based on the above theory and observations we divided each study basin into five channel types, representing channel segments that are potentially usable versus potentially inhospitable for salmonid spawning (Table 4.1). Our analysis assesses spawning habitat availability based on the proportion of each of these channel types within a watershed. Our approach is not meant to predict actual reach-average grain size or actual channel type, but rather to provide an assessment of the maximum potential spawning habitat under ideal morphologic conditions (i.e., conditions that would produce the necessary channel types and grain sizes for the slope and shear stress ranges listed in Table 4.1).

Magnitudes of hydraulic roughness and consequent textural fining depend on site-specific characteristics (i.e., size, frequency, amount, and effectiveness of hydraulic roughness, as well as sediment caliber and availability). Prediction of usable spawning habitat based on the channel types presented in Table 4.1 assumes that the empirical data of Figure 4.1 (in particular the roughness magnitudes and corresponding degrees of textural fining) are generally representative. This assumption is reasonable for our study sites, as they are from the same general geographic and geomorphic provinces as those from which the empirical data are derived [Buffington and Montgomery, in review (b)].

Results

Maps of the study sites and predicted channel-segment types are shown in Figures 4.4-6. In these mountain drainage basins, the largest proportion of channel segments are those with slopes $> 4\%$ (pink segments). These steep segments comprise 85-87% of the total stream length in each watershed (Table 4.1), and are generally inhospitable to spawning salmonids due to boulder-bed channel morphologies. Our predictions indicate that in the remaining stream segments, plane-bed channels containing suitable spawning gravel are quite rare (cyan segments), comprising 0-6% of the stream length with slopes $\leq 4\%$. However, 41-73% of the stream length with slopes $\leq 4\%$ can be opened to spawning if characterized by a pool-riffle morphology and consequent textural fining caused by bar form-drag (green segments). An additional 25-53% of the stream length with slopes $\leq 4\%$ is potentially available for salmonid spawning if characterized by a wood-forced pool-riffle morphology and textural fining resulting from the combined effects of bar and wood form drag (deep blue segments). In these steep watersheds, only 3% of the stream length with slopes $\leq 4\%$ is predicted to have grain sizes too small for spawning (red segments) (Willapa basin, Table 4.1).

Discussion

The results obtained for each watershed are strikingly similar, despite differences in basin lithology, geomorphic history, and physical size. In each basin, roughly 85% of the total stream length is predicted to be ill-suited for spawning due to steep slopes ($> 4\%$) and associated boulder-bed morphologies (i.e., step-pool and cascade channels). Moreover, in each watershed hydraulic roughness is predicted to control more than 90% of the available spawning habitat. The predicted locations of each channel type also are quite similar within each basin. Channel segments with suitable spawning gravels tend to be confined to mainstem reaches (Figs. 4.4-6), with bar roughness important for spawning-gravel production in lower-mainstem reaches, and wood roughness important for production of spawning gravels in the steeper, upper-mainstem channels. The upstream sequence of channel types predicted in this analysis is consistent with that observed in other mountain drainage basins [Montgomery and Buffington, 1997; 1998].

The actual occurrence of the predicted channel types depends on a variety of factors, such as channel slope, sediment supply and caliber, valley confinement, and wood loading. For example, plane-bed channels are rare in many forest environments due to the

preponderance of in-channel wood debris that forces pool-and-bar morphology [Montgomery et al., 1995]. Nevertheless, channel slope frequently is a useful indicator of likely channel type. For example, self-formed pool-riffle channels are most common on slopes of less than 1-2%, while plane-bed channels typically occur in reaches with gradients of 1-3% [Montgomery and Buffington, 1997]. Comparison of typical slope distributions observed in natural pool-riffle and plane-bed channels with those of the segment types identified in this analysis indicates that many of the channel segments classified here as potentially-usable pool-riffle channels have slopes greater than 2% (Fig. 4.7). Consequently, it is unlikely that many of these channels would have a self-formed pool-riffle morphology and the associated bar roughness needed to produce suitable spawning gravels. However, in forest environments these channel segments still could offer potential spawning habitat due to forcing of pool-and-bar morphology by wood debris. This indicates that wood debris may be of even greater importance in creating spawning habitat than suggested by the above analysis. 26-44% of what is identified in this analysis as potentially-usable pool-riffle spawning habitat may require morphologic forcing by wood debris. Similarly, 43-95% of the channel segments identified as potentially-usable plane-bed reaches have gradients either greater than or less than the typical 1-3% range (Fig. 4.7). Therefore it is unlikely that plane-bed channels with suitable spawning gravels would occur in these segments, further reducing the already minor role of plane-bed channels in producing useful spawning-gravel sizes. Slopes of natural wood-forced pool-riffle channels typically span those observed for pool-riffle and plane-bed channels (i.e., < 1-5%) [Montgomery et al., 1995; Montgomery and Buffington, 1997]. This range of observed slopes also spans those of interest in this study (i.e., < 1-4%). Consequently in this analysis, the potential occurrence of wood-forced pool-riffle channels depends more on wood production to the channel network, than channel slope.

Although we focus on the potential availability of salmonid spawning grounds as influenced by hydraulic roughness, the rate and caliber of sediment supply also may be an important control on bed-surface grain size [Buffington and Montgomery, in review (b)]. In particular, increased sediment supply can cause textural fining through size-selective deposition of fine-grained particles. While sediment-related textural fining has the potential to increase spawning habitat extent, it may induce higher embryo mortality, offsetting any potential gains in spawning-habitat availability. Increased sediment supply can cause bed mobility at stages less than bankfull, and thus more frequent scour and a higher probability

of egg excavation [Montgomery et al., 1996]. Furthermore, increased sediment loading may lead to greater interstitial filling of bed material, resulting in reduced intra-gravel flow of oxygen to buried salmonid embryos, as well as creating a physical barrier to emergence [Everest et al., 1987; Chapman, 1988; Bjornn and Reiser, 1991].

Conclusions

Results of our analysis indicate that textural fining due to bar and wood resistance has the potential to dramatically affect the extent of salmonid spawning habitat in mountain drainage basins. In particular, wood roughness can be a first order control on the availability of spawning gravel in steep, upper-mainstem reaches (slopes of 2-4%).

Land management practices of splash damming, riparian clearcutting and 'stream cleaning' have decreased the amount of wood debris in many channels throughout North America. Our results suggest that consequent textural coarsening in response to wood loss may have decreased salmonid spawning habitat availability and may be a factor in historic declines of fish populations. The impact of wood loss can range from significant textural coarsening that may destroy spawning habitat for salmonids in general, to less severe changes in grain size that may alter the species-specific appeal of a given channel reach (i.e., textural coarsening may stimulate a shift in the particular species-type using a given portion of the channel network). Wood loss can further compound impacts on fish populations by decreasing pool frequency and area, and thus the availability of potential rearing habitat [Montgomery et al., 1995; Wood-Smith and Buffington, 1995].

Our analysis is intended to predict potential availability of spawning habitat based on general hydrologic controls on grain size. It is a first-order assessment of basin conditions that is not species specific. Nor does our analysis consider watershed-specific controls on salmonid access to various portions of the drainage network. For example, both the Boulder River watershed and the Finney Creek basin have waterfalls that limit anadromous fish to the lower reaches of each basin. However, because our analysis is purposefully general, basin-specific or species-specific issues can be overlain on our approach.

Although our analysis does not predict actual channel types and grain sizes, it can be used to guide restoration efforts by locating potentially productive, but unrealized, habitat sites. Furthermore, the watershed-scale nature of the analysis can facilitate rapid assessment of financial costs and benefits associated with specific restoration plans.

Alternatively, our approach can be used to reconstruct potential historical extents of salmonid spawning grounds (i.e., spawning habitat prior to anthropogenic disturbance of basin hydrology, wood loading, and geomorphology).

Because our analysis focuses on reach-scale predictions of grain size it should be viewed as a coarse-level quantification of potential spawning habitat. Uncertainties associated model parameters, such as depth-drainage area relationships and DEM prediction of channel slope, prohibit use of our model for detailed, site-specific predictions of shear stress and median bed-surface grain size. Moreover, subreach-scale grain size patches and textural variability (Fig. 4.8) are not captured by this analysis, but may be important factors in spawning-site selection and overall reach suitability. Nevertheless, there is a general association between reach-level channel types and textural-patch complexity. Both the number and frequency of textural patches within a reach increase across plane-bed, pool-riffle, and wood-forced pool-riffle channel types (Fig. 4.9) due to increasing spatial variability of shear stress and sediment supply forced by subreach-scale roughness elements [Buffington and Montgomery, in review (b)]. Consequently, reach-level predictions provide a first-order assessment of habitat quality that has implications for subreach usage. Inoue et al. [1997] found that reach-scale channel morphology provides a dominant control on subreach habitat availability and is a better predictor of salmonid abundance than that obtained from reach-specific channel-unit characteristics.

It is also important to note that our approach is not a dynamic process-response model. Our analysis does not include specific predictions of channel response, and is not intended for that use. While, our predictions can be used to identify potential locations that might benefit from additional roughness (such as the addition of wood debris), a channel may respond in many different ways to this roughness. For example, addition of roughness elements may cause changes in channel width, depth, or slope in addition to, or in place of, the intended effect of textural fining.

Table 4.1: Stream-segment types

Slope	D₅₀ (mm)*	Bankfull τ_0 (Pa)	Description[†]
> 4 %	>> 47	--	step-pool or cascade channel with D ₅₀ much larger than preferred by spawning salmonids
≤ 4%	≤ 7	< 3	dune-ripple or low-gradient pool-riffle channel with D ₅₀ smaller than typically preferred by spawning salmonids
≤ 4%	7-47	3-23	plane-bed channel with suitable spawning gravels
≤ 4%	> 47	> 23-140	pool-riffle channel with suitable spawning gravels
≤ 4%	> 47	> 140-440	wood-forced pool-riffle channel with suitable spawning gravels

* predicted from equation (4.11).

[†] channel types of Montgomery and Buffington [1997; 1998].

Table 4.2: Stream-segment statistics

	Segment types	Percent of stream length*		
		<u>Willapa</u>	<u>Finney</u>	<u>Boulder</u>
$S > 4\%$, $D_{50} >> 47$ mm	boulder-bed step-pool or cascade with D_{50} much larger than preferred	87	85	85
$S \leq 4\%$, $D_{50} \leq 7$ mm	low-gradient pool-riffle or dune- ripple with D_{50} smaller than preferred	3	0	0
$S \leq 4\%$, $D_{50} = 7 - 47$ mm	usable plane-bed	4	0	6
$S \leq 4\%$, $D_{50} > 47$ mm, $23 \leq \tau_0 < 140$ Pa	usable pool-riffle	68	73	41
$S \leq 4\%$, $D_{50} > 47$ mm, $140 \leq \tau_0 < 440$ Pa	usable wood-forced pool-riffle	25	27	53

* the first entries are percentages of the total basin stream length, while the other entries are percentages of the stream length with $S \leq 4\%$.

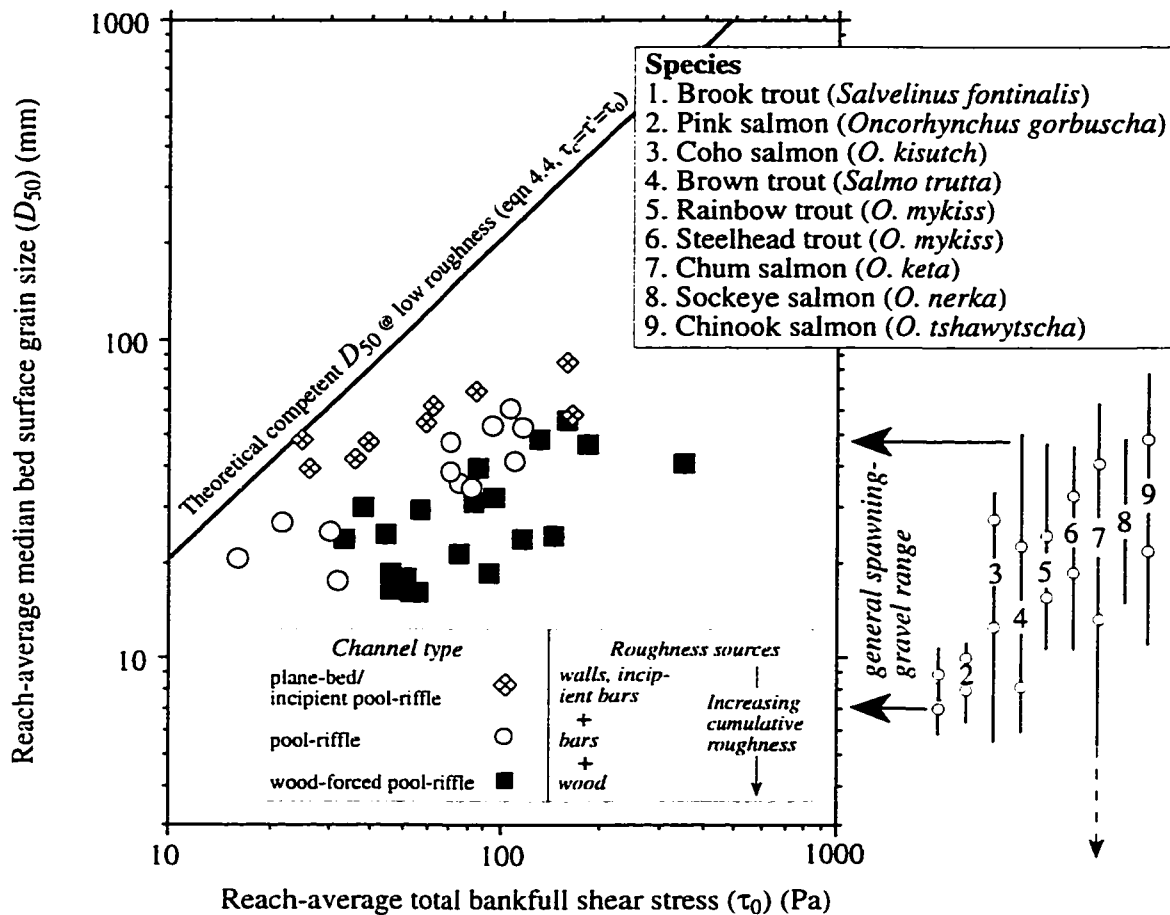


Figure 4.1: Effects of hydraulic roughness on reach-average median bed-surface grain size (D_{50}) (redrafted from Buffington and Montgomery [in review (b)]). For a given total boundary shear stress (τ_0), D_{50} systematically decreases away from the predicted value of competent median grain size (largest mobile D_{50}) with increasing hydraulic roughness and lowered bed stress (τ'). D_{50} ranges preferred by different salmonid species [Kondolf and Wolman, 1993] are shown at the right of the figure, with open circles indicating the inner and outer quartiles of each distribution of median grain sizes.

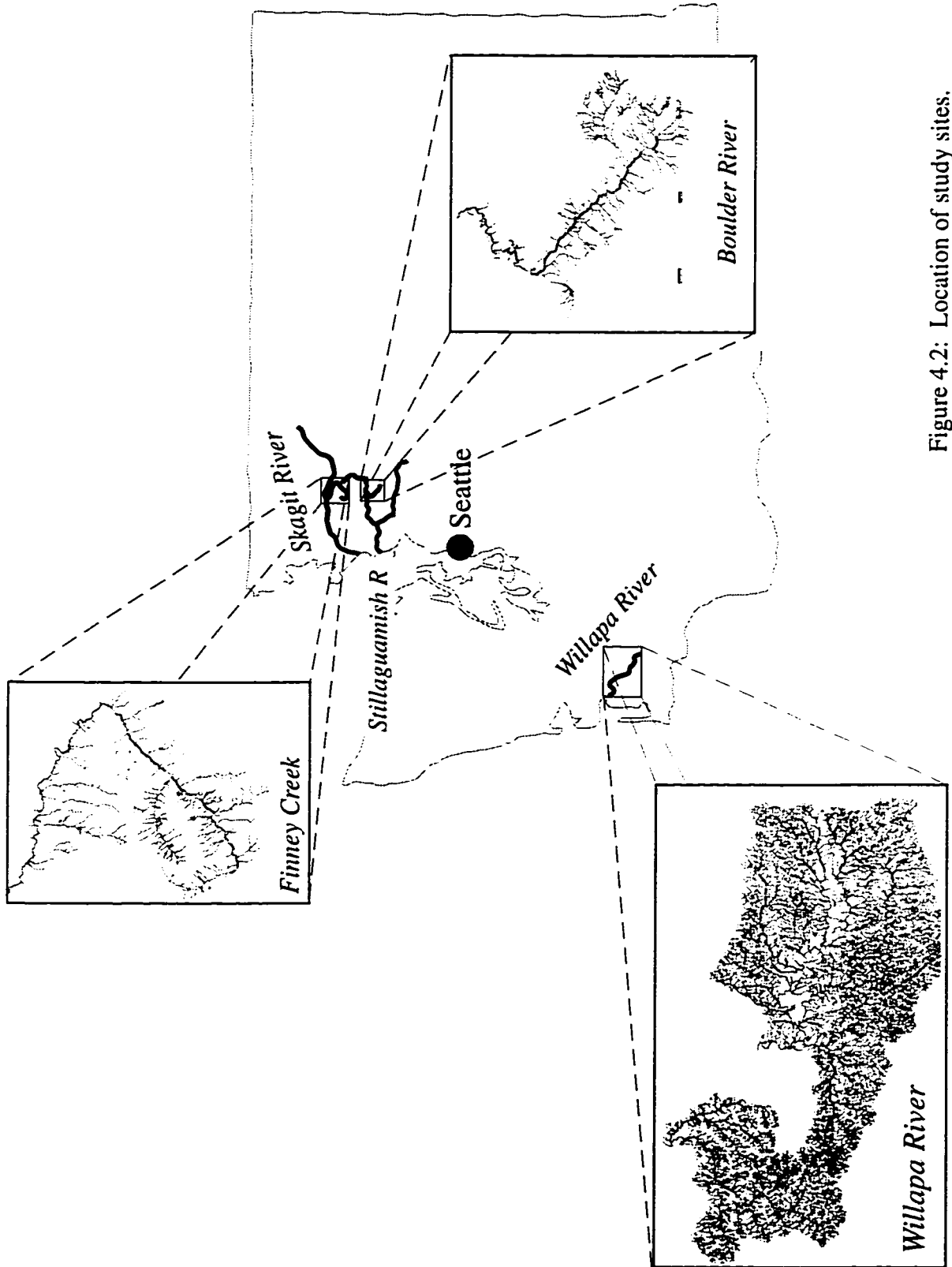


Figure 4.2: Location of study sites.

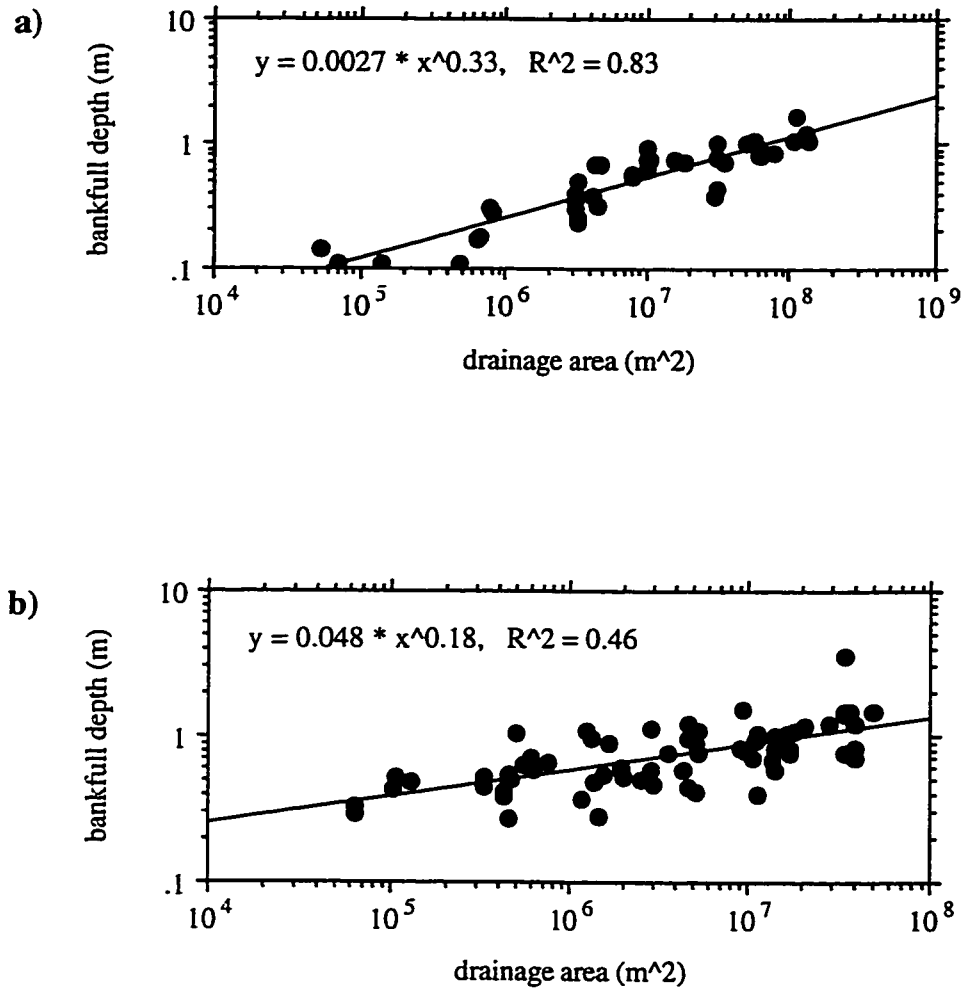
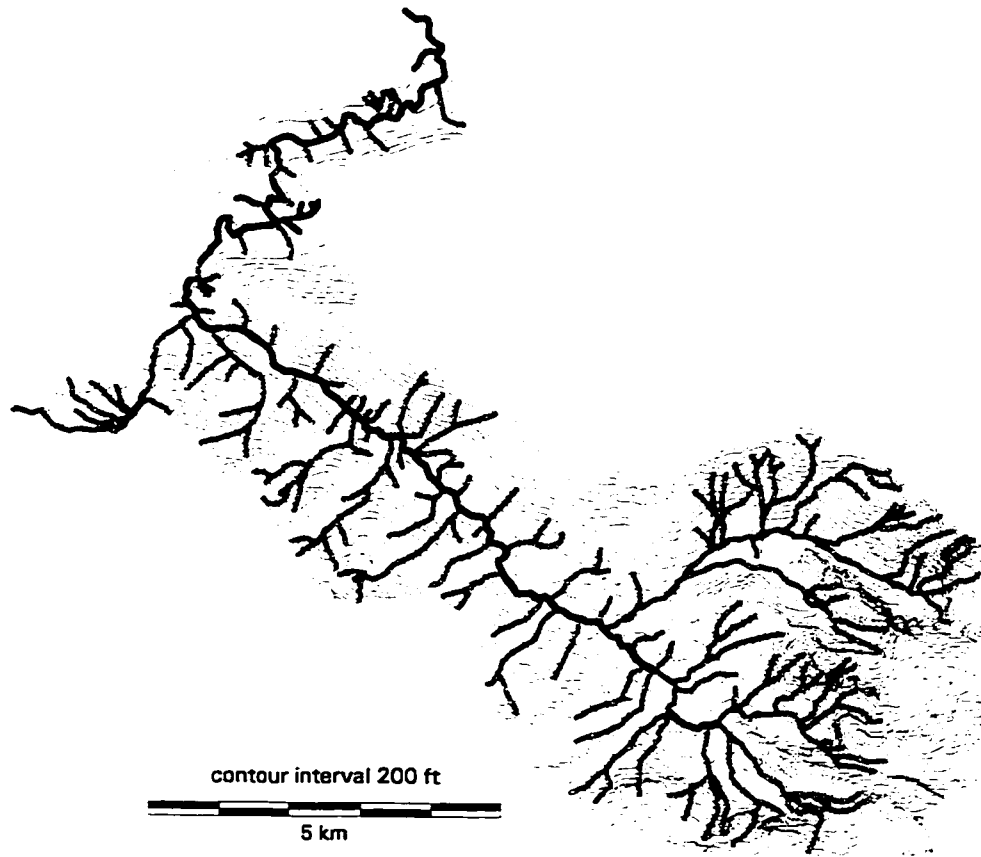


Figure 4.3: Field-relationships between channel depth and drainage area for a) the Boulder River and Finney Creek drainage basins (data from Montgomery et al. [1998]), and b) the Willapa River watershed (data from Massong [1998]).

Figure 4.4: Predicted channel-segment types for the Boulder River watershed. Characteristics of each channel type are presented in Table 4.1. Pink segments (headwater reaches) are generally not preferred by salmonids due to slopes $> 4\%$ and associated boulder-bed morphologies. Cyan segments (lower mainstem reaches) are plane-bed channels with usable spawning-gravel sizes. Green segments (lower mainstem reaches) are usable pool-riffle channels. Deep blue segments (upper mainstem reaches) are usable wood-forced pool-riffle segments. Numbers and lengths of each channel type are listed in the figure key.







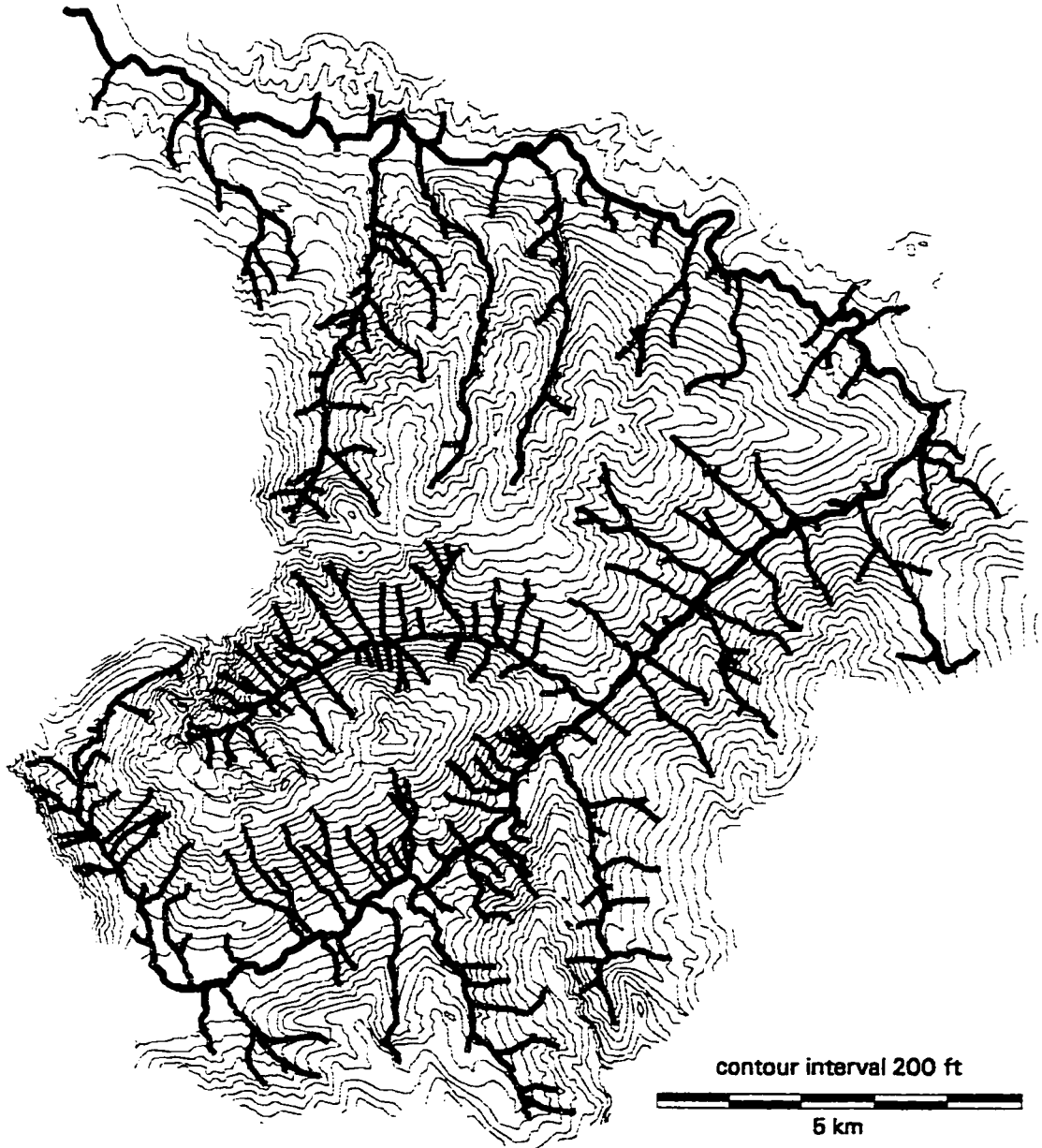
	Slope	Grain	Shear	Number	Length	
	> 4%			4185	123616	not preferred by salmonids
	≤ 4%	> 7 - 47 mm		7	1225	plane-bed
	≤ 4%	> 47 mm	23 - 140 Pa	41	8675	pool-riffle
	≤ 4%	> 47 mm	140 - 440 Pa	70	11290	LWD pool-riffle

Figure 4.5: Predicted channel-segment types for the Finney Creek basin. See Figure 4.4 for explanation of legend.






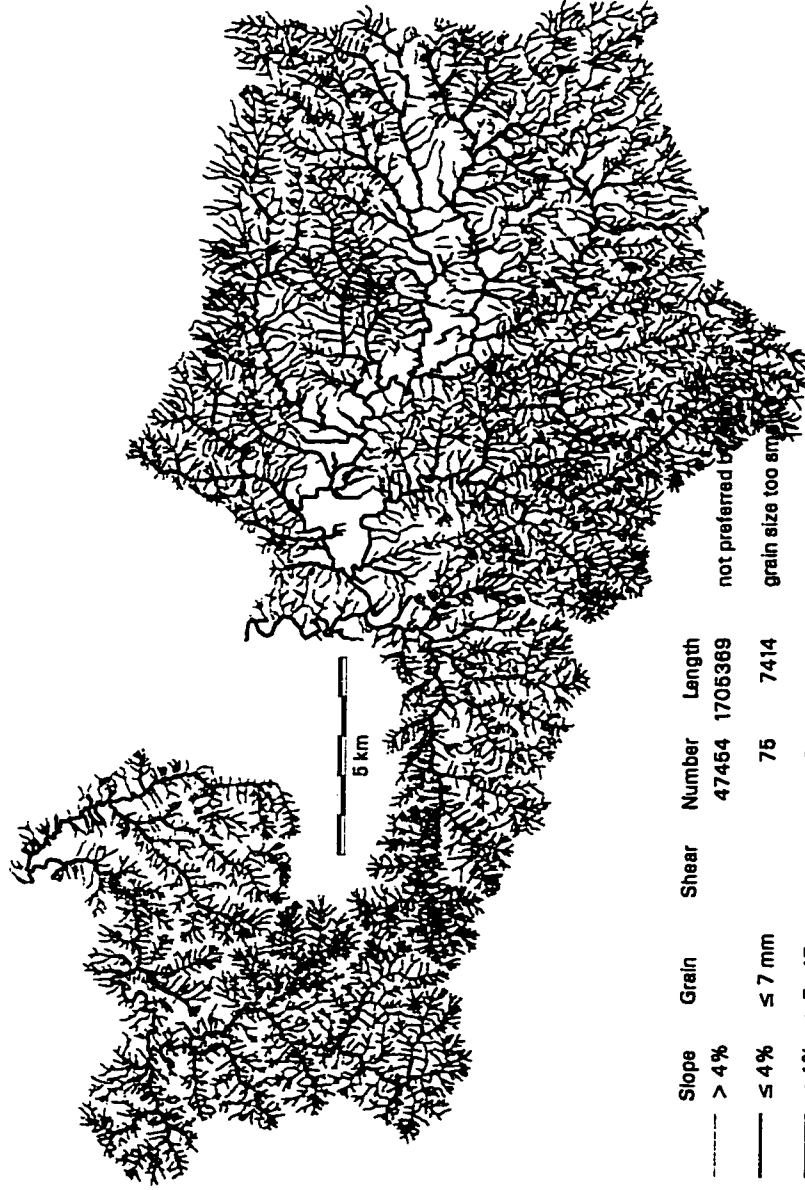
Slope	Grain	Shear	Number	Length	
 > 4%			6494	221213	not preferred by salmonids
 ≤ 4%	>47 mm	23 - 140 Pa	86	27614	pool-riffle
 ≤ 4%	>47 mm	140 - 440 Pa	61	10290	LWD pool-riffle

Figure 4.6: Predicted channel-segment types for the Willapa River watershed. In addition to the channel types discussed in the Figure 4.4 caption, red segments shown here (lower mainstem reaches) are lower-gradient pool-riffle and dune-ripple channels predicted to have grain sizes smaller than those typically preferred by spawning salmonids.



Slope	Grain	Shear	Number	Length	
> 4%			47454	1706369	not preferred to
≤ 4%	≤ 7 mm		75	7414	grain size too small
≤ 4%	> 7 - 47 mm		61	10282	plane-bed
≤ 4%	> 47 mm	23 - 140 Pa	1689	173746	pool-riffle
≤ 4%	> 47 mm	140 - 440 Pa	737	66401	LWD pool-riffle

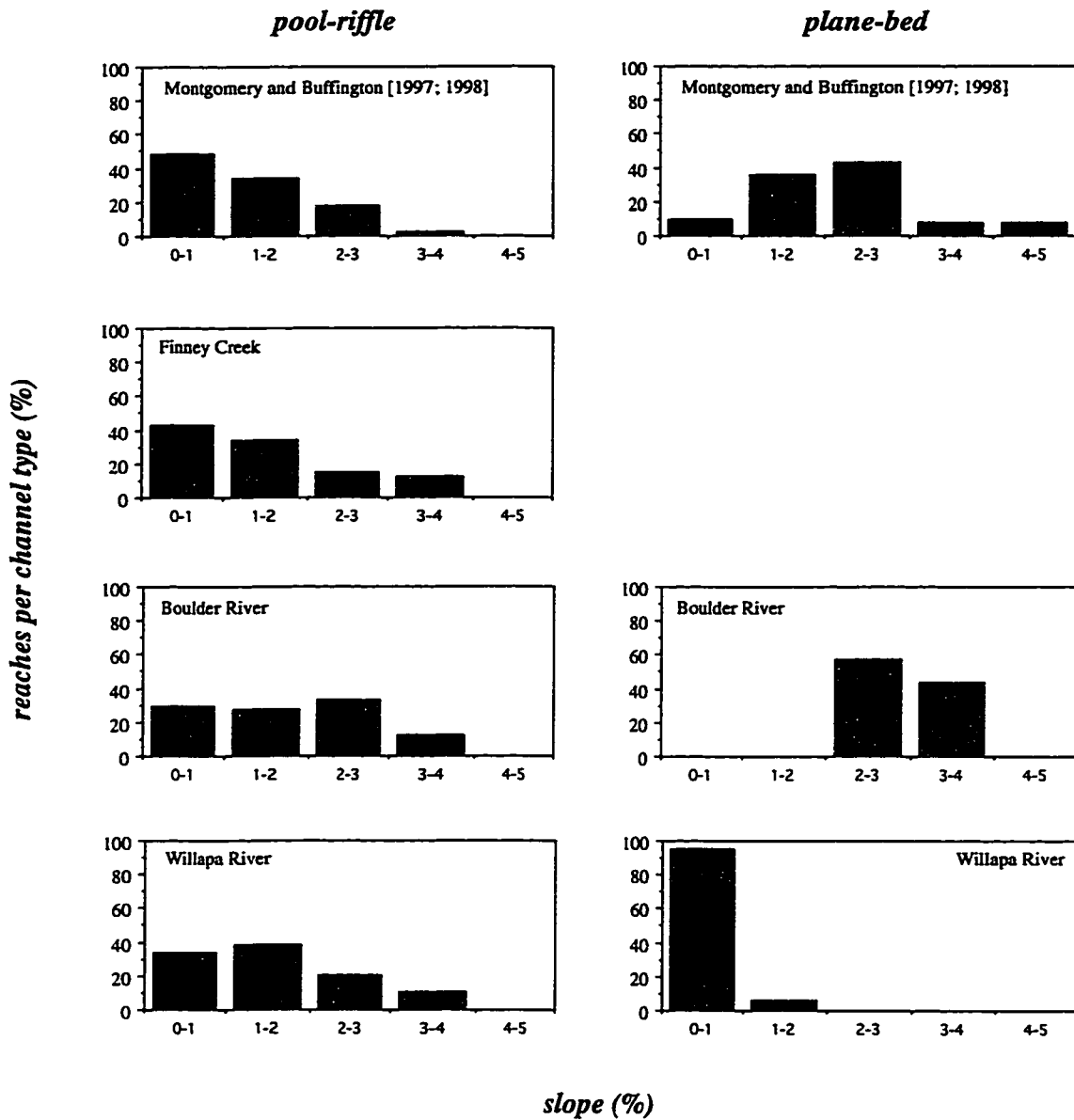


Figure 4.7: Typical frequency distributions of reach slope in natural pool-riffle and plane-bed channels [Montgomery and Buffington, 1997; 1998] compared with slope distributions of pool-riffle and plane-bed segment-types identified in this analysis. Numbers of reaches per channel type in each basin are reported in Figures 4.4-6.

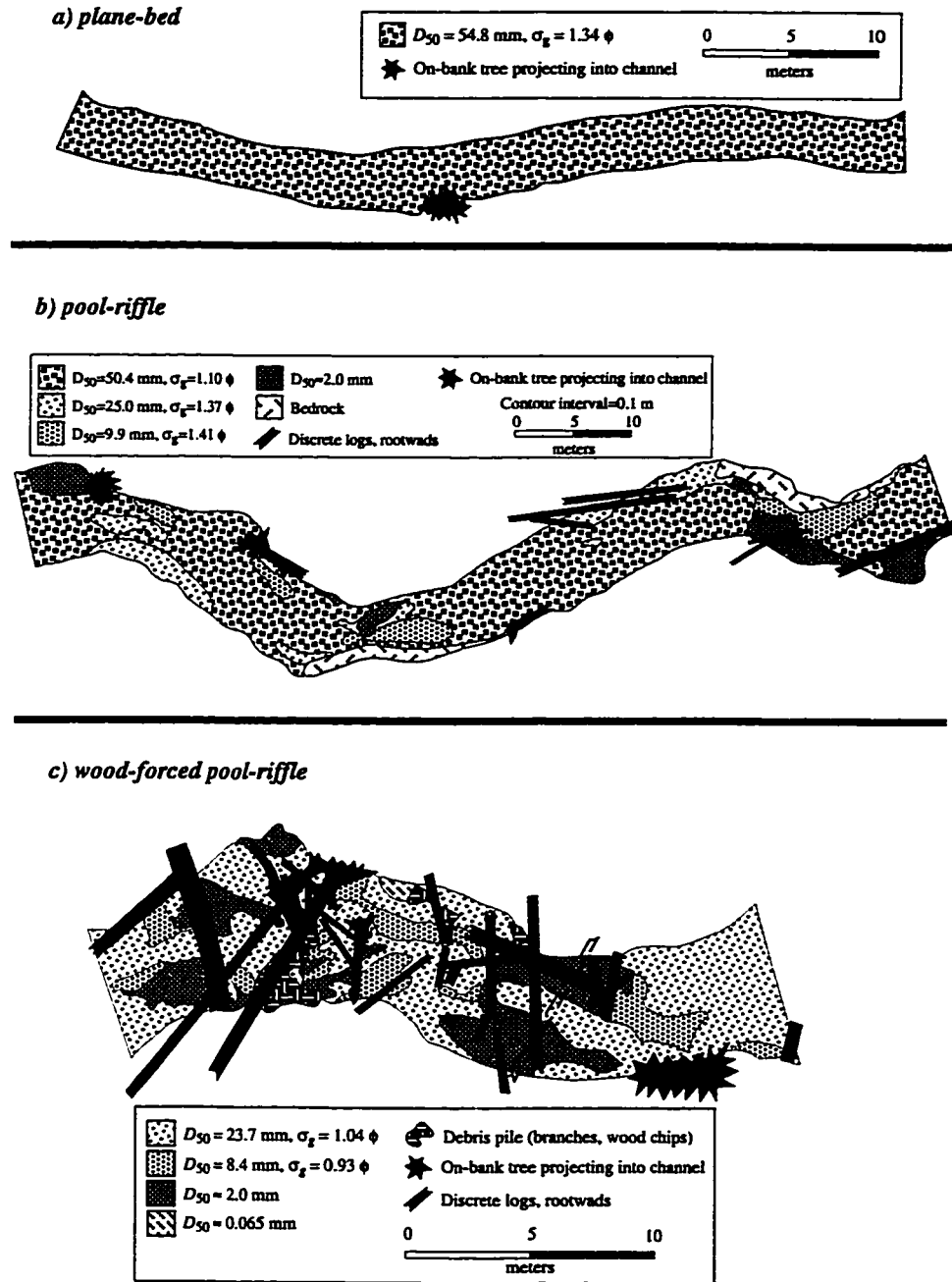


Figure 4.8: Typical textural maps for plane-bed, pool-riffle, and wood-forced pool-riffle channel types redrafted from Buffington and Montgomery [in review (a; b)]. σ_g is Folk's [1974] graphic standard deviation in units of phi [Krumbein, 1936].

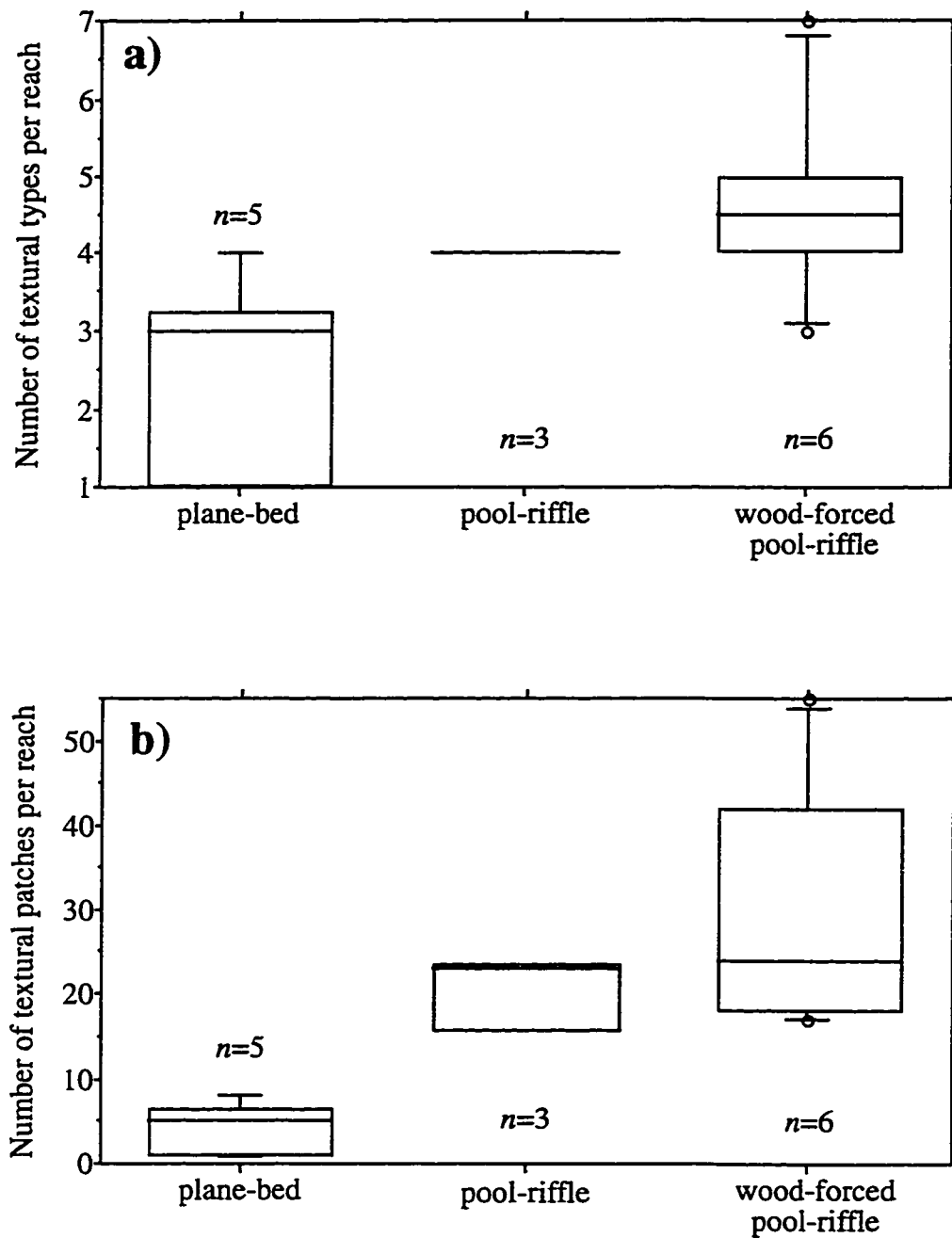


Figure 4.9: Box plots of a) the number of different types of textural patches per reach and b) the total frequency of textural patches per reach in plane-bed, pool-riffle, and wood-forced pool-riffle channels (redrafted from Buffington and Montgomery [in review (b)]). n is the number of channels surveyed per morphologic type.

List of References

- Abrahams, A. D., Luk, S.-H. and Parsons, A. J., Threshold relations for the transport of sediment by overland flow on desert hillslopes, *Earth Surf. Processes Landforms*, 13, 407-419, 1988.
- Andrews, E. D., Bed-material entrainment and hydraulic geometry of gravel-bed rivers in Colorado, *Geol. Soc. Amer. Bull.*, 95, 371-378, 1984.
- Bathurst, J. C., Graf, W. H. and Cao, H. H., Initiation of sediment transport in steep channels with coarse bed material, in *Mechanics of Sediment Transport*, edited by B. M. Sumer and A. Müller, pp. 207-213, A. A. Balkema, Rotterdam, 1983.
- Bevenger, G. S. and King, R. M., A pebble count procedure for assessing watershed cumulative effects, U.S. Dept. Agric., *Forest Service Res. Pap. RM-RP-319*, 17 pp., 1995.
- Bjornn, T. C. and Reiser, D. W., Habitat requirements of salmonids in streams, In: *Influence of forest and rangeland management on salmonid fishes and their habitats*, edited by W. R. Meehan, pp. 83-138, Am. Fish. Soc. Spec. Pub. 19, Bethesda, MD, 1991.
- Buffington, J. M. and Montgomery, D. R., A systematic analysis of eight decades of incipient motion studies, with special reference to gravel-bedded rivers, *Water Resour. Res.*, 33, 1993-2029, 1997.
- Buffington, J. M. and Montgomery, D. R., A procedure for classifying and mapping textural facies in gravel-bed rivers, *Water Resour. Res.*, in review (a).
- Buffington, J. M. and Montgomery, D. R., Effects of sediment supply and hydraulic roughness on surface textures of gravel-bed rivers, *Water Resour. Res.*, in review (b).
- Buffington, J. M., Dietrich, W. E. and Kirchner, J. W., Friction angle measurements on a naturally formed gravel streambed: Implications for critical boundary shear stress, *Water Resour. Res.*, 28, 411-425, 1992.
- Calkins, D. and Dunne, T., A salt tracing method for measuring channel velocities in small mountain streams, *J. Hydrol.*, 11, 379-392, 1970.
- Carling, P., The concept of dominant discharge applied to two gravel-bed streams in relation to channel stability thresholds, *Earth Surf. Processes Landforms*, 13, 355-367, 1988.

- Carling, P. A. and Hurley, M. A., A time-varying stochastic model of the frequency and magnitude of bed load transport events in two small trout streams, In: *Sediment Transport in Gravel-bed Rivers*, edited by C. R. Thorne, J. C. Bathurst and R. D. Hey, pp. 897-920, John Wiley, New York, 1987.
- Chang, H. H., Geometry of gravel streams, *J. Hydraul. Div. Am. Soc. Civ. Eng.*, *106*, 1443-1456, 1980.
- Chapman, D. W., Critical review of variables used to define effects of fines in redds of large salmonids, *Trans. Amer. Fish. Soc.*, *117*, 1-21, 1988.
- Chien, N., The present status of research on sediment transport, *Trans. Amer. Soc. Civ. Eng.*, *121*, 833-884, 1956.
- Chitale, S. V., River channel patterns, *J. Hydr. Div. Amer. Soc. Civ. Eng.*, *96*, 201-221, 1970.
- Church, M., Electrochemical and fluorometric tracer techniques for streamflow measurements, *12*, Brit. Geomorph. Res. Group, 1974.
- Church, M., Channel morphology and typology, In: *The Rivers Handbook*, edited by P. Carlow and G. E. Petts, pp. 126-143, Blackwell, Oxford, 1992.
- Church, M. A., McLean, D. G. and Wolcott, J. F., River bed gravels: Sampling and analysis, in *Sediment Transport in Gravel-bed Rivers*, edited by C. R. Thorne, J. C. Bathurst and R. D. Hey, pp. 43-88, John Wiley, New York, 1987.
- Crowder, D. W. and Diplas, P., Sampling heterogeneous deposits in gravel-bed streams, *J. Hydr. Eng.*, *123*, 1106-1117, 1997.
- Cummins, K. W. and Lauff, G. H., The influence of substrate particle size on the microdistribution of stream macrobenthos, *Hydrobiologia*, *34*, 145-181, 1969.
- Darcy, H. and Bazin, H., Recherches hydrauliques, prem. part., *Mém. Prés. Divers Savants*, L'Institut Impérial de France, 501 pp., 1865.
- Day, T. J., Field procedures and evaluation of a slug dilution gauging method in mountain streams, *J. Hydrol., New Zeal.*, *16*, 113-133, 1977.
- Deer, W. A., Howie, R. A., and Zussman, J., *An introduction to the rock-forming minerals*, 528 pp., Longman, Essex, 1982.
- Dietrich, R. V. and Skinner, B. J., *Rocks and rock minerals*, 319 pp., John Wiley, New York, 1979.
- Dietrich, W. E., Settling velocity of natural particles, *Water Resour. Res.*, *18*, 1615-1626, 1982.

- Dietrich, W. E., Kinerson, D. and Collins, L., Interpretation of relative sediment supply from bed surface texture in gravel bed rivers, *Eos, Trans. AGU*, 74, 151, 1993.
- Dietrich, W. E., Kirchner, J. W., Ikeda, H. and Iseya, F., Sediment supply and the development of the coarse surface layer in gravel-bedded rivers, *Nature*, 340, 215-217, 1989.
- Dietrich, W. E. and Smith, J. D., Bed load transport in a river meander, *Water Resour. Res.*, 20, 1355-1380, 1984.
- Dietrich, W. E., Smith, J. D. and Dunne, T., Flow and sediment transport in a sand bedded meander, *J. Geol.*, 87, 305-315, 1979.
- Dietrich, W. E., Smith, J. D. and Dunne, T., Boundary shear stress, sediment transport and bed morphology in a sand-bedded river meander during high and low flow, in *River Meandering, Proc. of the Conference Rivers '83*, edited by C. M. Elliot, pp. 632-639, Am. Soc. Civ. Eng., New York, 1984.
- Diplas, P. and Sutherland, A. J., Sampling techniques for gravel sized sediments, *J. Hydr. Eng.*, 114, 484-501, 1988.
- du Boys, P., Le Rhône et les rivières a lit affouillable, *Annales Ponts Chaussées, Mémoires Documents, Ser. 5, 18*, 141-195, 1879.
- Einstein, A., Der hydraulische oder profil-radius, *Schweizerische Bauzeitung*, 103, 89-91, 1934.
- Einstein, H. A., Formulas for the transportation of bed load, *Trans. Amer. Soc. Civ. Eng.*, 107, 561-597, 1942.
- Einstein, H. A. and Banks, R. B., Fluid resistance of composite roughness, *Eos Trans. AGU*, 31, 603-610, 1950.
- Einstein, H. A. and Barbarossa, N. L., River channel roughness, *Trans. Amer. Soc. Civ. Eng.*, 117, 1121-1146, 1952.
- Estep, M. A. and Beschta, R. L., Transport of bedload sediment and channel morphology of a southeast Alaska stream, U.S. Dept. Agric., *Forest Service Res. Note PNW-430*, 15 pp., 1985.
- Everest, F. H., Beschta, R. L., Scrivener, J. C., Koski, K. V., Sedell, J. R. and Cederholm, C. J., Fine sediment and salmonid production: A paradox, In: *Streamside Management: Forestry and Fishery Interactions*, edited by E. O. Salo and T. W. Cundy, pp. 98-142, Univ. of Wash. Inst. Forest Res., Seattle, 1987.
- Ferguson, R. I., Prestegard, K. L. and Ashworth, P. J., Influence of sand on hydraulics

- and gravel transport in a braided gravel bed river, *Water Resour. Res.*, 25, 635-643, 1989.
- Fisher, R. A., On a distribution yielding the error functions of several well known statistics, *Proc. Internat. Math. Cong.*, Univ. of Toronto Press, Toronto, 805-813, 1928.
- Flintham, T. P. and Carling, P. A., The prediction of mean bed and wall boundary shear in uniform and compositely rough channels, In: *International Conference on River Regime*, edited by W. R. White, pp. 267-287, Wiley, New York, 1988.
- Folk, R. L., The distinction between grain size and mineral composition in sedimentary-rock nomenclature, *J. Geol.*, 62, 344-359, 1954.
- Folk, R. L., *Petrology of Sedimentary Rocks*, 182 pp., Hemphill Publ., Austin, Tex., 1974.
- Fripp, J. B. and Diplas, P., Surface sampling in gravel streams, *J. Hydr. Eng.*, 119, 473-490, 1993.
- Gehrels, G. E. and Berg, H. C., Geologic map of southeastern Alaska, *U.S. Geol. Surv. Map I-1867*, 1992.
- Gehrels, G. E., McClelland, W. C., Samson, S. D., Patchett, P. J. and Jackson, J. L., Ancient continental margin assemblage in the northern Coast Mountains, southeast Alaska and northwest Canada, *Geol.*, 18, 208-211, 1990.
- Gilbert, G. K., Report on the geology of the Henry Mountains, *U.S. Geograph. and Geol. Surv. of the Rocky Mountain Reg.*, Washington, D. C., 155 pp., 1877.
- Gilbert, G. K., The transportation of débris by running water, *U.S. Geol. Surv. Prof. Pap. 86*, 263 pp., 1914.
- Gilbert, G. K., Hydraulic-mining débris in the Sierra Nevada, *U.S. Geol. Surv. Prof. Pap. 105*, 154 pp., 1917.
- Goldfarb, R. J., Leach, D. L., Pickthorn, W. J. and Paterson, C. J., Origin of lode-gold deposits of the Juneau gold belt, southeastern Alaska, *Geol.*, 16, 440-443, 1988.
- Greenberg, H. M., Streams, Mountain Drainage Basin Research Group, Univ. of Wash. web site: <http://duff.geology.washington.edu/mdbrg/mdbrg/streams/index.html>, 1997.
- Henderson, F. M., Stability of alluvial channels, *Transactions Am. Soc. Civ. Eng.*, 128, 657-720, 1963.
- Hey, R. D., Flow resistance in gravel-bed rivers, *J. Hydraul. Div. Am. Soc. Civ. Eng.*, 105, 365-379, 1979.

- Hey, R. D., Bar form resistance in gravel-bed rivers, *J. Hydraul. Eng.*, 114, 1498-1508, 1988.
- Hey, R. D. and Thorne, C. R., Accuracy of surface samples from gravel bed material, *J. Hydr. Eng.*, 109, 842-851, 1983.
- Higginson, N. N. J. and Johnston, H. T., Estimation of friction factor in natural streams, in *International Conference on River Regime*, edited by W. R. White, pp. 251-266, John Wiley, New York, 1988.
- Hoerner, S. F., *Fluid-dynamic Drag*, Hoerner Fluid Dynamics, Vancouver, WA, 1965.
- Houjou, K., Shimizu, Y. and Ishii, C., Calculation of boundary shear stress in open channel flow, *J. Hydrosoci. Hydr. Eng.*, 8, 21-37, 1990.
- Ibbeken, H. and Schleyer, R., Photo-sieving: A method for grain-size analysis of coarse-grained, unconsolidated bedding surfaces, *Earth Surf. Processes Landforms*, 11, 59-77, 1986.
- Inoue, M., Nakano, S., and Nakamura, F., Juvenile masu salmon (*Oncorhynchus masou*) abundance and stream habitat relationships in northern Japan, *Can. J. Fish. Aquat. Sci.*, 54, 1331-1341, 1997.
- Ikeda, S., Parker, G. and Kimura, Y., Stable width and depth of straight gravel rivers with heterogeneous bed materials, *Water Resour. Res.*, 24, 713-722, 1988.
- Iseya, F. and Ikeda, H., Pulsations in bedload transport rates induced by a longitudinal sediment sorting: A flume study using sand and gravel mixtures, *Geog. Ann.*, 69A, 15-27, 1987.
- Kellerhals, R., Stable channels with gravel-paved beds, *J. Waterways Harbors Div. Am. Soc. Civ. Eng.*, 63-83, 1967.
- Kellerhals, R. and Bray, D. I., Sampling procedures for coarse fluvial sediments, *J. Hydr. Eng.*, 97, 1165-1180, 1971.
- Kenney, B. C., Beware of spurious self-correlations!, *Water Resour. Res.*, 18, 1041-1048, 1982.
- Keulegan, G. H., Laws of turbulent flow in open channels, *J. Res. Nat. Bureau Stand.*, 21, 707-741, 1938.
- Kinerson, D., Bed surface response to sediment supply, M.S. thesis, 420 pp., Univ. of Calif., Berkeley, 1990.
- Kirchner, J. W., Dietrich, W. E., Iseya, F. and Ikeda, H., The variability of critical shear stress, friction angle, and grain protrusion in water worked sediments, *Sedimentology*,

- 37, 647-672, 1990.
- Knight, D. W., Boundary shear in smooth and rough channels, *J. Hydraul. Div. Am. Soc. Civ. Eng.*, 107, 839-851, 1981.
- Kondolf, G. M., Application of the pebble count: Notes on purpose, method, and variants, *J. Amer. Water Resour. Assoc.*, 33, 79-87, 1997.
- Kondolf, G. M. and Li, S., The pebble count technique for quantifying surface bed material size in instream flow studies, *Rivers*, 3, 80-87, 1992.
- Kondolf, G. M. and Wolman, M. G., The sizes of salmonid spawning gravels, *Water Resour. Res.*, 29, 2275-2285, 1993.
- Krumbein, W. C., Application of logarithmic moments to size frequency distribution of sediments, *J. Sed. Petrol.*, 6, 35-47, 1936.
- Krumbein, W. C., Statistical designs for sampling beach sand, *Eos, Trans. AGU*, 34, 857-868, 1953.
- Krumbein, W. C., The "geological population" as a framework for analysing numerical data in geology, *Liverpool Manchester Geol. J.*, 2, 341-368, 1960.
- Kuhnle, R. A. and Southard, J. B., Bed load transport fluctuations in a gravel bed laboratory channel, *Water Resour. Res.*, 24, 247-260, 1988.
- Lane, E. W., Progress report on studies on the design of stable channels by the bureau of reclamation, *Proc. Am. Soc. Civ. Eng.*, 79, 1-30, 1953.
- Langbein, W. B. and Leopold, L. B., River channel bars and dunes--Theory of kinematic waves, *U.S. Geol. Surv. Prof. Pap. 422-L*, 20 pp., 1968.
- Leighly, J. B., Toward a theory of the morphologic significance of turbulence in the flow of water in streams, *Univ. Calif. Publ. Geog.*, 6, 1-22, 1932.
- Leopold, L., An improved method for size distribution of stream bed gravel, *Water Resour. Res.*, 6, 1357-1366, 1970.
- Leopold, L. B. and Maddock, T., The hydraulic geometry of stream channels and some physiographic implications, *U. S. Geol. Surv. Prof. Pap. 252*, 57 pp., 1953.
- Leopold, L. B., Wolman, M. G. and Miller, J. P., *Fluvial Processes in Geomorphology*, 522 pp., W. H. Freeman, San Francisco, 1964.
- Li, R., Simons, D. B. and Stevens, M. A., Morphology of cobble streams in small watersheds, *J. Hydraul. Div. Am. Soc. Civ. Eng.*, 102, 1101-1117, 1976.
- Lindley, E. S., Regime channels, in *Proceedings of the Punjab Engineering Congress*, pp. 63-74, 1919.

- Lisle, T. E., Effects of coarse woody debris and its removal on a channel affected by the 1980 eruption of Mount St. Helens, Washington, *Water Resour. Res.*, 31, 1797-1808, 1995.
- Lisle, T. E. and Hilton, S., The volume of fine sediment in pools: An index of sediment supply in gravel-bed streams, *Water Resour. Bull.*, 28, 371-383, 1992.
- Lisle, T. E., Iseya, F. and Ikeda, H., Response of a channel with alternate bars to a decrease in supply of mixed-size bed load: A flume experiment, *Water Resour. Res.*, 29, 3623-3629, 1993.
- Lisle, T. E. and Madej, M. A., Spatial variation in armouring in a channel with high sediment supply, in *Dynamics of Gravel-bed Rivers*, edited by P. Billi, R. D. Hey, C. R. Thorne and P. Tacconi, John Wiley, New York, pp. 277-293, 1992.
- Mackin, J. H., Concept of the graded river, *Bull. Geol. Soc. Am.*, 59, 463-512, 1948.
- Manning, R., On the flow of water in open channels and pipes, *Trans. Institution Civ. Eng. Ireland*, 20, 161-207, 1891.
- Marcus, W. A., Roberts, K., Harvey, L. and Tackman, G., An evaluation of methods for estimating Manning's n in small mountain streams, *Mountain Res. Development*, 12, 227-239, 1992.
- Massong, T., Influence of lithology, sediment supply, and log jams on the distribution of bedrock and alluvial channels, unpublished Masters thesis, Univ. of Wash., Seattle, 62 pp., 1998.
- McNeil, W. J. and Ahnell, W. H., Measurement of gravel composition of salmon stream beds, Fisheries Res. Inst., College of Fisheries, Univ. of Wash., *Circular 120*, 2 pp., 1960.
- Meyer-Peter, E. and Müller, R., Formulas for bed-load transport, in *Proceedings of the 2nd Meeting of the International Association for Hydraulic Structures Research*, pp. 39-64, Inter. Assoc. for Hydraul. Res., Delft, Netherlands, 1948.
- Middleton, G. V. and Southard, J. B., *Mechanics of Sediment Movement*, 401 pp., Soc. of Econ. Paleontol. and Mineral., Tulsa, OK, 1984.
- Milhaus, R. T., Sediment transport in a gravel-bottomed stream, Ph.D. dissertation, 232 pp., Oreg. State Univ., Corvallis, 1973.
- Miller, R. T. and Byrne, R. J., The angle of repose for a single grain on a fixed rough bed, *Sedimentology*, 6, 303-314, 1966.
- Mizuyama, T., Bedload transport in steep channels, Ph.D. dissertation, 118 pp., Kyoto

- Univ., Kyoto, Japan, 1977.
- Montgomery, D. C. and Runger, G. C., *Applied statistics and probability for engineers*, 895 pp., John Wiley, New York, 1994.
- Montgomery, D. R., Road surface drainage, channel initiation, and slope instability, *Water Resour. Res.*, 30, 1925-1932, 1994.
- Montgomery, D. R., Abbe, T. B., Buffington, J. M., Peterson, N. P., Schmidt, K. M. and Stock, J. D., Distribution of bedrock and alluvial channels in forested mountain drainage basins, *Nature*, 381, 587-589, 1996.
- Montgomery, D. R. and Buffington, J. M., Channel-reach morphology in mountain drainage basins, *Geol. Soc. Amer. Bull.*, 109, 596-611, 1997.
- Montgomery, D. R. and Buffington, J. M., Channel processes, classification, and response, In: *River Ecology and Management*, edited by Naiman, R. and Bilby, R., Springer-Verlag, New York, 13-42, 1998.
- Montgomery, D. R., Buffington, J. M., Peterson, N. P., Schuett-Hames, D. and Quinn, T. P., Streambed scour, egg burial depths and the influence of salmonid spawning on bed surface mobility and embryo survival, *Can. J. Fish. Aquat. Sci.*, 53, 1061-1070, 1996.
- Montgomery, D. R., Buffington, J. M., Smith, R. D., Schmidt, K. M. and Pess, G., Pool spacing in forest channels, *Water Resour. Res.*, 31, 1097-1105, 1995.
- Montgomery, D. R., Dietrich, W. E., and Sullivan, K., The role of GIS in watershed analysis, *Landform Monitoring and Analysis*, edited by Lane, S. N., Richards, K. S., and Chandler, J. H., Wiley, New York, 241-261, 1998.
- Montgomery, D. R., Fournelle-Georgiou, E., Channel network source representation using digital elevation models, *Water Resour. Res.*, 29, 3925-3934, 1993.
- Mosely, M. P. and Tindale, D. S., Sediment variability and bed material sampling in gravel-bed rivers, *Earth Surf. Processes Landforms*, 10, 465-482, 1985.
- Naden, P. S. and Brayshaw, A. C., Small- and medium-sized bedforms in gravel-bed rivers, In: *River Channels: Environment and Process*, edited by K. S. Richards, pp. 249-271, Blackwell, Oxford, 1987.
- Naot, D., Response of channel flow to roughness heterogeneity, *J. Hydr. Eng.*, 110, 1568-1587, 1984.
- Nelson, J. M. and Smith, J. D., Flow in meandering channels with natural topography, in *River Meandering, Geophys. Monogr. Ser.*, vol. 12, edited by S. Ikeda and G. Parker,

- pp. 69-102, AGU, Washington, D.C., 1989.
- O'Brien, M. P. and Rindlaub, B. D., The transportation of bed-load by streams, *Eos Trans. AGU*, 15, 593-603, 1934.
- Paola, C. and Mohrig, D., Paleohydraulics revisited: palaeoslope estimation in coarse-grained braided rivers, *Basin Res.*, 8, 243-254, 1996.
- Paola, C. and Seal, R., Grain size patchiness as a cause of selective deposition and downstream fining, *Water Resour. Res.*, 31, 1395-1407, 1995.
- Parker, G., Self-formed straight rivers with equilibrium banks and mobile bed. Part 1. The sand-silt river, *J. Fluid Mech.*, 89, 109-125, 1978a.
- Parker, G., Self-formed straight rivers with equilibrium banks and mobile bed. Part 2. The gravel river, *J. Fluid Mech.*, 89, 127-146, 1978b.
- Parker, G. and Andrews, E. D., Sorting of bed load sediment by flow in meander bends, *Water Resour. Res.*, 21, 1361-1373, 1985.
- Parker, G. and Klingeman, P. C., On why gravel bed streams are paved, *Water Resour. Res.*, 18, 1409-1423, 1982.
- Parker, G. and Peterson, A. W., bar resistance of gravel-bed streams, *J. Hydraul. Div. Am. Soc. Civ. Eng.*, 106, 1559-1575, 1980.
- Parker, G., Dhamotharan, S. and Stefan, H., Model experiments on mobile, paved gravel bed streams, *Water Resour. Res.*, 18, 1395-1408, 1982.
- Pizzuto, J. E., Numerical simulation of gravel river widening, *Water Resour. Res.*, 26, 1971-1980, 1990.
- Platts, W. S., Megahan, W. F. and Minshall, G. W., Methods for evaluating stream, riparian, and biotic conditions, U.S. Dept. Agric., *Forest Service Gen. Tech. Rep. GTR-INT-138*, 70 pp., 1983.
- Potter, K. W., Derivation of the probability density function of certain biased samples of coarse riverbed material, *Water Resour. Res.*, 15, 21-22, 1979.
- Powell, D. M. and Ashworth, P. J., Spatial pattern of flow competence and bed load transport in a divided gravel bed river, *Water Resour. Res.*, 31, 741-752, 1995.
- Prestegard, K. L., Bar resistance in gravel bed streams at bankfull stage, *Water Resour. Res.*, 19, 473-476, 1983.
- Reed, J. C., Southeastern Alaska, in *Landscapes of Alaska*, edited by H. Williams, pp. 9-18, Univ. of California Press, Berkeley, 1958.
- Reice, S. R., The role of substratum in benthic macroinvertebrate microdistribution and

- litter decomposition in a woodland stream, *Ecology*, 61, 580-590, 1980.
- Reid, L. M. and Dunne, T., Sediment production from forest road surfaces, *Water Resour. Res.*, 20, 1753-1761, 1984.
- Rice, S., Towards a model of changes in bed material texture at the drainage basin scale, in *Process Models and Theoretical Geomorphology*, edited by M. J. Kirkby, pp. 160-172, John Wiley, New York, 1994.
- Rice, S. and Church, M., Sampling surficial fluvial gravels: The precision of size distribution percentile estimates, *J. Sedimentary Res.*, A, 66, 654-665, 1996.
- Ritter, J. R., Bed-material movement, Middle Fork Eel River, California, *U.S. Geol. Surv. Prof. Pap. 575-C*, 3 pp., 1967.
- Robert, A., Roy, A. G. and De Serres, B., Changes in velocity profiles at roughness transitions in coarse grained channels, *Sedimentology*, 39, 725-735, 1992.
- Rouse, H., Critical analysis of open-channel resistance, *J. Hydraul. Div. Am Soc. Civ. Eng.*, 191, 1-25, 1965.
- Russell, I. C., *River Development*, 327 pp., John Murray, London, 1907.
- Schumm, S. A., Fluvial geomorphology: Channel adjustment and river morphology, in *River Mechanics*, edited by H. W. Shen, pp. 5:1-22, H. W. Shen, Fort Collins, 1971.
- Shields, A., Anwendung der Aehnlichkeitsmechanik und der Turbulenzforschung auf die Geschiebebewegung, *Mitt. Preuss. Versuchsanst. Wasserbau Schiffbau*, 26, 26 pp., 1936.
- Shields, F. D. and Gippel, C. J., Prediction of effects of woody debris removal on flow resistance, *J. Hydraul. Eng.*, 121, 341-354, 1995.
- Shirazi, M. A. and Seim, W. K., Stream system evaluation with emphasis on spawning habitat for salmonids, *Water Resour. Res.*, 17, 592-594, 1981.
- Shirazi, M. A., Seim, W. K. and Lewis, D. H., Characterization of spawning gravel and stream evaluation, in *Salmon-Spawning Gravel: A Renewable Resource in the Pacific Northwest?*, pp. 227-278, State of Wash. Water Res. Center Rep. 39, Pullman, Wash., 1981.
- Sidle, R. C., Bed load transport regime of a small forest stream, *Water Resour. Res.*, 24, 207-218, 1988.
- Sidle, R. C., Pearce, A. J. and O'Loughlin, C. L., *Hillslope Stability and Land Use*, *Water Resour. Monogr. Ser.*, vol. 11, 140 pp., AGU, Washington, D.C., 1985.
- Simons, D. B. and Albertson, M. L., Uniform water conveyance channels in alluvial

- material, *Trans. Amer. Soc. Civ. Eng.*, 128, 65-167, 1963.
- Smarrt, P. F. M. and Grainger, J. E. A., Sampling for vegetation survey: some aspects of the behaviour of unrestricted, restricted, and stratified techniques, *J. Biogeog. 1*, 193-206, 1974.
- Smith, J. D. and McLean, S. R., Spatially averaged flow over a wavy surface, *J. Geophys. Res.*, 82, 1735-1746, 1977.
- Smith, R. D., Sidle, R. C. and Porter, P. E., Effects on bedload transport of experimental removal of woody debris from a forest gravel-bed stream, *Earth Surf. Processes Landforms*, 18, 455-468, 1993.
- Smith, R. D., Sidle, R. C., Porter, P. E. and Noel, J. R., Effects of experimental removal of woody debris on the channel morphology of a forest gravel-bed stream, *J. Hydrol.*, 152, 153-178, 1993.
- Student (Gosset, W. S.), The probable error of a mean, *Biometrika*, 6, 1-25, 1908.
- Sullivan, K., Hydraulics and fish habitat in relation to channel morphology, Ph.D. dissertation, 407 pp., Johns Hopkins Univ., Baltimore, 1986.
- Tabor, R. W. and Cady, W. M., Geologic map of the Olympic Peninsula, Washington, *U.S. Geol. Surv. Map I-994*, 1978a.
- Tabor, R. W. and Cady, W. M., The structure of the Olympic Mountains, Washington: Analysis of a subduction zone, *U.S. Geol. Surv. Prof. Pap. 1033*, 38 pp., 1978b.
- Tabor, R. W., Booth, D. B., Vance, J. A., Ford, A. B., and Ort, M. H., Preliminary geologic map of the Sauk River 30 by 60 minute quadrangle, Washington, *U.S. Geol. Surv. Open File Map 88-692*, 1988.
- Townsend, C. R., The patch dynamics concept of stream community ecology, *J. North Amer. Benthological Soc.*, 8, 36-50, 1989.
- Trimble, S. W., Stream channel erosion and change resulting from riparian forests, *Geol.*, 25, 467-469, 1997.
- Udden, J. A., The mechanical composition of wind deposits, Augustana College and Theological Seminary, *Augustana Lib. Pub. no. 1*, 69 pp., Rock Island, IL, 1898.
- Udden, J. A., Mechanical composition of clastic sediments, *Bull. Geol. Soc. Amer.*, 25, 655-744, 1914.
- U. S. Waterways Experiment Station (USWES), Study of river-bed material and their use with special reference to the Lower Mississippi River, *Pap. 17*, 161 pp., Vicksburg, Miss., 1935.

- Wentworth, C. K., A scale of grade and class terms for clastic sediments, *J. Geol.*, 30, 377-392, 1922.
- Whiting, P. J. and Dietrich, W. E., Boundary shear stress and roughness over mobile alluvial beds, *J. Hydraul. Eng.*, 116, 1495-1511, 1990.
- Whiting, P. J., Dietrich, W. E., Leopold, L. B., Drake, T. G. and Shreve, R. L., Bedload sheets in heterogeneous sediment, *Geol.*, 16, 105-108, 1988.
- Wiberg, P. L. and Smith, J. D., Calculations of the critical shear stress for motion of uniform and heterogeneous sediments, *Water Resour. Res.*, 23, 1471-1480, 1987.
- Wiberg, P. L. and Smith, J. D., Model for calculating bed load transport of sediment, *J. Hydraul. Eng.*, 115, 101-123, 1989.
- Wiberg, P. L. and Smith, J. D., Velocity distribution and bed-roughness in high-gradient streams, *Water Resour. Res.*, 27, 825-838, 1991.
- Williams, G. P., Bank-full discharge of rivers, *Water Resour. Res.*, 14, 1141-1154, 1978.
- Williams, H., Turner, F. J., and Gilbert, C. M., *Petrography*, 626 pp., W. H. Freeman, New York, 1982.
- Wolcott, J. and Church, M., Strategies for sampling spatially heterogeneous phenomena: The example of river gravels, *J. Sed. Petrol.*, 61, 534-543, 1990.
- Wolman, M. G., A method of sampling coarse bed material, *Trans. AGU*, 35, 951-956, 1954.
- Wolman, M. G. and Brush, L. M., Factors controlling the size and shape of stream channels in coarse noncohesive sands, *U.S. Geol. Surv. Prof. Pap. 282-G*, 37 pp., 1961.
- Wolman, M. G. and Leopold, L. B., River flood plains: Some observations on their formation, *U.S. Geol. Surv. Prof. Pap. 282-C*, 107 pp., 1957.
- Wolman, M. G. and Miller, J. P., Magnitude and frequency of forces in geomorphic processes, *J. Geol.*, 68, 54-74, 1960.
- Wood-Smith, R. D. and Buffington, J. M., Multivariate geomorphic analysis of forest streams: Implications for assessment of land use impact on channel condition, *Earth Surf. Processes Landforms*, 21, 377-393, 1996.
- Yotsukura, N. and Cobb, E. D., Transverse diffusion of solutes in natural streams, *U.S. Geol. Surv. Prof. Pap. 582-C*, 19 pp., 1972.

Vita

John Mason Buffington VI

University of Washington

1998

Born: **January 27, 1966, Oakland, California**

Parents: **Lana Leigh Buffington**

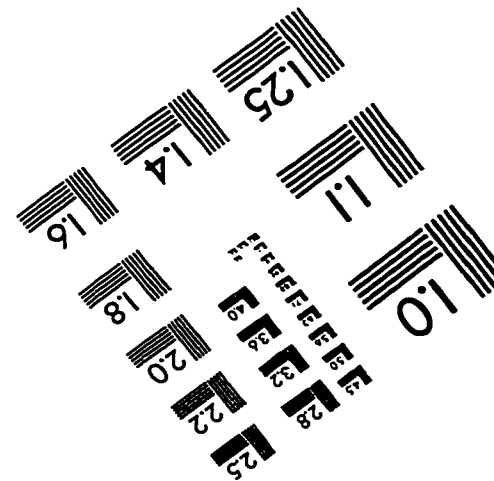
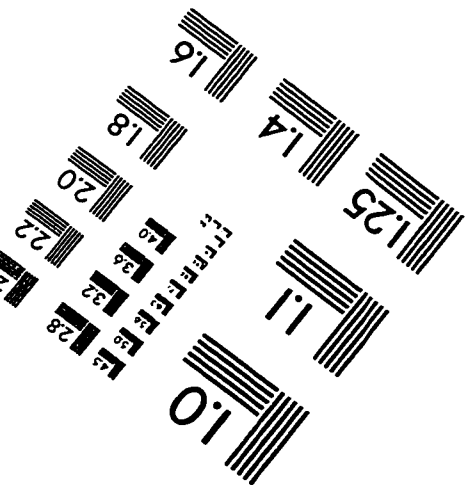
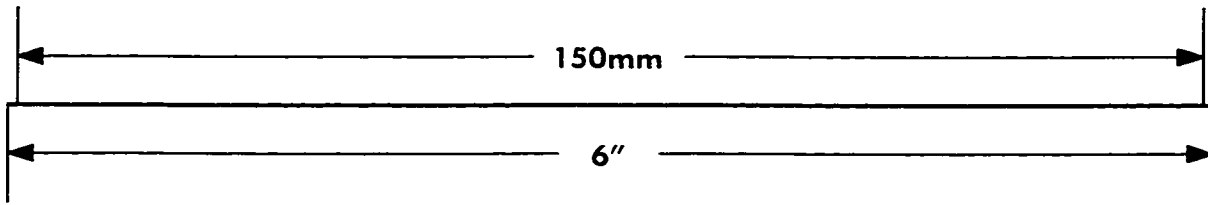
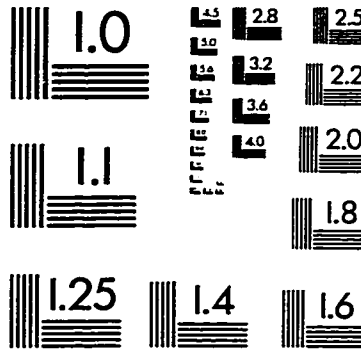
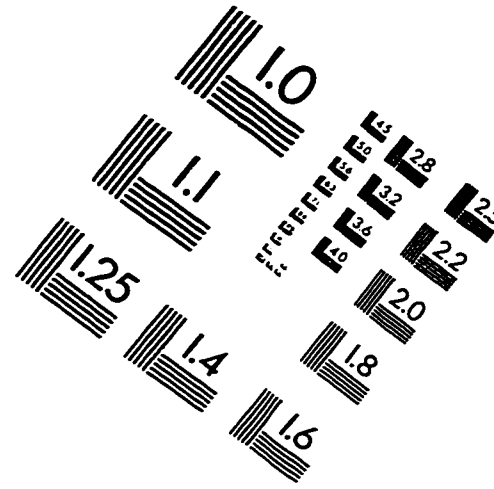
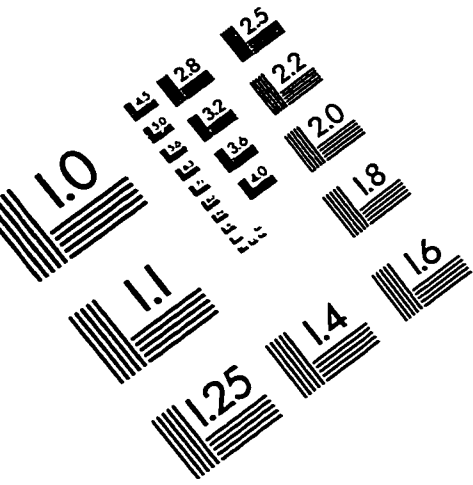
John Mason Buffington V

Education: **Skyline High School, Oakland California, graduated 1984**

University of California Berkeley, B.A. 1988

University of Washington, M.S. 1995

IMAGE EVALUATION TEST TARGET (QA-3)



APPLIED IMAGE, Inc
1653 East Main Street
Rochester, NY 14609 USA
Phone: 716/482-0300
Fax: 716/288-5989

© 1993, Applied Image, Inc., All Rights Reserved